UNIVERSITY OF WEST BOHEMIA IN PILSEN

Faculty of Electrical Engineering
Department of Power Electronics and Machines

THESIS

Analysis of the plant's connection to the electricity grid

Author: **bc. Josef Kolerus**
Thesis supervisor: **Ing. Martin Sirový, Ph.D.**
Specialist consultant: **Ing. Miloš Ryba**

2024

ZÁPADOČESKÁ UNIVERZITA V PLZNI

Fakulta elektrotechnická
Katedra výkonové elektroniky a strojů

DIPLOMOVÁ PRÁCE

Studie připojitelnosti elektrárny do elektrizační soustavy

Autor práce: **bc. Josef Kolerus**
Vedoucí práce: **Ing. Martin Sirový, Ph.D.**
Odborný konzultant: **Ing. Miloš Ryba**

2024

ZÁPADOČESKÁ UNIVERZITA V PLZNI
Fakulta elektrotechnická
Akademický rok: 2023/2024

ZADÁNÍ DIPLOMOVÉ PRÁCE

(projektu, uměleckého díla, uměleckého výkonu)

Jméno a příjmení:	**Bc. Josef KOLERUS**
Osobní číslo:	**E22N0038P**
Studijní program:	**N0713A060013 Výkonové systémy a elektroenergetika**
Specializace:	**Výkonové elektronické technologie a pohony**
Téma práce:	**Studie připojitelnosti elektrárny do elektrizační soustavy**
Zadávající katedra:	**Katedra výkonové elektroniky a strojů**

Zásady pro vypracování

1. Sestavení matematického modelu elektrárenského bloku cca 50-100MW v Matlab/Simscape (turbína, vícehmotový rotor, synchronní generátor, regulátor buzení, model vlastní spotřeby, blokový transformátor s přepínačem odboček, VVN síť).
2. Zpracování loadflow diagramů pro simulované případy a pro stacionární problémy (kapacita regulace jalového výkonu v síti v závislosti na napětí v připojovacím místě).
3. Ladění regulátorů – regulace výkonu turbíny a napětí a jalového výkonu generátoru.
4. Dynamické simulace definovaných dějů – poruchy v síti, injektované napěťové skoky, injektované frekvenční změny, koordinace základních ochran generátoru.
5. Preferovaný jazyk zpracování angličtina, čeština pouze v případě studie na základě kodexu ČEPS.

Rozsah diplomové práce: **40-60**
Rozsah grafických prací:
Forma zpracování diplomové práce: **elektronická**
Jazyk zpracování: **Angličtina**

Seznam doporučené literatury:

1. UK gridcode: https://www.nationalgrideso.com/document/162271/download (The Grid Code, National Grid Electricity System Operator Limited, 2023).
2. UK distribution code: https://www.nationalgrideso.com/document/162271/download (Engineering Recommendation G99, Energy Networks Association, 2021).

Vedoucí diplomové práce: **Ing. Martin Sirový, Ph.D.**
Research and Innovation Centre for Electrical Engineering

Datum zadání diplomové práce: **6. října 2023**
Termín odevzdání diplomové práce: **24. května 2024**

Západočeská univerzita v Plzni * Fakulta elektrotechnická

L.S.

Prof. Ing. Zdeněk Peroutka, Ph.D.
děkan

Prof. Ing. Václav Kůs, CSc.
vedoucí katedry

V Plzni dne 6. října 2023

Abstract

The thesis is focused on simulation and subsequent assessment of grid code tests for a newly connected power production unit to the grid. The issued is solved in Simulink, employing a Phasor-based solution method. The thesis deals with the particular models utilized in the simulation, i.e. Grid, Step-up transformer, Generator, Brushless excitation (type AC7B), Steam turbine and Mass. Custom models are developed either in accordance with standards or by utilizing implementations from the Simulink/Simscape/Power Systems library. In the final stage of the thesis, grid code compliance simulation results are presented.

Key Words

Grid Code, G99, Power Generating Unit, Power plant model, conditions of connection, Phasor-based solution, generator, AC7B excitation, turbine, mass, OLTC, PSS tuning, Reactive capability across the voltage range, FRT, LFSM, FSM

Acknowledgements

I would like to express my sincere acknowledgement to Ing. Miloš Ryba and Ing. Martin Sirový, Ph.D. for their supervision during the writing of my thesis. Their knowledge, valuable advice and constant availability of help contributed to the successful completion of my thesis.

Content

General list of symbols and shortenings

Shortenings

AC7B – type of the brushless alternator-rectifier excitation system, reference in [8]

AVR – Automatic Voltage Regulation

DNO – Distribution Network Operator

FRT – Fault Ride Through

GCP – Grid Connection Point

HP – High Pressure

IP – Intermediate Pressure

FSM – Frequency Sensitive Mode

LFSM – Limited Frequency Sensitive Mode

LP – Low Pressure

OLTC - On-Load Tap Changer

PSS – Power System Stabilizer

UEL – Under-Excitation Limiter

Symbols

a – phasor rotation operator

f – frequency

f (t) – general analysed function

F (f) – general function in the frequency spectre, after Fourier analysis

F (s) – transmission of signals, in the Laplace domain

H – inertia constant

i – general current

i_{sd} – stator winding current d-axis component

i_{sq} – stator winding current q-axis component

i_{fd} – field winding current (d-axis component)

i_{kd} – damper winding current d-axis component

i_{kq1} – damper winding current q-axis component 1

i_{kq2} – damper winding current q-axis component 2

I_{FD} – generator field current

I_{FE} – exciter field current

J – inertia moment

L – general inductance

L_d'' – sub-transient d-axis inductance

L_q'' – sub-transient q-axis inductance

L_d' – transient d-axis inductance

L_q' – transient q-axis inductance

L_d – stator d-axis inductance (stator leakage inductance plus mutual inductance)

L_q – stator q-axis inductance (stator leakage inductance plus mutual inductance)

L_l – leakage inductance of stator winding

L_{lfd} – leakage inductance of field winding

L_{lkd} – leakage inductance of damper winding d-axis component

L_{lkq1} – leakage inductance of damper winding q-axis component 1

L_{lkq2} – leakage inductance of damper winding q-axis component 2

L_{md} – matual inductance d-axis component

L_{mq} – matual inductance q-axis component

N – number of coils

P_G – generator terminal electric active power

P_{HL} – house load of Power Generating Unit

P_k – short circuit losses expressed in kW or as a percentage

P_M - turbine shaft power

P_{REF} – turbine set-point

P_{REG} – registered power = contracted rated output

R – general electrical resistance

R_s – stator winding resistance

R_{fd} – field winding resistance

R_{kd} – damper winding resistance d-axis component

R_{kq1} – damper winding resistance q-axis component 1

R_{kq2} – damper winding resistance q-axis component 2

R_K – short circuit resistance of the grid

S_K – short circuit power of the grid

S_N – nominal apparent power

T_E – exciter time constant

T_d'' – sub-transient short-circuit d-axis time constant

T_{d0}'' – sub-transient open-circuit d-axis time constant

T'_d – transient short-circuit d-axis time constant

T'_{d0} – transient open-circuit d-axis time constant

T''_q – sub-transient short-circuit q-axis time constant

T''_{q0} – sub-transient open-circuit q-axis time constant

T'_q – transient short-circuit q-axis time constant

T'_{q0} – transient open-circuit q-axis time constant

T – torque

u, V – general voltage

u_{sd} – stator winding voltage d-axis component

u_{sq} – stator winding voltage q-axis component

u_{fd} – field winding voltage (d-axis component)

u_{kd} – damper winding voltage d-axis component

u_{kq1} – damper winding voltage q-axis component 1

u_{kq2} – damper winding voltage q-axis component 2

V_F, E_{FD} – generator field voltage

V_{FE} – exciter field voltage

X_K – short circuit reactance of the grid

z_k – short circuit impedance (equal to short circuit voltage) of transformer in per unit

Z_K – short circuit impedance of the grid

δ – angular angle of rotation / load angle

Φ – general magnetic flux

Ψ – general coupled magnetic flux

Ψ_{sd} – stator d-axis flux

Ψ_{md} – matual d-axis flux

Ψ_{fd} – field (d-axis) flux

Ψ_{kd} – damper d-axis flux

Ψ_{sq} – stator q-axis flux

Ψ_{mq} – matual q-axis flux

Ψ_{kq1} – damper q-axis flux 1

Ψ_{kq2} – damper q-axis flux 2

ω – angular speed of rotation

Introduction

In today's context, the results of the feasibility study regarding the connection of the Power Generating Unit are essential for approving the connection of a newly manufactured Power Generating Unit to the grid. It is necessary to demonstrate the stable operation of the production unit in a specific power grid by performing simulation on an equivalent mathematical model.

The study has been conducted for the specific Rivenhall Waste-to-energy Power plant in England in collaboration with Doosan Škoda Power company. In Great Britain, the conditions that the production unit must satisfy are specified by the G99 [1] and Grid Code [2].

The main objective of the document is to prove compliance with the connection conditions of the production unit. The mathematical model has been developed in the Simulink program.

The first section of the thesis focuses on the selection of appropriate solution method.

In the following chapters from 2 to 8, the individual blocks of Power Generating Unit are defined. Figure 1 illustrates the connection of the partial blocks. Each individual chapter contains mathematical equations describing the specific part of the production unit and implementation of this equations. Where applicable, the structures of individual models are based on standards such as Std 421.5 or IEEEG1. The inputs into the blocks are either provided or computed within each chapter, parameters of PI controllers and PSS constants are determined by simulation. Each chapter includes a table summarizing the parameters of its corresponding block.

The final chapter, Simulation, is the most important chapter. In the Simulation chapter, the conditions are specifically listed, subsequently, evidence of meeting these conditions is presented using diagrams. The simulation is performed in accordance with G99 [1]. The most extensive is the chapter on PSS simulation, requiring initial tuning of PSS with the proper constants and subsequently demonstrating the correct tuning of these constants. Similarly, the Verification and Validation chapter demonstrates the proper tuning of PI controllers. Reactive capability across the voltage range is conducted near steady-state conditions to comply with the regulatory range illustrated in Figure 13.5 from reference [1]. Chapter 9.4 demonstrates the keeping of generator stability during specified disturbances. The LFSM testing illustrates the behavior of the production unit during a sudden changeover to island mode.

1 Method of solution

The proper choice of problem-solving method is crucial. The modelling of the production unit and its interaction with the grid is carried out in the Simulink environment, with the widely used Simscape library (Power systems – Specialize technology – Fundamental Blocks).

As an output from simulations, we are primarily interested in RMS values rather than the harmonic waveform. For this reason, phasor-based solution has been, as detailed in Chapter 1.2. The advantage of this approach lies in the simulation speed. Simulink handles operations with complex numbers, allowing for the utilization of a significantly larger solution step. The general structure of the production unit connected to the network is illustrated in Figure 1:

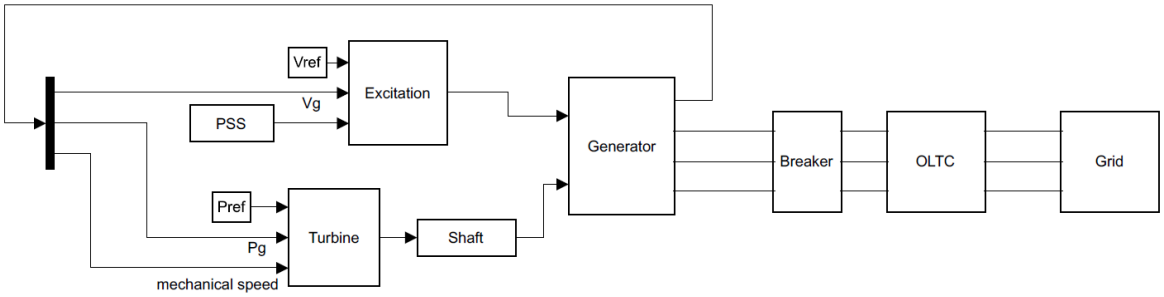

Figure 1 General connection diagram

All these blocks operate with per units. Specific block models are described in the following chapters.

1.1 Powergui (Power Graphical User Interface)

Powergui is necessary for simulating any block from the Power Systems Library. The Powergui stores an equivalent Simulink circuit that represents the connection of individual models. The electrical circuit can be solved in three different ways. I opted for phasor analysis to solve the issue (advantages have already been mentioned).

There are tools available, such as model initialization, to achieve a steady state for a particular model.

These functions can be helpful, but in my simulation, there are many models that are not from a library, and their steady state is not completely accurate. There are many initial states for the given simulation, therefore, initialization is always performed within an initialization

run of model with subsequent state saving. However, to achieve steady-state faster in the initialization run, a specific initialization function was utilized for the generator.

1.2 Phasor solution

Utilizing a phasor-based solution through Powergui offers the optimal method to simulate the capability of a Power Generating Unit connection. A large portion of the required simulations need to be carried out over a long-time interval, so utilizing a very small simulation step is not desirable. The very small simulation steps lead to increased computational demands and extended simulation duration. The phasor-based solution allows for precisely reducing these computational complications of the common real-time solution. The principle of phasor solution applied at these models will be explained. The individual voltages of the 3-phase grid are ideally shifted from each other by 120° and have the same amplitude.

We can imagine one phase as a vector rotating in space defined by a certain velocity. When simulating the voltage source of the network, the phasor (rotating vector) rotates at a frequency of 50 Hz. All voltage vectors rotate at an equal speed but with different phase delays. In Figure 2, harmonic waveforms of phases are transformed into rotating vectors.

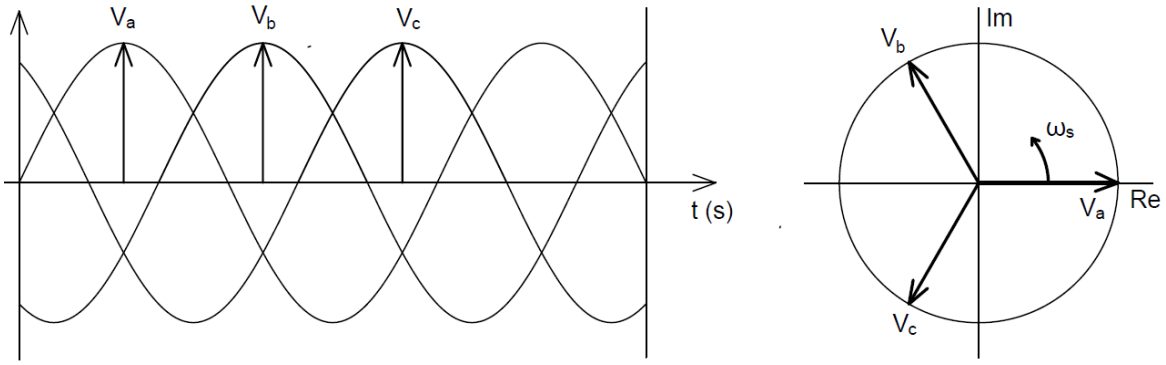

Figure 2 Harmonic waveforms of phases transform into phasors

If vectors rotate at a constant speed within a stationary coordinate system, they can be converted into stationary vectors within a rotating coordinate system. To include this transformation, it is necessary to enter the rotation speed into the Powergui, i.e. 50 Hz. The magnitude and orientation of the vector can be described using complex numbers.

Complex numbers can be calculated more effectively than instantaneous values. The simulation step for an instantaneous-based solution must be several times smaller compared to the phasor-based solution (especially in steady-state, where complex numbers remain constant).

1.3 PI controllers

A PI controller typically consists of proportional and integral components. The PI regulator tries to get the measured variable closer to the desired setpoint, however, it is not always possible due to limitations. These limitations prevent the controller from reaching an output a value that could potentially endanger the operation of the production unit. In response to this limitation, the integrator must react appropriately.

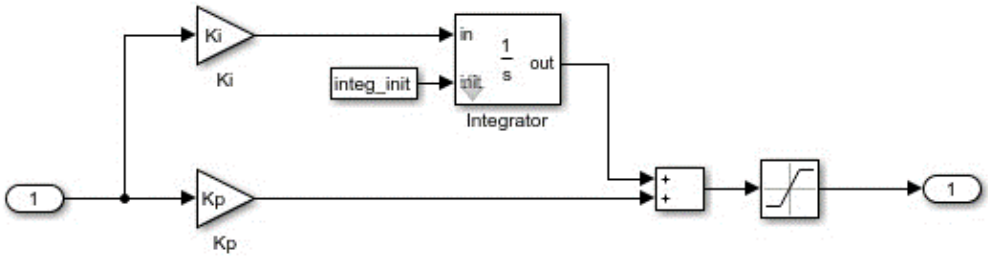

Figure 3 PI controller

Anti-Windup mechanism has been designed as illustrated in Figure 4. A limited output shall not stop the integration, but shall only limit the output from the controller, allowing integration to continue until it reaches the saturated level. The integrator remains active until its output reaches the limit value, therefore only the integrator output is monitored in the feedback loop. Reaching the saturation value is indicated by a dead-band block. Re-enabling the integration is possible only in case the input has the opposite sign than the output. In such cases, the integrator is re-enabled to perform de-integration. Converting to int8 supports the faster and more stable comparisons (Equal and AND are not able handle with small-value inputs).

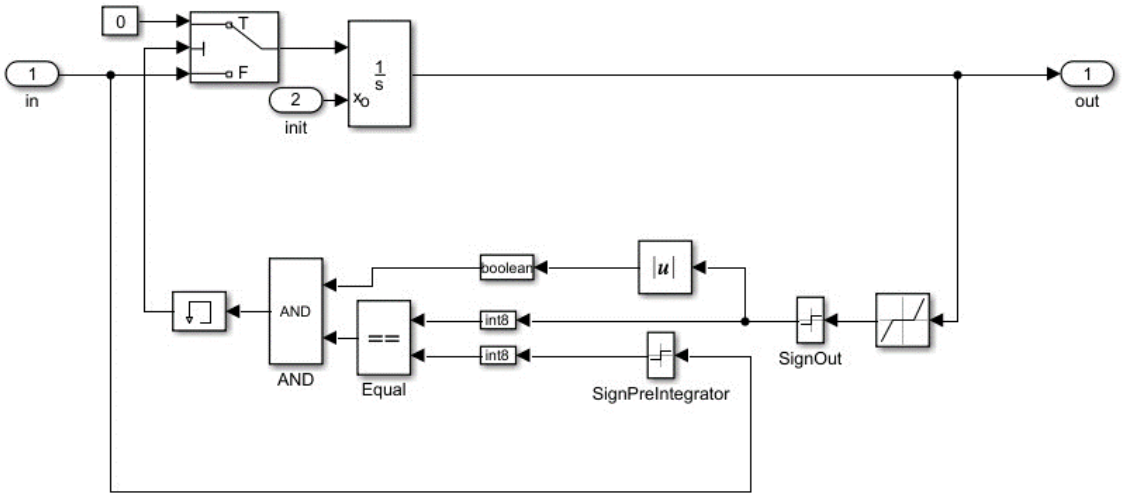

Figure 4 Anti-Windup of integrator

2 Generator

The Synchronous Machine pu Fundamental block from the library Simscape/Power Systems was used as the generator model. The model represents the voltage and flux equations, which are submitted to the solver. In addition, the mechanical part is also considered in the model (more information in the chapter Mass).

I can say that the clear advantage of this model to be its ability to solve problems using phase analysis, which means that it handles complex number mathematics. This allows simulations to be performed over longer time scales. The inputs excitation voltage and shaft torque are specified in per unit values, enabling the utilization of excitation and turbine models based on the Std 421.5 and IEEEG1 standards.

Disadvantage of this model is the computation of the space vector using positive sequence calculation. Consequently, it is not as suitable for applications involving asymmetric voltages at the generator terminals.

In the following chapters, fundamental parameters are calculated from measured standard parameters. The Synchronous Machine per Unit Standard is not utilized because it's not possible to identify how the conversion from standard parameters to fundamental parameters is performed and some inaccuracy was apparent in the experimental trials.

2.1 Derivation of voltage equations

The equations used in the model are accessible on the Mathworks website, the derivation of these equations is described in the following lines. The derivations of equations in the following chapter are based on source [3].

The synchronous generator has 3 types of windings: stator three-phase winding, field winding and damper winding. The Figure 5 is provided only for illustrative purposes.

The winding can be represented as a general RL circuit, where the voltage across the inductor is derived from the following considerations.

$$L = \frac{\mathrm{N}\Phi}{I} = \frac{\Psi}{I} \longrightarrow \Psi = L \cdot I \ldots u_L = L\frac{di}{dt} = \frac{d\Psi}{dt} \tag{2.01}$$

The equation for one phase of a stator winding can be formulated as follows:

$$u_{sa} = R_s i_{sa} + \frac{d\Psi_{sa}}{dt} \tag{2.02}$$

The phases b and c can be expressed in the same way.

$$u_{sb} = R_s i_{sb} + \frac{d\Psi_{sb}}{dt} \tag{2.03}$$

$$u_{sc} = R_s i_{sc} + \frac{d\Psi_{sc}}{dt} \tag{2.04}$$

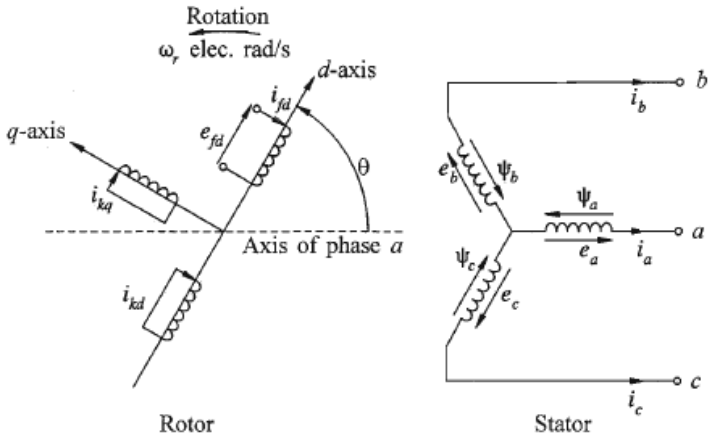

Figure 5 Synchronous machine windings and coordinate system [3]

2.1.1 Clarke transformation

By using the Clarke transformation, the three-phase voltage equations can be converted into a two-dimensional standing coordinate system. The Clarke transformation is only applicable for converting instantaneous 3-phase values into a space rotating vector (space phasor) within a αβ coordinate system. Clarke transformation:

$$\bar{u} = k\ (u_a + \bar{a} \cdot u_b + \bar{a}^2 \cdot u_c) \tag{2.05}$$

The coefficient k is selected to ensure that, following the conversion, the amplitude of the space vector in the coordinate system αβ corresponds to the voltage amplitude of one phase. Therefore, $k = \frac{2}{3}$ for the amplitude invariant transformation. For the zero-sequence component, it is necessary to execute the substitution $k_0 = \frac{1}{3}$ to satisfy the amplitude invariance condition.

After splitting into individual components:

$$u_\alpha = \frac{2}{3}\left(u_a - \frac{1}{2}u_b - \frac{1}{2}u_c\right) \tag{2.06}$$

$$u_\beta = \frac{2}{3}\left(u_a + \frac{\sqrt{3}}{2}u_b - \frac{\sqrt{3}}{2}u_c\right) \tag{2.07}$$

$$u_0 = \frac{2}{3}\left(\frac{1}{2}u_a + \frac{1}{2}u_b + \frac{1}{2}u_c\right) \tag{2.08}$$

We obtain the equation in the αβ coordinate system.

$$\bar{u}_{s\alpha\beta} = R_s \bar{\imath}_{s\alpha\beta} + \frac{d\bar{\Psi}_{s\alpha\beta}}{dt} \tag{2.09}$$

This rotating velocity of this vector is dependent on supply frequency.

Furthermore, we know that the same equations can be formulated for a rotor which rotates at velocity $\omega_m \cdot pp$, this coordinate system is marked as dq. For the rotor coordinate system, a similar general equation is applied:

$$\bar{u}_{rdq} = R_s \bar{\imath}_{rdq} + \frac{d\bar{\Psi}_{rdq}}{dt} \tag{2.10}$$

The angle between the rotor and stator coordinate system can be referred to as ϑ. The rotational speed of the rotor coordinate system relative to the stationary stator coordinate system can be considered as $\omega_m \cdot pp$, where ω_m is the angular velocity and pp is the number of pole pairs.

2.1.2 Park transformation

The Park transformation, also known as Direct-quadrature-zero transformation, generally converts vector from one coordinate system to another coordinate system. To convert a stator coordinate system to a rotor coordinate system, utilize the general relationship for vector conversion:

$$\bar{u}_1 = e^{j\alpha} \cdot \bar{u}_2 \tag{2.11}$$

The coordinate system $\bar{u}_1$ is ahead of the coordinate system $\bar{u}_2$ by the angle α. By applying it to the conversion of the voltage of the stator coordinate system to the rotor coordinate system, we obtain the following equation:

$$\bar{u}_{sdq} = e^{j\vartheta} \cdot \bar{u}_{s\alpha\beta} \tag{2.12}$$

Thus, the voltage $\bar{u}_{sdq}$ represents the stator vector in the rotor coordinate system. The same conversion rule is valid for stator current and stator flux.

The angle between the rotor and stator coordinate system varies depending on the rotation speed:

$$\vartheta = \int pp \cdot \omega_m \, dt + \vartheta_0 \tag{2.13}$$

The conversion is applied to equation (2.09) to obtain the following formula:

$$\bar{u}_{s\alpha\beta} \cdot e^{j\vartheta} = R_s \bar{\imath}_{s\alpha\beta} \cdot e^{j\vartheta} + \frac{d\bar{\Psi}_{s\alpha\beta} \cdot e^{j\vartheta}}{dt} \tag{2.14}$$

Subsequent derivation of the element $\bar{\Psi}_{s\alpha\beta} \cdot e^{j\vartheta}$ leads to the equation:

$$\begin{aligned}\bar{u}_{s\alpha\beta}\cdot e^{j\vartheta} &= R_s\bar{\imath}_{s\alpha\beta}\cdot e^{j\vartheta}+\frac{d\bar{\Psi}_{s\alpha\beta}}{dt}\cdot e^{j\vartheta}+\bar{\Psi}_{s\alpha\beta}\cdot\frac{de^{j\vartheta}}{dt}\\ &= R_s\bar{\imath}_{s\alpha\beta}\cdot e^{j\vartheta}+\frac{d\bar{\Psi}_{s\alpha\beta}}{dt}\cdot e^{j\vartheta}+\bar{\Psi}_{s\alpha\beta}\cdot e^{j\vartheta}\cdot j\cdot\frac{d\vartheta}{dt}\\ &= R_s\bar{\imath}_{s\alpha\beta}\cdot e^{j\vartheta}+\frac{d\bar{\Psi}_{s\alpha\beta}}{dt}\cdot e^{j\vartheta}+\bar{\Psi}_{s\alpha\beta}\cdot pp\cdot j\cdot\omega_m\cdot e^{j\vartheta}\end{aligned} \tag{2.15}$$

Equation (2.15) can be expressed like:

$$\bar{u}_{sdq}=R_s\bar{\imath}_{sdq}+\frac{d\bar{\Psi}_{sdq}}{dt}+j\bar{\Psi}_{sdq}\cdot pp\cdot\omega_m \tag{2.16}$$

For the steady state, the synchronous generator rotates at synchronous speed, thus $pp\cdot\omega_m=\omega_s$, so a deviation from the synchronous speed will cause a change in the ratio of the components dq of the voltage vector. When the current orientation in the generator schematic diagram is respected, the sign of the $R_s\bar{\imath}_{sdq}$ component is reversed. The equation can be split into components as follows:

$$u_{sd}=-R_s i_{sd}+\frac{d\Psi_{\mathrm{sd}}}{dt}-\Psi_{\mathrm{sq}}\cdot pp\cdot\omega_m \tag{2.17}$$

$$u_{sq}=-R_s i_{sq}+\frac{d\Psi_{\mathrm{sq}}}{dt}+\Psi_{\mathrm{sd}}\cdot pp\cdot\omega_m \tag{2.18}$$

After applying the Park transformation, the zero component remains in the same form.

$$u_{s0}=-R_s i_{s0}+\frac{d\Psi_{s0}}{dt} \tag{2.19}$$

The magnetic field from the excitation acts in the d-axis, the general rotor equation (2.10) is modified into a field equation:

$$u_{fd}=R_{fd}i_{fd}+\frac{d\Psi_{fd}}{dt} \tag{2.20}$$

In addition, the rotor of synchronous machine also contains a damper winding. From the equivalent diagrams of the synchronous machine, the remaining voltage equations can also be determined. These diagrams are different for the d-axis and for the q-axis. The equivalent diagram for the d-axis is shown in the following figure:

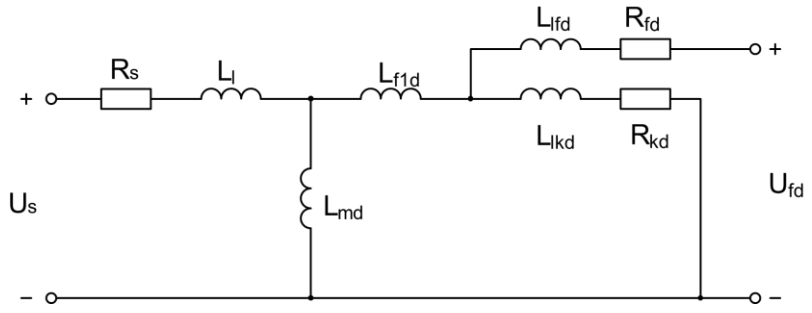

Figure 6 d-axis equivalent diagram

The damper winding is short-circuited, which leads to the formula:

$$u_{kd} = 0 = R_{kd} \cdot i_{kd} + \frac{d\Psi_{kd}}{dt} \tag{2.21}$$

The field does not act in the q-axis, just the damper, hence according to Figure 7 we only formulate the equations for the damper.

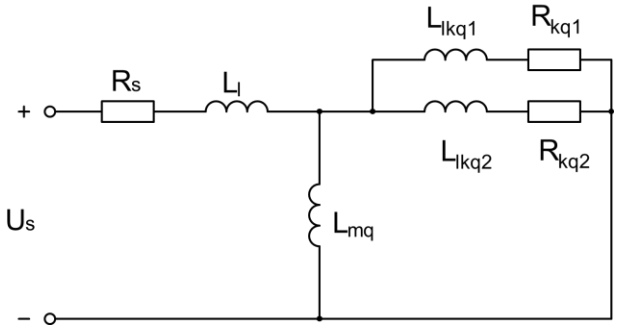

Figure 7 q-axis equivalent diagram

$$u_{kq1} = 0 = R_{kq1} \cdot i_{kq1} + \frac{d\Psi_{kq1}}{dt} \tag{2.22}$$

$$u_{kq2} = 0 = R_{kq2} \cdot i_{kq2} + \frac{d\Psi_{kq2}}{dt} \tag{2.23}$$

2.2 Derivation of flux equations

The derivations of equations in the following chapter are based on source [3]. Generally, the coupled flux is defined as:

$$L = \frac{N\Phi}{I} = \frac{\Psi}{I} \longrightarrow \Psi = L \cdot I \tag{2.24}$$

The fluxes that occur in a synchronous machine are illustrated in figure 8.

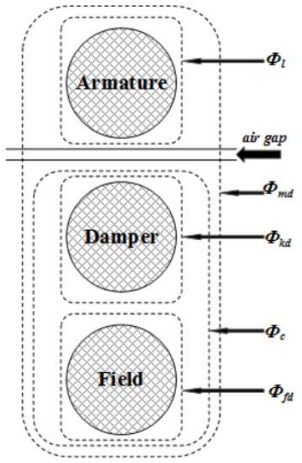

Figure 8 Magnetic fluxes illustration [4]

Where ϕ_l is leakage flux of stator winding, ϕ_{kd} is leakage flux of damper winding, ϕ_{fd} is leakage flux of damper winding, ϕ_m is mutual flux and ϕ_c is marked as Canay leakage flux, which represents the link between field and damper winding. In many studies it is used as correction element [4]. The Canay inductance is not specified by the manufacturer, thus it is neglected.

The equivalent schematic diagrams are again different for the d-axis and for the q-axis.

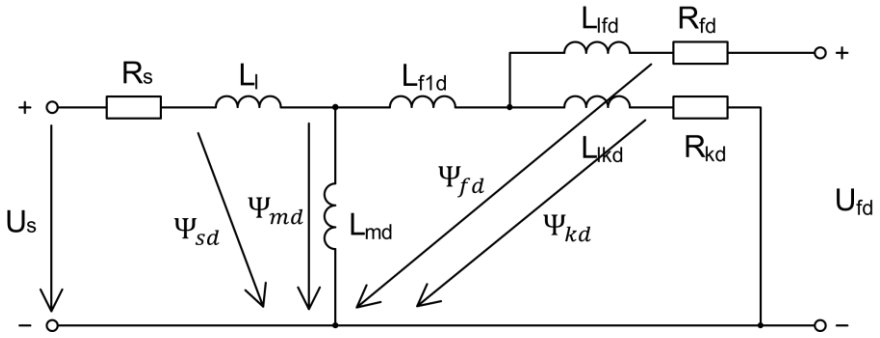

Figure 9 d-axis equivalent diagram with the fluxes

From the equivalent schematic diagram, the coupled fluxes Ψ_{sd}, Ψ_{md}, Ψ_{fd}, Ψ_{kd} can be determined as:

$$\Psi_{md} = L_{md}(-i_{sd} + i_{kd} + i_{fd}) \tag{2.25}$$

i_{sd} is negative when respecting the generator mode (reversed current polarity). All three currents contribute to the mutual flux. The other coupled fluxes are always sum of mutual flux and single leakage fluxes. The induction L_{f1} represents the coupled flux between damper and field, which is called Canay inductance.

$$\Psi_{sd} = L_{md}(-i_{sd} + i_{kd} + i_{fd}) + L_l(-i_{sd}) \tag{2.26}$$

$$\Psi_{kd} = L_{md}(-i_{sd} + i_{kd} + i_{fd}) + L_{f1d}(i_{kd} + i_{fd}) + L_{lkd}i_{kd} \tag{2.27}$$

$$\Psi_{fd} = L_{md}\left(-i_{sd} + i_{kd} + i_{fd}\right) + L_{f1d}\left(i_{kd} + i_{fd}\right) + L_{lfd}i_{fd} \tag{2.28}$$

The field winding operates only in the d-axis, thus an equivalent diagram for the q-axis is constructed with only the damper winding. Consequently, the Canay inductance does not feature in the equations.

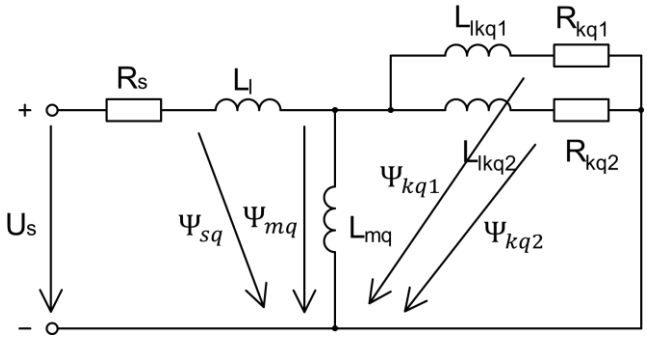

Figure 10 q-axis equivalent diagram with the fluxes

$$\Psi_{mq} = L_{mq}(-i_{sq} + i_{kq1} + i_{kq2}) \tag{2.29}$$

$$\Psi_{sq} = L_{mq}\left(-i_{sq} + i_{kq1} + i_{kq2}\right) + L_{l}\left(-i_{sq}\right) \tag{2.30}$$

$$\Psi_{kq1} = L_{mq}\left(-i_{sq} + i_{kq1} + i_{kq2}\right) + L_{lkq1}i_{kq1} \tag{2.31}$$

$$\Psi_{kq2} = L_{mq}\left(-i_{sq} + i_{kq1} + i_{kq2}\right) + L_{lkq2}i_{kq2} \tag{2.32}$$

The model accounts for parasitic phase-to-ground capacitances with values taken from Table 1 via a Three-phase RLC branch.

2.3 Standard parameters

The producer of the generator is unable to measure Fundamental parameters; these are theoretical values describing the machine's equivalent circuit. Practically, only Standard parameters from machine transients can be measured. The measured parameters of the machine are summarized in the following table.

Table 1 Datasheet of the manufactured generator

Load point				Load point A	
Apparent Power (MVA)				74.12	
Active Power (MW)				63	
Cold Air Temp. (°C)				45	
Colling Water Temp. (°C)				40	
Voltage (kV)				15	
Voltage deviation (-)				0.05	
Armature curent (kA)				2.853	
Reactances (tolerance 15%)	X_d" (%)	unsat.	sat.	17.7	14.3
	X_d' (%)	unsat.	sat.	24.9	22.4
	X_d (%)	unsat.	sat.	189	170
	X_q" (%)	unsat.	sat.	19.4	15.7
	X_q' (%)	unsat.	sat.	45.4	41.1
	X_q (%)	unsat.	sat.	179	152
	X_2 (%)	unsat.	sat.	18.5	15.0
	X_0 (%)	unsat.		8.8	
	X_{leak} (%)	unsat.		13.9	
Time constant at winding temp. 95 °C	T_d" (s)			0.029	
	T_d' (s)			0.832	
	T_{d0}' (s)			6.801	
	T_{d0}" (s)			0.042	
	T_q" (s)			0.071	
	T_q' (s)			0.518	
	T_{q0}' (s)			2.500	
	T_{q0}" (s)			0.150	
	T_a (s)			0.218	
Resistance at 20 °C (mΩ)	Stator winding / Phase			4.76	
	Rotor winding			104.37	
Capacities at 20 °C (uF)	Stator winding / Phase			0.288	
	Rotor winding			0.139	
Voltage regulation (%)	PF = rated			31.5	
	PF = 1.00			24.8	
Winding temp rise (K) (Winding temperature (°C))		Stator (RTD)		68 (113)	
		Rotor (avarage)		61 (106)	
Total losses (kW)				927	

The producer measures the transient and sub-transient time constants under short-circuit and open-circuit conditions with related reactance, then the leakage inductance is also relevant for recalculating the parameters. The equations (2.17 – 2.32) defining the model of the synchronous machine operate with the fundamental machine parameters. These fundamental parameters must be determined from standard values.

2.3.1 Parameters conversion

Transient (T_d') and sub-transient (T_d'') time constant and related reactance are determined, for example, by measuring sudden short circuits at the machine terminals. The short circuit at the machine terminals is kept to steady state to ensure clear determination of values.

Open-circuit time constants such as T_{d0}'' and T_{d0}' can be calculated from armature open-circuit tests, such as: load rejection, voltage recovery and field short circuit with armatures in open circuit [5].

The transient effect of the stator current caused by disturbance can be derived from the Theorem of constant flux, which asserts that the magnetic energy can't change instantly [3]. At the time of disturbance t_0, the flux change in the rotor winding is zero $\frac{d\Psi}{dt} = 0$, this is depicted in the following figure.

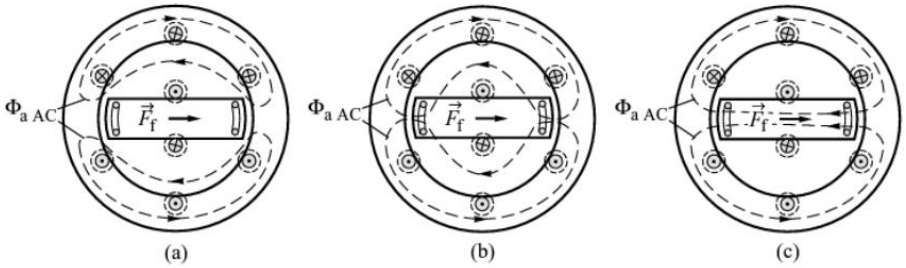

Figure 11 a) Sub-transient flux, b) Transient flux, c) Steady-state flux (d-axis) [6]

The main flux, sometimes referred to as mutual or magnetizing flux, flows in the non-failure state from the stator through the air gap to the rotor and back. During a sudden short circuit, a portion of the main flux still flows through the rotor circuit. The stator current to rapidly increase due to the short circuit at the generator terminals.

The increased current causes an increased flux on the stator side, which according to constant-flux theorem cannot close across the rotor windings, as indicated in Figure 11 a). Therefore, this part of flux closes through the air gap with high magnetic resistance and causes high amplitude of transient currents.

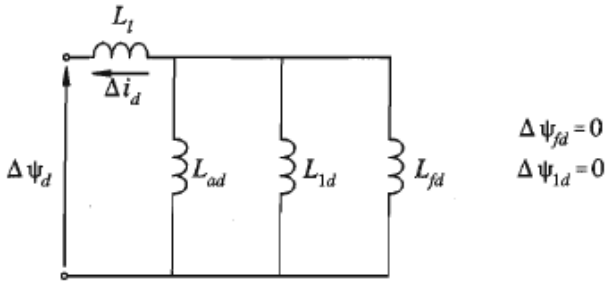

Figure 12 Flux deviation in the equivalent circuit [3]

This effect can be imagined in the following figure, where we assume a change in Δi_d and associated with change in $\Delta\Psi_\mathrm{d}$. At time t_0, the change in rotor fluxes remains zero [3].

$$L_d'' = \frac{d\Psi_\mathrm{d}}{di_d} \tag{2.33}$$

With the assumption of zero resistance in the field winding and damper winding, the short-circuit current level after a fault would remain constant.

$$i = k \cdot e^{-\frac{R}{L}t} + i_\infty \tag{2.34}$$

The general transient equation of an ordinary series RL circuit with zero resistance or infinite inductance leads to a state of constant current after a fault. However, with finite resistance in the rotor windings, the field current increases, following an exponential curve with the winding time constant τ, to a new steady-state current value:

$$\tau = \frac{L}{R} \tag{2.35}$$

As the current in a particular rotor winding increases, the flux of that winding also increases, causing the portion closing across the air gap to begin decreasing. The damper has generally much larger resistance than the field, therefore after the decay of the transient in the damper there is still decay of the transient in the field [3]. That is why we identify two time constants.

2.3.2 Inductance calculations

The sub-transient time constant, T_d'', is much shorter than the transient constant, T_d'. Within defined time intervals, it is possible to construct equivalent circuits determining the sub-transient inductance, L_d'', and the transient inductance, L_d', which correspond to the behaviour of the transients [3].

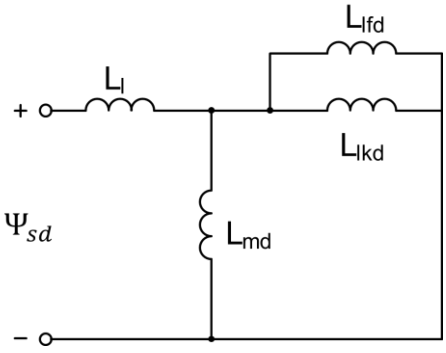

Figure 13 Equivalent circuit for Ld''

Figure 11 b) represents the transient flux corresponds to Ld'. At the transient state, the flux passes through the damper winding, but does not yet pass through the field. The flux is forced to complete its circuit through an air gap.

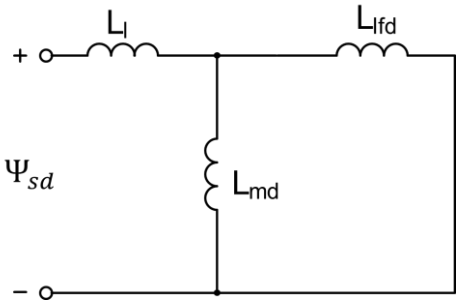

Figure 14 Equivalent circuit for Ld'

The value of the inductance Ld is obtained by series connection of the stator leakage inductance and the mutual inductance, the machine is in steady state.

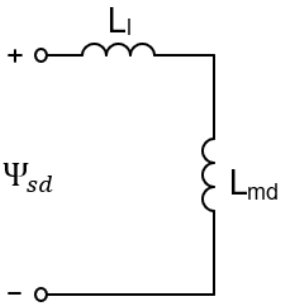

Figure 15 Equivalent circuit for Ld

Based on these alternative schematic diagrams, the equations for inductance are derived:

$$L_d'' = L_l + \frac{1}{\frac{1}{L_{md}} + \frac{1}{L_{lfd}} + \frac{1}{L_{lkd}}} \tag{2.36}$$

$$L'_d = L_l + \frac{1}{\frac{1}{L_{md}} + \frac{1}{L_{lfd}}} \tag{2.37}$$

$$L_d = L_l + L_{md} \tag{2.38}$$

Similar considerations are possible for a sub-transient and transient interval in the quadrature direction of the rotor.

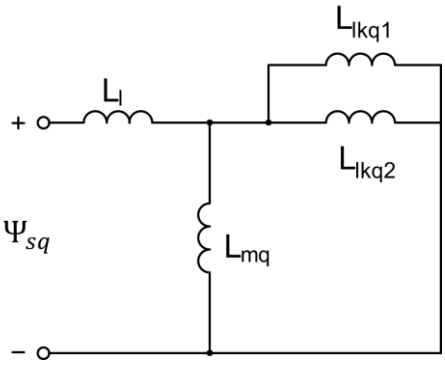

Figure 16 Equivalent circuit for Lq''

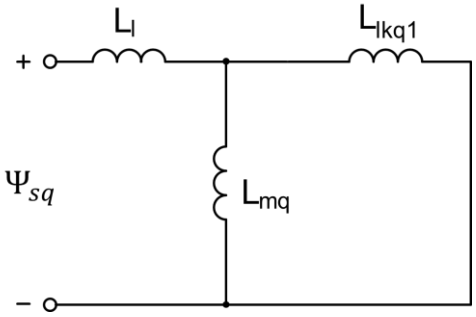

Figure 17 Equivalent circuit for Lq'

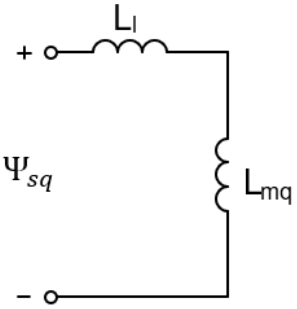

Figure 18 Equivalent circuit for Lq

Analogous equations are also applied:

$$L''_q = L_l + \frac{1}{\frac{1}{L_{mq}} + \frac{1}{L_{lkq1}} + \frac{1}{L_{lkq2}}} \tag{2.39}$$

$$L'_q = L_l + \frac{1}{\frac{1}{L_{mq}} + \frac{1}{L_{lkq1}}} \tag{2.40}$$

$$L_q = L_l + L_{mq} \tag{2.41}$$

From these equations, the unknown mutual inductances are expressed:

$$L_{md} = L_d - L_l \tag{2.42}$$

$$L_{mq} = L_q - L_l \tag{2.43}$$

By adjusting equations (2.37) we get L_{lfd}.

$$\begin{aligned} L'_d - L_l = \frac{1}{\frac{1}{L_{md}} + \frac{1}{L_{lfd}}} \longrightarrow \frac{1}{L'_d - L_l} = \frac{1}{L_{md}} + \frac{1}{L_{lfd}} \longrightarrow \frac{1}{L_{lfd}} \\ = \frac{1}{L'_d - L_l} - \frac{1}{L_{md}} \longrightarrow L_{lfd} = \frac{1}{\frac{L_{md} - (L'_d - L_l)}{(L'_d - L_l)L_{md}}} \\ = L_{md}\frac{L'_d - L_l}{L_{md} - L'_d + L_l} = L_{md}\frac{L'_d - L_l}{L_d - L'_d} \end{aligned} \tag{2.44}$$

L_{kq1} is determined by the same procedure from equation (2.40).

$$L_{kq1} = L_{mq}\frac{(L'_q - L_l)}{L_q - L'_q} \tag{2.45}$$

By adjusting equations (2.36) we get L_{kd}.

$$\begin{aligned} L''_d - L_l = \frac{1}{\frac{1}{L_{md}} + \frac{1}{L_{lfd}} + \frac{1}{L_{lkd}}} \longrightarrow \frac{1}{L''_d - L_l} = \frac{1}{L_{md}} + \frac{1}{L_{lfd}} + \frac{1}{L_{lkd}} \\ \longrightarrow \frac{1}{L''_d - L_l} = \frac{1}{L_d{}' - L_l} + \frac{1}{L_{lkd}} \longrightarrow L_{lkd} \\ = \frac{1}{\frac{1}{L''_d - L_l} - \frac{1}{L_d{}' - L_l}} = \frac{1}{\frac{(L'_d - L_l) - (L''_d - L_l)}{(L''_d - L_l)(L_d{}' - L_l)}} \\ = \frac{(L''_d - L_l)(L_d{}' - L_l)}{(L'_d - L''_d)} \end{aligned} \tag{2.46}$$

L_{kq2} is determined by the same procedure from equation (2.39).

$$L_{lkq2} = \frac{(L''_q - L_l)(L_q{}' - L_l)}{(L'_q - L''_q)} \tag{2.47}$$

2.3.3 Resistance calculations

As previously mentioned, the short-circuit sub-transient time T_d'' constant represents the shorter time interval. The damping of the transient event is caused by the large resistance of the damper winding [3]. The general equivalent diagram during the sub-transient interval is shown in figure 19.

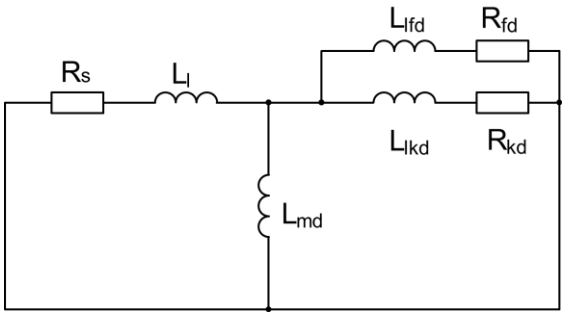

Figure 19 General short-circuited diagram for the sub-transient interval

At this moment, it is important not to overlook that the time constant interval T_d' begins at the time of the disturbance t_0! Thus, during the time interval T_d'', both the damper winding and the field winding acts to damp the current. This results in a slight distortion of the derived time constant of the particular RL circuit from the measured time constant. With this negligible error, according to [3], standard calculations are performed. For a more precise determination of the time constants, I recommend referring to [3].

So, let's assume that for the time interval T_d'', the dominant resistance is R_{kd}.

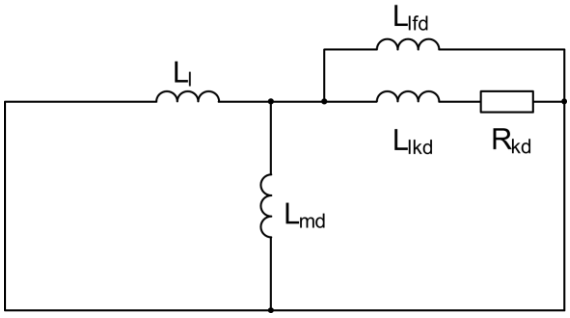

Figure 20 Simplified short-circuited diagram for the sub-transient interval (Td'')

A similar simplified schematic diagram can also be applied to T_{d0}'', which represents the open-circuit time constant. See Figure 21.

The time constant of the equivalent circuit from Figure 20 is illustrated by the following equation.

$$T_d'' = \frac{L_{lkd} + \frac{1}{\frac{1}{L_l} + \frac{1}{L_{md}} + \frac{1}{L_{lfd}}}}{R_{lkd}} \tag{2.48}$$

The value of the time constant thus is defined in pu units (radians), because resistance and inductances are in pu, therefore the constant has to be divide by rated angular frequency ($\omega_0 = 2\pi f_0$) [3]. Similar consideration and calculation is applied to constants T_{d0}'', T_d',T_{d0}', for which equivalent diagrams are provided in the following section.

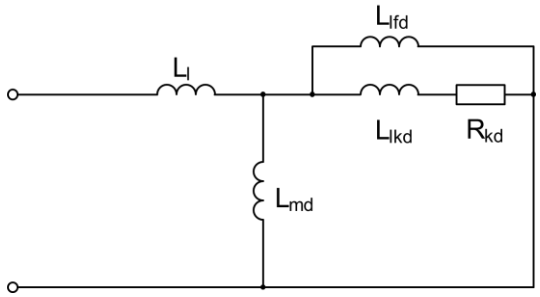

Figure 21 Simplified open-circuited diagram for the sub-transient interval (Td0'')

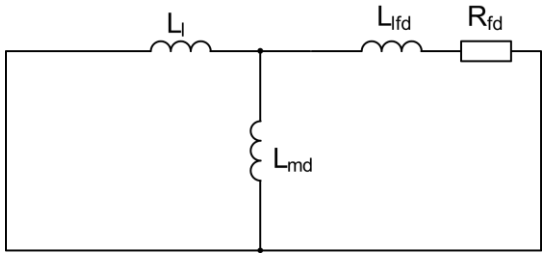

Figure 22 Simplified short-circuited diagram for the transient interval (Td')

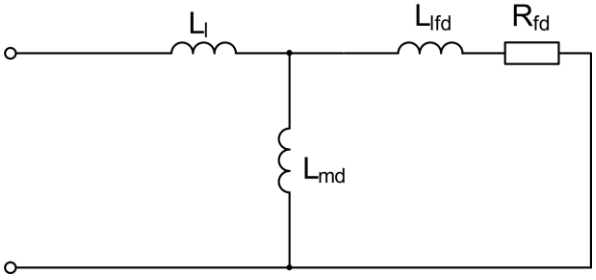

Figure 23 Simplified open-circuited diagram for the sub-transient interval (Td0')

These equations can be used to determine the individual winding resistances, which are the input parameters to the machine model. The following equations show that resistances can be calculated in two different ways (with T_d or T_{d0}).

$$R_{kd} = \frac{L_{lkd} + \frac{1}{\frac{1}{L_l} + \frac{1}{L_{md}} + \frac{1}{L_{lfd}}}}{T_d'' \cdot 2\pi f_0} \tag{2.49}$$

$$R_{fd} = \frac{L_{lfd} + \frac{1}{\frac{1}{L_l} + \frac{1}{L_{md}}}}{T_d' \cdot 2\pi f_0} \tag{2.50}$$

$$R_{kd} = \frac{L_{lkd} + \frac{1}{\frac{1}{L_{lfd}} + \frac{1}{L_{md}}}}{T_{d0}'' \cdot 2\pi f_0} \tag{2.51}$$

$$R_{fd} = \frac{L_{lfd} + L_{md}}{T_{d0}' \cdot 2\pi f_0} \tag{2.52}$$

For the q-axis components of the resistances, the deductions and calculations are the same.

$$R_{kq2} = \frac{L_{lkq2} + \frac{1}{\frac{1}{L_l} + \frac{1}{L_{mq}} + \frac{1}{L_{lkq1}}}}{T_q'' \cdot 2\pi f_0} \tag{2.53}$$

$$R_{kq1} = \frac{L_{lkq1} + \frac{1}{\frac{1}{L_l} + \frac{1}{L_{mq}}}}{T_q' \cdot 2\pi f_0} \tag{2.54}$$

$$R_{kq2} = \frac{L_{lkq2} + \frac{1}{\frac{1}{L_{lkq1}} + \frac{1}{L_{mq}}}}{T_{q0}'' \cdot 2\pi f_0} \tag{2.55}$$

$$R_{kq1} = \frac{L_{lkq1} + L_{mq}}{T_{q0}' \cdot 2\pi f_0} \tag{2.56}$$

The reactances listed in Table 1 can be swapped for inductances because the inductance per unit is equal to the reactance per unit, as indicated by equation (2.57).

$$L\ (p.u.) = \frac{L\ (\mathrm{H})}{L_{base}\ (H)} = \frac{X/\omega}{Z_{base}/\omega} = \frac{X}{Z_{base}} = X\ (p.u.) \tag{2.57}$$

2.4 Synchronous Machine pu Fundamental block – Phasor solution

As I mentioned before, the models operate with a phasor solver. The space voltage vector is not determined from instantaneous values; therefore, Clark's transformation is not used. Instead, the space voltage vector is determined from phasors using the positive sequence calculation.

$$\bar{V} = \frac{1}{3}(\bar{V}_a + \bar{V}_b \cdot \bar{a} + \bar{V}_c \cdot \bar{a}^2) \\ = \frac{1}{3}\left(V \cdot e^{j0^\circ} + V \cdot e^{-j120^\circ} \cdot e^{+j120^\circ} + V \cdot e^{-j240^\circ} \cdot e^{+j240^\circ}\right) \tag{2.58}$$

It is clearly illustrated in the following Figure:

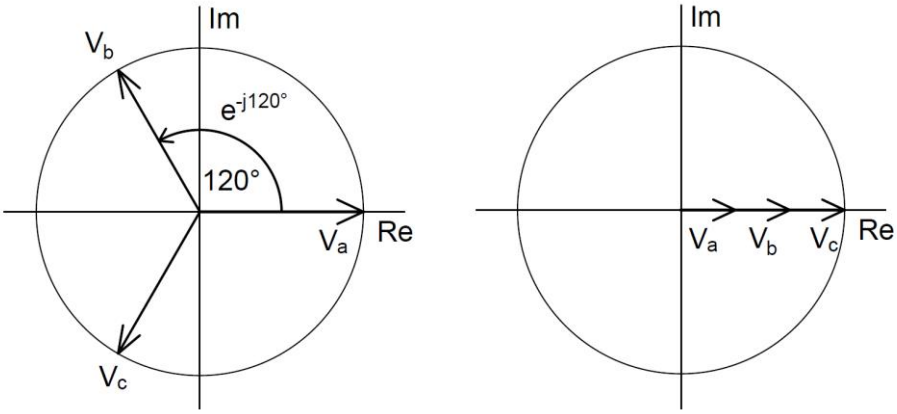

Figure 24 a) Phasors b) Positive sequence illustration

The dq system is related to the position of the rotor (equal to the position of the rotor flux) of a synchronous machine. For phasor solution, it is necessary to determine relative position rotor flux phasor and stator flux phasor. This is accomplished by employing a mechanical model that determines the deviation in rotational speed. By integrating this speed deviation, the deviation angle (rotor angle) is subsequently established. So, the phasor of the stator voltage is recalculated to the dq coordinate system.

The stator voltage phases are simultaneously shifted in relation to the ideal grid source mainly due to the star-delta transformer connection, detailed in the chapter Grid.

3 Excitation

3.1 Description

In the simulation, AC7B excitation is used, which includes brushless excitation consisting of a permanent magnet pilot exciter, an alternating exciter and rotating diode rectifier

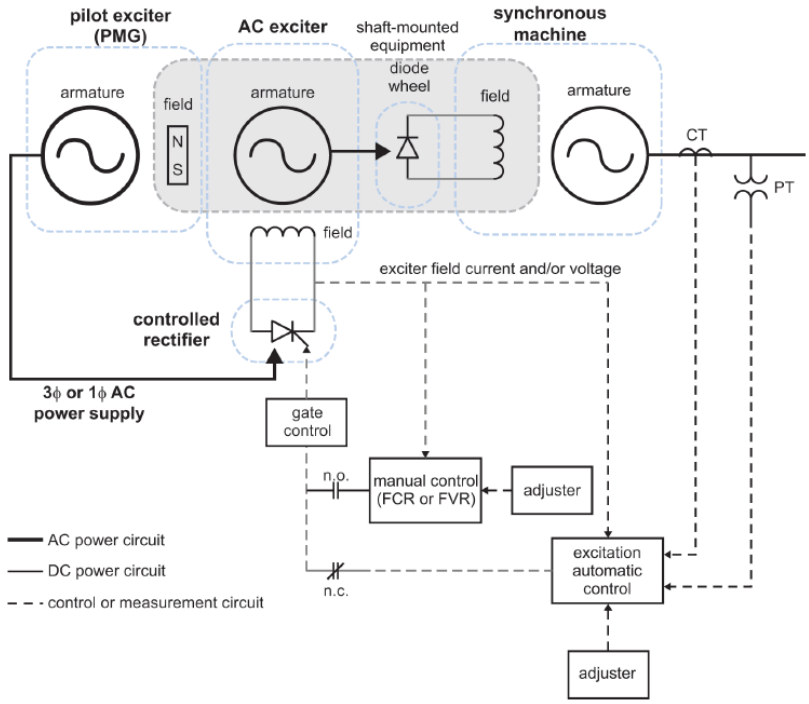

Figure 25 Brushless excitation system AC7B [7]

Rotating pilot exciter generates AC power to its armature, which is then rectified to DC power in a controlled manner. The magnitude of the rectified current entering to the main exciter's stator is regulated by Automatic Voltage Regulation (AVR) system. AVR adjusts the voltage level of the main exciter field to reach required level of the exciter filed current. Due to rotation, the armature of the main exciter induces AC voltage, which is then rectified by a rotating diode rectifier. Consequently, a DC current enters to the field of the synchronous machine.

The advantage of this type of excitation system is that there is no need for brushes and rings to transmit power. The frequent replacement of brushes with new ones is eliminated and allows the rotating system to operate continuously for much longer periods.

Both the auxiliary and main exciters are deliberately manufactured as multipole three-phase. This results in a higher frequency of induced AC voltage in the exciter's armature, which positively impacts the ripple of the subsequently rectified current.

3.2 Exciter model

The (main) exciter model is based on standard Std 421.5.

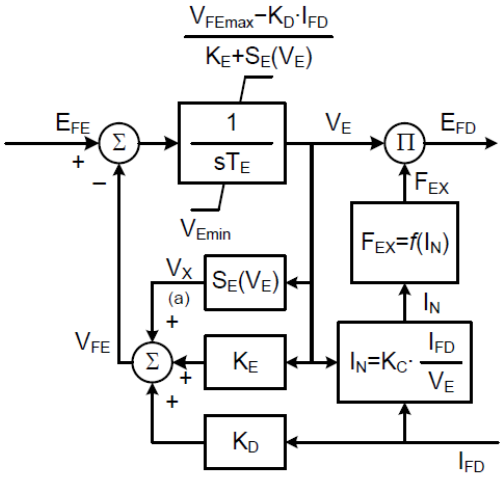

Figure 26 Model of the exciter [8]

Summary of variables and parameters:

E_{FE} – voltage of exciter stator, adjusted by controllers.

V_E – unrectified voltage induced into the rotor of the exciter.

$S_E(V_E)$ – respecting the exciter's magnetic circuit saturation.

K_E – excitation field constant is typically equal to 1 for AC exciters, while a different value may be applied in a self-excited DC exciters.

K_D – demagnetization constant respecting effects caused by the exciter load depending on the magnitude of I_{FD}.

Fex – considers the energy loss due to the load on the uncontrolled rotating rectifier, the calculation is derived from the rectifier loading current.

K_C – the constant respecting the commutation reactance of the rectifier.

E_{FD} (also referred to as V_F) – field voltage of generator.

I_{FD} (also referred to as I_F) – field current of generator.

T_E – time constant of exciter

3.3 Calculations

3.3.1 Constant respecting the commutation reactance

It is based on the Fex load characteristic according to the calculated load current I_N. The function Fex respects the voltage drop at the rectifier.

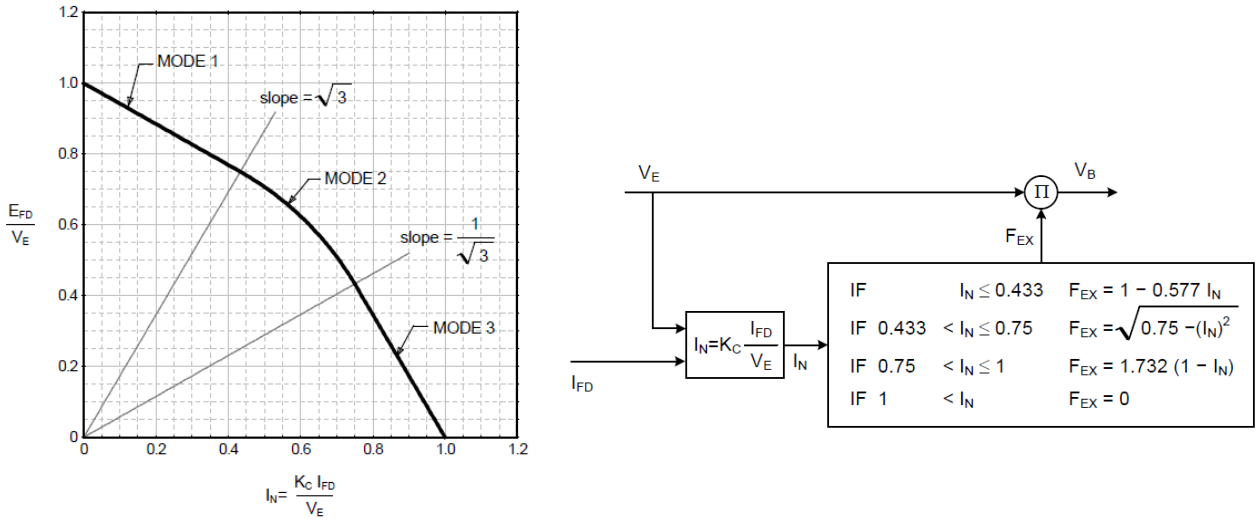

Figure 27 Function respecting the voltage drop at the rectifier (F_{EX}) [8]

The model performs Fex calculations according to Figure 6 for time-variable simulation. However, the coefficients in this section are derived from the nominal excited state based on calculations referenced in source [9].

The load current is determined by the formula:

$$I_N = K_c \cdot \frac{I_{fd}}{V_E} \tag{3.01}$$

For an uncontrolled three-phase bridge rectifier, equation (3.02) is used to calculate K_c [9]:

$$K_c = \frac{3 \cdot \sqrt{3}}{\pi} \frac{X''_{de} + X_{2e}}{2} \frac{1}{R_f} \frac{V_{FN}^2}{S_N} \tag{3.02}$$

X''_{de} and X_{2e} are sub-transient and negative sequence reactance of the main exciter. S_N is a nominal power of the main exciter and is derived from the nominal current and voltage ($S_N = I_{fN} \cdot V_{fN}$). R_L is the resistance of the circuit powered by the exciter, typically the resistance of the generator field winding. Therefore, the calculation of the load resistance is performed as follows: $R_f = \frac{V_{fN}}{I_{fN}}$. This resistance is also provided by the generator manufacturer.

For nominal values, equation (3.02) can be simplified to:

$$K_c = \frac{3 \cdot \sqrt{3}}{\pi} \frac{X''_{de} + X_{2e}}{2} \tag{3.03}$$

I_N calculation

If $I_N \leq 0.433$:

$$Fex = 1 - 0.577 I_N = 1 - \frac{1}{\sqrt{3}} I_N \Longrightarrow I_N = (1 - Fex)\sqrt{3} \tag{3.04}$$

$$I_N = K_c \cdot \frac{I_{fd}}{V_E} \Longrightarrow K_c = I_N \cdot \frac{V_E}{I_{FD}} \tag{3.05}$$

By substituting equation (3.04) into equation (3.05), we obtain the equation:

$$K_c = I_N \cdot \frac{V_E}{I_{FD}} = (1 - Fex)\sqrt{3} \cdot \frac{V_E}{I_{FD}} \tag{3.06}$$

Furthermore, from Figure 26, it is evident that the output voltage of the exciter V_E is the induced voltage into the exciter rotor. The voltage decreased by the rectifier voltage drop E_{FD} corresponds to the voltage of generator field.

$$Fex \cdot V_E = E_{FD} \tag{3.07}$$

Due to the fact that the energy source primarily has an internal impedance of an inductive nature, it causes a nonlinear voltage drop during commutation depending on the load current. [8] (see Figure 27).

The constant K_c is typically calculated from the rated steady-state values, where the following is valid:

$$I_{fd}(p.u.) = E_{fd}\ (p.u.) \tag{3.08}$$

The per unit values are detailed describe at following chapter.

These assumptions allow us to simplify equation (3.06):

$$\begin{aligned} K_c = (1 - Fex)\sqrt{3} \cdot \frac{V_E}{I_{fd}} &= \sqrt{3} \cdot \frac{V_E}{I_{fd}} - \sqrt{3} \cdot \frac{V_E}{I_{fd}} \cdot Fex = \sqrt{3} \cdot \frac{V_E}{I_{fd}} - \sqrt{3} \frac{E_{FD}}{I_{fd}} \\ &= \sqrt{3} \cdot \frac{V_E}{I_{fd}} - \sqrt{3} = \sqrt{3}\left(\frac{V_E}{I_{fd}} - 1\right) \\ \Longrightarrow \frac{V_E}{I_{fd}} &= \frac{K_c + \sqrt{3}}{\sqrt{3}} = \frac{K_c}{\sqrt{3}} + 1 = \frac{3}{\pi} \cdot \frac{X''_{de} + X_{2e}}{2} + 1 \end{aligned} \tag{3.09}$$

In its final form, it is thus possible to directly estimate the ratio $\frac{V_E}{I_{fd}}$ from the transient excitation reactance X''_{de} and the negative sequence reactance X_{2e}.of the exciter.

As a final step, I_N is directly expressed from the exciter parameters for subsequent substitution into Fex. The computed values are summed in the Table 4.

$$I_N = K_c \cdot \frac{I_{fd}}{V_E} = \frac{\frac{3 \cdot \sqrt{3}}{\pi} \frac{X''_{de} + X_{2e}}{2}}{\frac{3}{\pi} \frac{X''_{de} + X_{2e}}{2} + 1} \tag{3.10}$$

Based on the resulting I_N, a region is selected to determine the calculation of the Fex

3.3.2 Demagnetization coefficient

The derivation of the calculation of the factor K_D is based on the equation [9]:

$$K_D = \frac{I_{fe\ LOAD}}{I_{fe\ OC}} - 1 - \frac{K_c}{\sqrt{3}} \tag{3.11}$$

Where $I_{FE\ LOAD}$ is equal to rated load of exciter, derived from the rated load of the generator. This refers to the current necessary to supply the generator field winding during nominal operation. I_{FE0} is the exciter current needed to excite the exciter for its open-circuit state, but $I_{FE\ OC}$ represents the excitation current needed to excite the generator field winding while the generator is open-circuited.

By substituting equation (3.09) into equation (3.11), we obtain formula:

$$K_D = \frac{I_{fe\ LOAD}}{I_{fe\ OC}} - \frac{V_E}{I_{fd}} \tag{3.12}$$

3.3.3 Calculation of coefficient values

Calculation of coefficient K_c:

$$K_c = \frac{3 \cdot \sqrt{3}}{\pi} \frac{X''_{de} + X_{2e}}{2} = \frac{3 \cdot \sqrt{3}}{\pi} \cdot 0.19 = 0.3143 \tag{3.13}$$

Calculation of load current:

$$I_N = \frac{\frac{3 \cdot \sqrt{3}}{\pi} \frac{X''_{de} + X_{2e}}{2}}{\frac{3}{\pi} \frac{X''_{de} + X_{2e}}{2} + 1} = 0.266\ (-) \tag{3.14}$$

The variable I_N belongs to sector 1, for which this equation was derived. No adjustment to the calculation is necessary. Furthermore, Fex for steady state is calculated as follows:

$$Fex = 1 - 0.577 I_N = 0.846\ (-) \tag{3.15}$$

Calculation of coefficient K_D:

$$K_D = \frac{I_{fe\ LOAD}}{I_{fe\ OC}} - \frac{V_E}{I_{fd}} = \frac{I_{fe\ LOAD}}{I_{fe\ OC}} - \frac{E_{fd}}{I_{fd}} \cdot \frac{1}{Fex} = \frac{13.3}{4.7} - \frac{1}{0.846} = 1.648 \tag{3.16}$$

$I_{fe\ OC} = 4.7$ A is determined from the rebuilt $I_{fe\ OC}/V_f$ characteristic corresponding to the characteristic provided by the excitation manufacturer, see Figure 28 b). E_{fd} is equal to I_{fd} in steady state.

Another approach for calculation is possible:

$$K_D = \frac{I_{fe\ LOAD}}{I_{fe\ OC}} - 1 - \frac{K_c}{\sqrt{3}} = \frac{13.3}{4.7} - 1 - \frac{0.3143}{\sqrt{3}} = 1.648 \tag{3.17}$$

3.3.4 Calculation of parameters in relative units

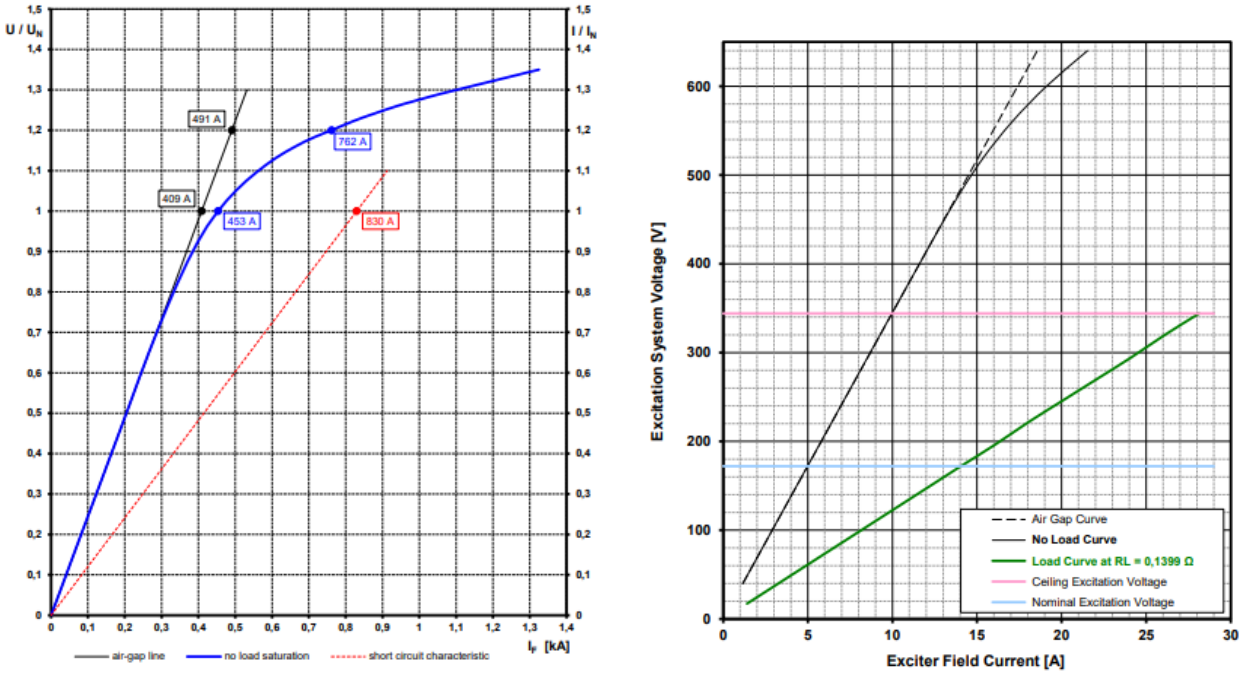

Figure 28 a) Generator characteristic, b) Exciter characteristic

These following excitation values are subtracted from the generator datasheet.

Table 2 Excitation values from datasheet

I_{fN}	1162	(A)	nominal current of generator field winding
I_{f0}	409	(A)	unsaturated open-circuited current of generator field winding
I_{feN}	13.3	(A)	nominal current of exciter field winding
V_{fn}	162	(V)	nominal voltage of generator field winding
V_{feN}	67.7	(V)	nominal voltage of exciter field winding

In the rated state, the resistance of the generator field winding R_f is given by V_{fN}/I_{fN}, where V_{fN} and I_{fN} are provided by the manufacturer. Alternatively, the field winding resistance is noted in the manufacturer's datasheet, where it is calculated in this manner.

The resistance of the generator field winding in the nominal state can be calculated as:

$$R_f = \frac{V_{fN}}{I_{fN}} = \frac{162}{1162} = 0.14\ \Omega \tag{3.18}$$

Thanks to knowing the unsaturated open-circuited current of the generator field winding, the equivalent voltage can be calculated as:

$$V_{f0} = I_{f0} \cdot R_f = 57,02\ V \tag{3.19}$$

The proportional units in this model define the relative load, for voltage applies:

$$\ddot{V}_f = \frac{V_{fN}}{V_{f0}} = \frac{162}{57.02} = 2.841\ (p.u.) \tag{3.20}$$

In a steady state, the relative value of voltage and current is equal, which is confirmed by the following calculations:

$$\ddot{V}_f = \ddot{I}_f \tag{3.21}$$

$$\ddot{I}_f = \frac{I_{fN}}{I_{f0}} = \frac{1162}{409} = 2.841\ (p.u.) \tag{3.22}$$

The resistance of the exciter (stator winding of the exciter) is computed in a similar manner.

$$R_e = \frac{V_{feN}}{I_{feN}} = \frac{67.7}{13.3} = 5.09\ \Omega \tag{3.23}$$

The relative exciter voltage can be calculated from the known values according to Figure 27.

$$\begin{aligned} \ddot{V_{fe}} &= K_E \cdot \ddot{V_E} + K_D \cdot \ddot{V}_f + saturation \\ &= K_E \cdot \frac{\ddot{V}_f}{FEX} + K_D \cdot \ddot{V}_f + saturation \\ &= 1 \cdot \frac{2.841}{0.846} + 1.648 \cdot 2.841 + 0.01 = 8.066\ (p.u.) \end{aligned} \tag{3.24}$$

Saturation is determined using a graphical-iterative method. The deviation of the saturated curve from the linear curve is reconstructed using Se [Ve].

Subsequently, it is possible to determine the current and voltage in the exciter's open-circuit state.

$$I_{fe0} = \frac{I_{feN}}{\ddot{V_{fe}}} = \frac{13.3}{8.066} = 1.649\ A \tag{3.25}$$

$$V_{fe0} = I_{fe0} \cdot R_E = 1.649 \cdot 5.09 = 8.393\ V \tag{3.26}$$

All calculated parameters are summarized in the following tables:

Table 3 Calculated significant excitation values

Parameter	Value	Unit	Description
Physical values			
I_{fN}	1162	(A)	nominal current of generator field winding
I_{f0}	409	(A)	unsaturated open-circuited current of generator field winding
V_{fn}	162	(V)	nominal voltage of generator field winding
V_{f0}	57.02	(V)	unsaturated open-circuited voltage of generator field winding
I_{feN}	13.3	(A)	nominal current of exciter field winding
$I_{fe\ OC}$	4.7	(A)	generator open-cicuit current of exciter field winding
I_{fe0}	1.649	(A)	exciter open-circuit current of exciter field winding
V_{feN}	67.7	(V)	nominal voltage of exciter field winding
V_{fe0}	8.3936	(V)	exciter open-circuit voltage of exciter field winding

R_f	0.1394	(Ω)	resistance of generator field winding
R_e (Ω)	5.0902	(Ω)	resistance of exciter field winding
Per unit values			
V_f	2.841	(p.u.)	rated voltage (or current) of generator field winding
V_E	3.357	(p.u.)	rated unrectified voltage of generator field winding
V_{fe}	8.066	(p.u.)	rated voltage (or current) of exciter field winding
V_{fem}	36.706	(p.u.)	maximum voltage of exciter field winding

Table 4 Parameters of excitation model

Ke	1	FEX	0.84643	X_{de}"	0.19
Kc	0.3143	In	0.266	X_{2e}	0.19
Kd	1.653	Ve/If	1.18144		

Se[VE]	VE (p.u.)	VE (V)	Se
Se [0.92]	11.8953	678.275	0.2
Se [0.68]	8.79214	501.334	0.01

3.4 AVR

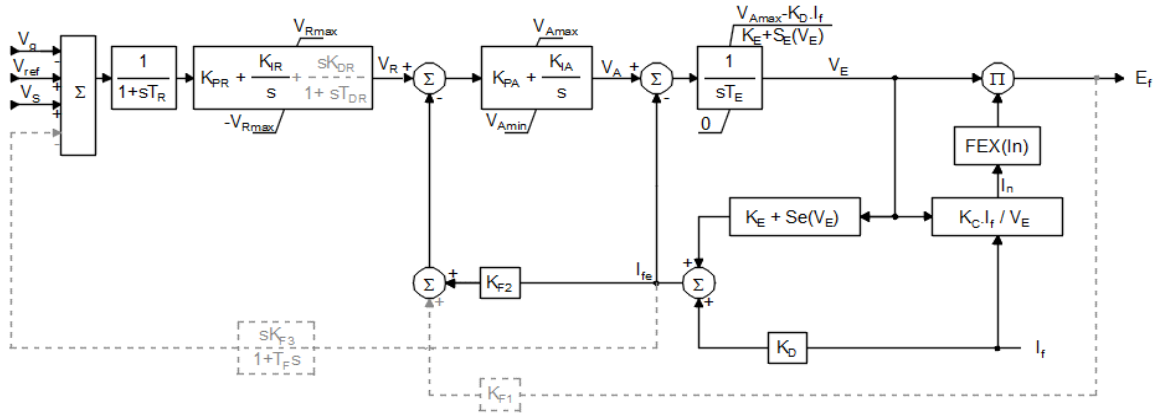

Figure 29 AVR of AC7B

The AC7B regulation of the alternator excitation is based on standard Std 421.5. Within the AC7B model, three potential feedback loops, PI and PID regulators are specified. The PID_R regulator controls the voltage at the generator terminals to match the reference voltage. The reference voltage can be adjusted using signal Vs from the Power System Stabilizer (PSS). The output from the PID_R sets the setpoint of the exciter field current. The PI_A controller is used to regulate measured field current normalized by the gain Kf2 to achieve the required (setpointed) field current value. The sufficient dynamic of exciter current loop, which has the derive character, allows the D component of PID_R controller to be omitted.

Additionally, other feedback loops (Kf1 and Kf3) are available for the AC7B excitation model, but they are not utilized in this case.

For practical purposes, the feedback signal used to control exciter current is commonly normalized from exciter per unit system to different per unit system that has rated exciter current as its base.

$$K_{f2} = \frac{1}{\ddot{V_{fe}}} = \frac{1}{8.066} = 0.124 \tag{3.27}$$

The main regulator is limited to 2 p.u., which is ceiling value of the exciter current in this case. The PI_A controller adjusts dynamic variations in the exciter field voltage to achieve a more dynamic regulation of the exciter field current. Therefore, it is limited only by the maximum available instantaneous voltage from the auxiliary PM exciter, denoted as the V_{fem} value.

The calibration of the regulators can be easily verified by applying a step change in the desired terminal voltage of the generator around its rated value. Typically, a step from 0.9 Un to 1.0 Un is used in accordance with C.7.8.3. of [1], as outlined in the Chapter 9.7. The overshoot during the change of the desired voltage at the generator terminals should not optionally exceed 10% in open-circuited generator. The tuned parameters of PID controllers are summarized in the following table:

Controller Parameters			
KPR	5	KIR	2.7
KPA	130	KIA	130
VRMAX	2	VRMIN	-2
VAMAX	34	VAMIN	-34

4 Turbine

The Registered Capacity in the Connection offer is 55 MW. However, the Power Generating Unit shall guarantee a value of 55.6 MW, as commissioned by the DNO (Distribution Network Operator). Furthermore, the DNO estimated the parasitic load (house load) for this Power Generating Unit to be around 5.5 MW.

It is based on the general model of a steam turbine IEEEG1, which can be divided into Governor and Turbine.

The IEEEG1 model respects all pressure levels that the turbine can have, from HP trough IP to LP. In the Rivenhall project the turbine is single casing, so only a high pressure part is used in the model; thus the other pressure levels are zero (K4=1, K5= 0, K6 = 0). The control of steam valves, which regulates the power input to the turbine, is simulated too. The valves are limited by the opening/closing speed U and the minimum/maximum valve opening relative to respective p.u. power G.

The standard IEEEG1 model does not include a power controller, because the constant output from load control is considered. The primary purpose of this model is to introduce frequency sensitive response to the shaft power. Therefore, it includes the simple Lead-lag block, which is often inactive and replaced the PI controller. PI controller is utilized for both load control and frequency sensitive response.

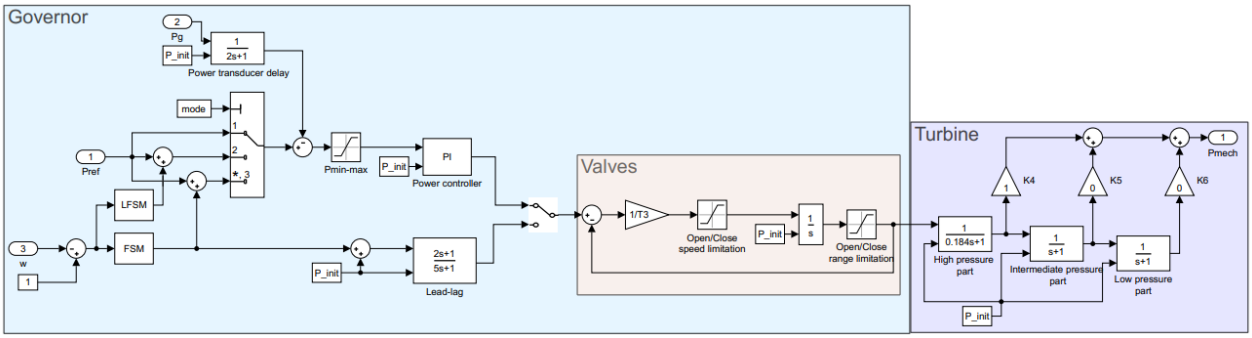

Figure 30 Simplified turbine model

4.1 Turbine model

The steam transport delay is represented by a time constant of an aperiodic transfer block. During the operation, the time constant is determined by swallowing capability of the turbine. We are interested in the highest time constant, which is related to sudden load changes. This time constant is determined by the thermal energy of steam spread within the turbine blades, steam chamber, and piping directly linked to the turbine. To determine this

amount of accumulated energy, it is necessary to know the partial volumes and partial specific energies. The energy is related to the reference power of the turbine.

$$\frac{Stored\ Energy\ (MJ)}{Ref\ Power\ (MW)} = time\ constant\ (s) \tag{4.01}$$

For an accurate result, I can consider the provided value of 0.184. The torque produced by steam flow through turbine causes the rotation of the turbine mass. The turbine shaft-mass moment transmitted through the flexible shaft connection to the generator mass is modelled in the Chapter 5.

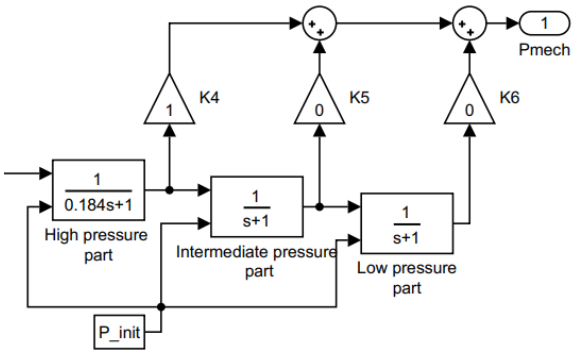

Figure 31 Turbine model

4.2 Valve model

The valve model is simulated using an aperiodic block with a time constant T3, as can be seen in Figure 31. Furthermore, it is limited by the mentioned opening/closing speed Umin/Umax and the minimum/maximum power of steam Gmin/Gmax.

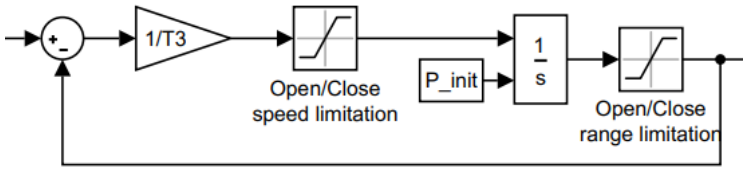

Figure 32 Valve model

4.3 Governor

The input to the controller is the deviation between the required power and actual power at the generator's output terminals. The feedback from the generator is filtered out by an aperiodic block with a time constant usually around 2 s. This long time constant is set to filter out the power variation caused by electrical transient, mainly local mode oscillation, and prevent interactions of turbine control and AVR and PSS. The reference signal may then be corrected, according to the FSM or LFSM mode, to keep the rotation frequency around the electrical 50 Hz.

The implemented PI controllers are based on the model from chapter 1.3. The tuning of the The tuning of the PI of the controllers is carried out by the response of the turbine torque to the speed step when the FSM is switched on.

The PI controllers tuning is performed as response to the injected speed step within FSM turn on. The torque of the turbine with an injected step of 0.2 Hz is depicted in Figure 22 in Capture 9.7. The tuned PI coefficients are summarized in Table 6.

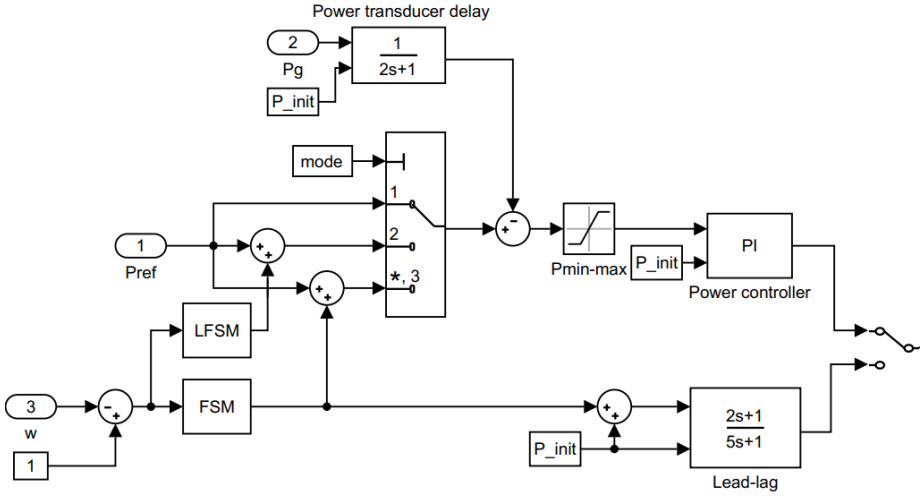

Figure 33 Simplified governor model

4.3.1 FSM

Frequency sensitive mode – the mode when the output power is corrected by frequency or by speed rotation of turbine. If the speed deviates from rated value, the power into turbine increase/decrease.

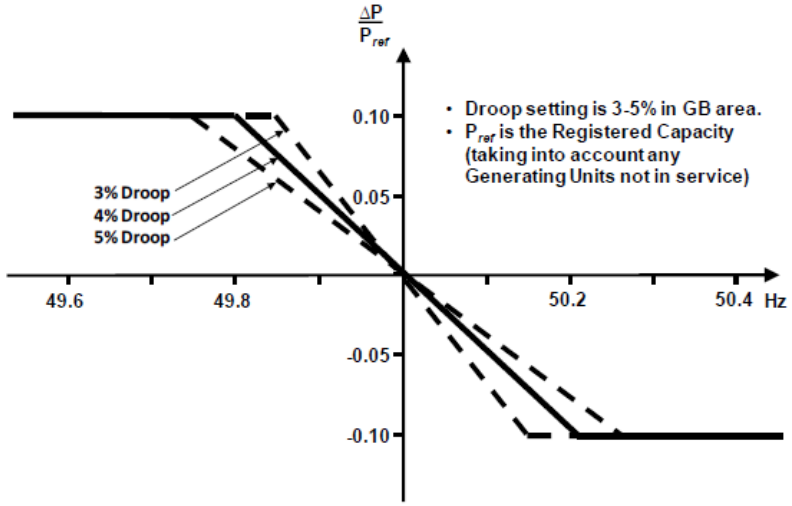

Figure 13.5 – Frequency Sensitive Mode capability of Power Generating Modules and Power Park Modules

Figure 34 Active power frequency response of FSM [1]

The active power response to the frequency deviation is depicted in the Figure 34. The sensitivity of power-proportional reaction determines the droop. Additionally, the power response is limited to 10% of the registered power for additional power.

Droop can be in range 3-5%, as shown the Figure 34. For this project 5% has been selected.

The general formula for calculating the droop is following:

$$droop = \frac{|\Delta f|}{f_N} \cdot \frac{P_{reg}}{|\Delta P|} \cdot 100 \tag{4.02}$$

Subsequently, the power response can be expressed as follows:

$$\Delta P_{FSM\ p.u.} = \Delta f_{p.u.} \cdot \frac{1}{\left(\frac{droop}{100}\right)} P_{reg\ p.u.} \tag{4.03}$$

Where P_{reg} is registered power capacity, i.e. output electric power to the grid minus the house load. Droop is set at 5%. The house load power of the power plant unit is unknown, but it is estimated on the base of similarity with power plants of similar capacity by DNO. The estimated house load 5.5 MW includes the anticipated step-up transformer losses 306 kW.

$$P_{gN} = \frac{61.1\ MW}{74.12\ MVA} = 0.8243\ p.u. \tag{4.04}$$

$$P_{regN} = P_{gN} - P_{HL} = 61.1 - 5.5 = 55.6\ MW \ldots \frac{55.6}{74.12} = 0.75\ p.u. \tag{4.05}$$

P_{gN} represents the nominal output power in per unit, while P_{regN} denotes the registered power in per unit of the power unit. P_{HL} represents the house load power including the step-up transformer power losses.

As already mentioned, FSM responds to a change in speed by adjusting the output power. This adjustment is implemented in the model by multiplying the output by $(P_{gN} - P_{HL})/S_N$ because the entire simulation utilizes per-unit values related to the nominal power of the generator.

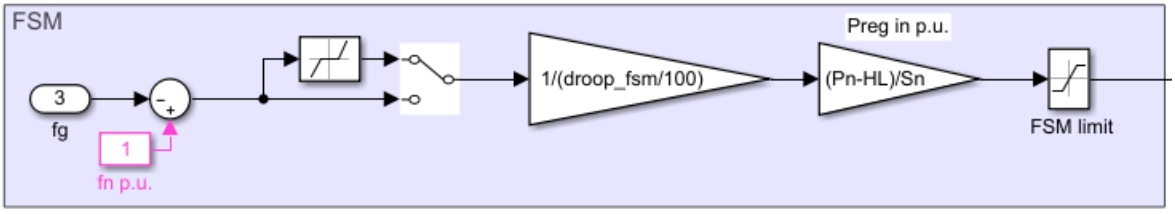

Figure 35 FSM implementation

The frequency response insensitivity according to [1] is set to 15 mHz.

The maximum limitation of the adjusted FSM power is defined according to Figure 34 as:

$$P_{regmax} = P_{regN} \cdot 0.1 = 0.75 \cdot 0.1 = 0.075\ p.u. \tag{4.06}$$

The maximum frequency deviation for which the FSM can provide power response until output saturation occurs can be evaluated as follows:

$$droop = \frac{f_{MAX}}{f_N} \cdot \frac{P_{reg}}{\Delta P_{FSM_{MAX}}} \rightarrow f_{MAX} = droop \cdot f_N \cdot \frac{\Delta P_{FSM_{MAX}}}{P_{reg}} = \frac{5}{100} \cdot 50 \cdot 0.1 = 0.25\ Hz \tag{4.07}$$

Due to the insensitivity of 0.015 Hz, the saturated power is corrected to a frequency of 0.265 Hz. The FSM is validated in the Chapter 9.

4.3.2 LFSM

Power output correction based on machine speed can be performed according to the mentioned FSM or the Limited Frequency Sensitive Mode, or a combination of both. Unlike FSM, LFSM must operate in much wider limits, practically from plant minimum stable load to its max. registered capacity., its purpose is to keep the system running during network disturbances. If the frequency exceeds the threshold of 50.4 Hz, the LFSM control adjusts the load setpoint to make it lower by closing the control valves (referred to as LFSM-O). Analogically, when the frequency drops below 49.5 Hz, the controller responds by increasing turbine load. This mode is referred to as LFSM-U.

The application of the LFSM-U shall consider the availability of all primary sources because the single generating unit may not currently have higher available power. The available power depends on the reserved power at the boiler. It is not anticipated that Power Generating Units operate in an inefficient mode, but rather they frequently operate in constant pressure mode. This means that the Power Generating Units work at max. available load while keeping a constant pressure at the boiler.

During energy-efficient operation, the boiler does not reserve any power in advance. All the steam produced goes into the turbine, so the boiler control determines the actual output of the turbine. The turbine is responsible for keeping the steam pressure at a stable value, ensuring safe operation of the boiler.

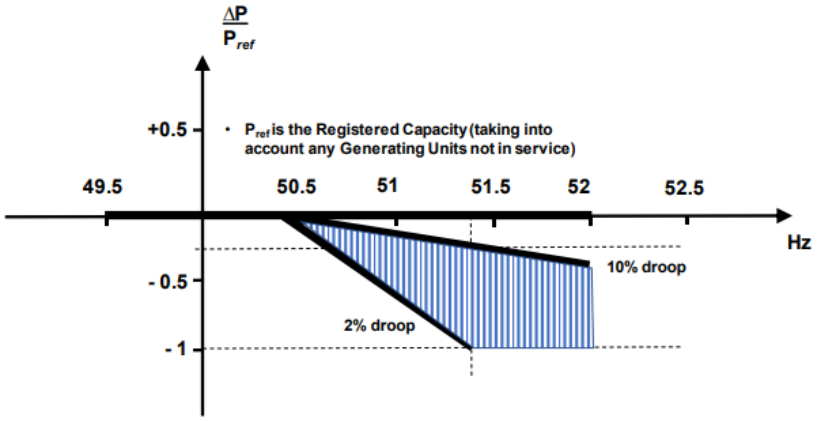

Figure 36 Active power frequency response of LFSM [1]

LFSM droop is set in the same way as FSM droop (5%). The other properties and settings are summarized in the Chapter 9.

4.4 Turbine Parameters

Table 5 Turbine parameters

Parameter	Value	Unit	Description
Turbine parameters			
T4	0.184	s	Time constant of the inlet piping/steam bowl (HP turbine)
T5	0	s	Time constant of second boiler pass (IP turbine)
T6	0	s	Time constant of third boiler pass (LP turbine)
K4	1	p.u.	Fraction of shaft power after first boiler pass
K5	0	p.u.	Fraction of shaft power after second boiler pass
K6	0	p.u.	Fraction of shaft power after third boiler pass
Valve parameters			
T3	0.035	s	Valve positioner time constant
U_{MIN}	0.7	p.u.	Maximum valve closing velocity
U_{MAX}	-0.7	p.u.	Maximum valve opening velocity
G_{min}	0	p.u.	Maximum valve closing
G_{MAX}	0.9	p.u.	Maximum valve opening
Controller parameters			
Kp	0.8	p.u.	Proportional gain
Ki	1/2.5	p.u.	Integration gain
T1	2	s	Governor lag time constant (not used)
T2	5	s	Governor lead time constant (not used)
Power			
S_N	74.12	MVA	Apparent generator power, reference power
P_G	61.1	MW	Output power
P_{REG}	55.6	MW	Registered power
P_{HL}	5.5	MW	House load
P_{REF}	0.824	p.u.	Turbine power set-point

FSM			
droop	5	%	Droop based on P_{REG}
	6.665	%	Droop based on Sn
db	0.015	Hz	Frequency dead band
FSM max	0.1	p.u.	FSM upper limit based on P_{REG}
	0.075	p.u.	FSM upper limit based on S_N
FSM min	-0.1	p.u.	FSM lower limit based on P_{REG}
	-0.075	p.u.	FSM lower limit based on S_N
LFSM			
f_N	50	Hz	nominal frequency (1 p.u. = 3000 rpm)
f_{MAX}	50.4	Hz	Upper frequency limit for disabled LFSM
f_{MIN}	49.5	Hz	Lower frequency limit for disabled LFSM
df_{MAX}	0.5/50	p.u.	upper value for LFSM deadband
df_{MIN}	0.4/50	p.u.	lower value for LFSM deadband
P_{MAX}	0.2	p.u.	Maximum power to controller (P_{REF} + LFSM)
P_{MIN}	0.9	p.u.	Minimum power to controller (P_{REF} + LFSM)
dP_{MAX}	0.075	p.u.	Maximum immediate power change *
dP_{MIN}	-0.075	p.u.	Minimum immediate power change *

* Depends on turbine design

The dP_{MAX}/dP_{MIN} value allows an immediate power change of the turbine and is commonly limited to 10% to protect the lifetime of the turbine. Larger changes are limited by ramp based on thermal stress calculations, with a typical ramp rate of 5% per minute. For our purposes, it is required to determine the maximum power change during islanding, so the ramp is not used/modelled.

5 Mass

The rules of motion for 2 rotating masses connected by a shaft with stiffness K can be illustrated in the following Figure:

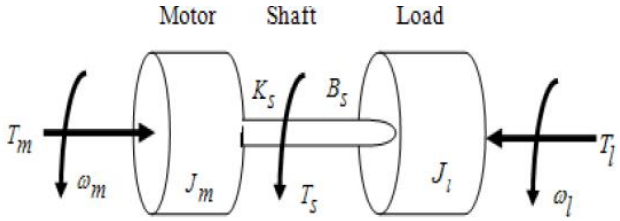

Figure 37 Rotating mass connected through shaft [10]

For this arrangement, the following three equations can be formulated [10]:

$$J_T \frac{d\omega_T}{dt} = T_T - T_S - D_T\omega_T \tag{5.01}$$

$$T_S = K(\delta_T - \delta_G) \tag{5.02}$$

$$J_G \frac{d\omega_G}{dt} = T_S - T_G - D_G\omega_G \tag{5.03}$$

Where J is moment of inertia, T is torque, D is damping torque (usually expressed as losses), K is stiffness of the flexible shaft. The partial indices denote: G – generator, S – shaft, T – turbine.

Furthermore, there is a known relationship between angular velocity and angle of rotation:

$$\omega_T = \frac{d\delta_T}{dt}, \omega_G = \frac{d\delta_G}{dt} \tag{5.04}$$

By applying the Laplace transform to equation (5.01), we obtain equation (5.06), which is then modified to equation (5.08).

$$J_G\omega_T s \ = (T_T - T_S - \omega_T D_T) \tag{5.05}$$

$$\delta_T = \frac{1}{s}\omega_T = \ (T_T - T_S - \omega_T D_T)\frac{1}{J_T s^2} \tag{5.06}$$

$$J_T\delta_T s^2 = \ (T_T - T_S - \omega_T D_T) \tag{5.07}$$

$$J_T \frac{d^2\delta_T}{dt^2} = T_T - T_S - D_T\omega_T \tag{5.08}$$

The simplified model is shown in Figure 38 (the used model is slightly more complicated due to converting between real values and per unit values), where equation (5.01) corresponds to the red rectangle.

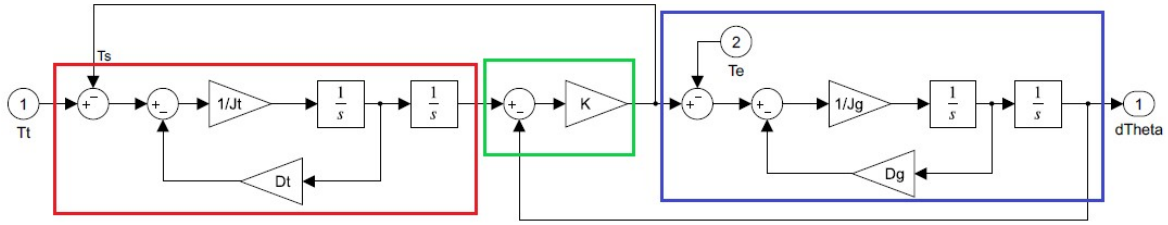

Figure 38 Implementation of mass equations

The shaft self-damping is disregarded because it is already included in the total turbine shaft losses. The green rectangle response to equation (5.02) and blue rectangle to equation (5.03).

$$T_S = K(\delta_T - \delta_G) \tag{5.09}$$

Equation (5.03), similarly to equation (5.01), is modified into the following form:

$$J_G \omega_G s = (T_S - T_E - \omega_G D_G) \tag{5.10}$$

$$\delta_G = \frac{1}{s}\omega_G = (T_S - T_E - \omega_G D_G)\frac{1}{J_G s^2} \tag{5.11}$$

$$J_G \delta_G s^2 = (T_S - T_E - \omega_G D_G) \tag{5.12}$$

$$J_G \frac{d^2\delta_G}{dt^2} = T_S - T_E - D_G \omega_G \tag{5.13}$$

Equation (5.03) has already been incorporated into the synchronous machine model. Where T_E means electro-magnetic torque (corresponding to the generator torque T_G).

5.1 Per unit values

5.1.1 Expression of the equation

The whole model operates with per unit values, so the equations need to be recalculated to per unit. We proceed again from the motion equation:

$$J\frac{d\omega_m}{dt} = \Delta T \tag{5.14}$$

ΔT – refers to the difference between T_T and T_S.

Definition of inertia constant [3]:

$$J = 2H\frac{S_{base}}{\omega_{0m}^2} \tag{5.15}$$

Where H is inertia contant (s), S_{base} is the reference power and ω is mechanical angular velocity.

This equation is important for determining the reference torque. By substituting equation (5.15) into equation (5.14), we get:

$$\frac{2H}{\omega_{0m}}\frac{d\omega_m}{dt} = \frac{\Delta T}{\frac{S_{base}}{\omega_{0m}}} = \Delta\ddot{T} \tag{5.16}$$

Where the marking $\Delta\ddot{T}$ is per unit torque.

Relative angular velocity $\ddot{\omega}_r$ can be expressed as the ratio of mechanical velocity to reference mechanical velocity and can be converted to electrical values.

$$\ddot{\omega}_r = \frac{\omega_m/pp}{\omega_{0m}/pp} = \frac{\omega_e}{\omega_0} \tag{5.17}$$

After substituting this equation (5.17) into equation (5.16), we obtain the following formula:

$$2H\frac{d\ddot{\omega}_r}{dt} = \Delta\ddot{T} \tag{5.18}$$

Similar to equation (5.01), self-damping must be taken into account:

$$2H\frac{d\ddot{\omega}_r}{dt} = \Delta\ddot{T} - D\ddot{\omega}_r \tag{5.19}$$

We can use equation (5.04) and modify it to express the relative velocity as follows:

$$\frac{d^2\delta}{dt^2} = \frac{d\omega_e}{dt} = \omega_0\frac{d\ddot{\omega}_r}{dt} \tag{5.20}$$

By subsequently substituting the expressed relative velocity, we obtain the equation:

$$\frac{2H}{\omega_0}\frac{d^2\delta}{dt^2} = \Delta\ddot{T} - \frac{D}{\omega_0}\frac{d\delta}{dt} \tag{5.21}$$

5.1.2 Implementation into the model

For a simple visualization, the model consists of transfer functions. The Laplace transform is utilized for conversion, subsequently adjusted into a suitable form in following steps:

$$F(s) = \frac{\delta}{\Delta\ddot{T}} \tag{5.22}$$

$$\Delta\ddot{T} = \frac{2H}{\omega_0}s^2\delta + \frac{D}{\omega_0}s\delta = s\frac{\delta}{\omega_0}(2Hs + D) \tag{5.23}$$

$$F(s) = \frac{\delta}{\Delta\ddot{T}} = \frac{\omega_0}{s(2Hs + D)} = \frac{1}{(2Hs + D)}\frac{\omega_0}{s} \tag{5.24}$$

This equation can be visualized as:

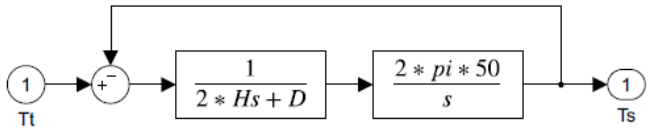

Figure 39 Implementation of mass equation in per unit

The transfer functions were subsequently split into smaller elements. An important aspect is defining the initial state to achieve steady state. The overview of the entire model is shown in the following picture:

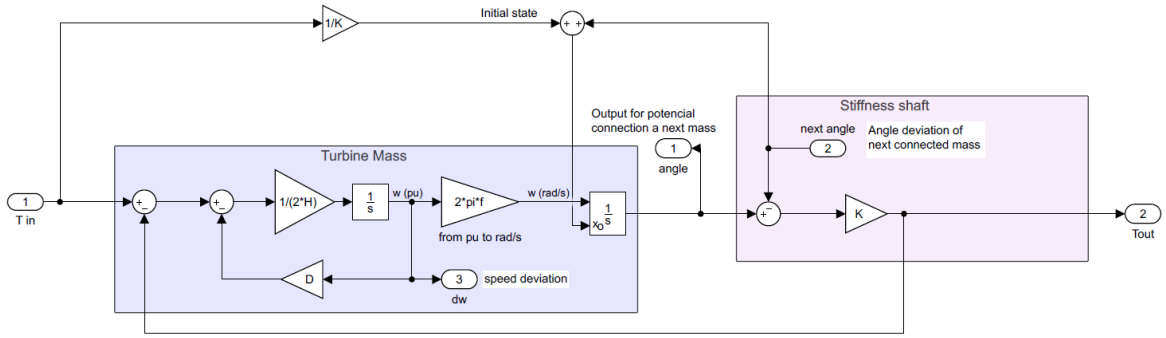

Figure 40 Final model used in the simulation

The Table 7 provides a summary of the model parameters.

Table 6 Mass model parameters

Parameter	Value	Unit	Description
H	2.125	s	Inertia constant
D	0.01	p.u.	Damping factor
K	80	p.u./rad	Shaft stiffness
f_N	50	Hz	Nominal rotation frequency

6 OLTC Transformer

The OLTC (On-Load Tap Change Power Transformer) is modelled using the 1-Ph *Multi-winding transformer* available in the Simscape library.

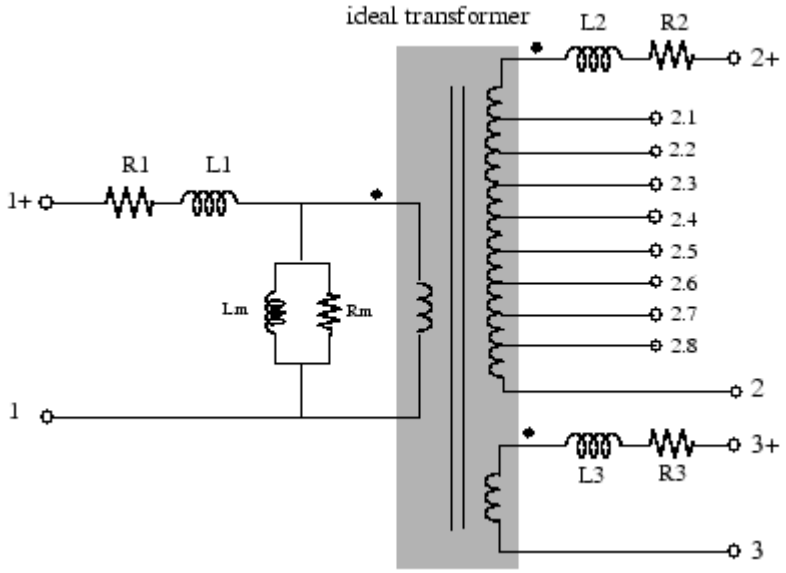

Figure 41 Equivalent circuit diagram of Multi-winding transformer [11]

Parameters of the Grid Transformer provided by customer are summarized in the following table.

Table 7 OLTC parameters

S_N (MVA)	k (-)	z_k (%)	P_k (kW/%)	Taps	single Tap
70	132/15	19	306/0.44	-12.5 % +17.5 %	1.25 %

On-load tap switching occurs on the higher voltage side, thus we consider terminals 1,1+ as LV (Low Voltage). The HV side is represented by fix winding 3,3+ and winding with taps 2,2+. The nominal operation of the transformer occurs when the tap position is set to 0.

The switching of taps is controlled by logic. During nominal operation of the transformer, it is linked to the output terminals 3 and +3. If the tap setting is positive, winding 2 and 2+ are connected in phase. In the opposite case, if the tap setting is negative, the winding is connected in reverse phase.

In the Multi-winding transformer block, winding resistance, leakage inductance and magnetizing inductance can only be entered in per unit. The resistance respecting magnetizing losses and the magnetizing inductance cannot be derived from the provided step-up transformer data.

The values of these elements in the equivalent circuit are normally significantly higher. Considering that the transformer operates under heavy load, their influence on the simulation is minimum. Therefore, default values are retained in the model.

The short-circuit impedance value (Z_K = 19%) is substantial times greater than the percentage value of the short-circuit losses (P_K = 0.44%), so it is not a significant mistake to consider the short-circuit reactance equal to the short-circuit impedance.

$$z_k(p.u.) = \frac{Z_k}{Z_{base}} \cong \frac{X_k}{Z_{base}} = x_k(p.u.) \tag{6.01}$$

Both winding sides ideally have the same relative reactance and resistance. This leads to the consideration that the winding side of the transformer has half the reactance in its nominal state. In the following calculations, this is illustrated, where L (H) – real-value inductance, L (p.u.) – per-unit inductance.

$$Z_k = z_k \cdot Z_n \cong X_1 + X_2' = 2 \cdot X = 2 \cdot \omega \cdot L \rightarrow L\ (H) = \frac{Z_k}{2 \cdot \omega} \tag{6.02}$$

$$L_1(p.u.) = L_2(p.u.) = \frac{L(H)}{L_{base}} = \frac{\frac{Z_k}{2 \cdot \omega}}{\frac{Z_{base}}{\omega}} = \frac{1}{2}\frac{z_k \cdot Z_{base}}{Z_{base}} = \frac{1}{2} z_k \tag{6.03}$$

Similarly, the resistance of individual windings is calculated.

$$R_1(p.u.) = R_2(p.u.) = \frac{1}{2} P_k \tag{6.04}$$

Increasing the taps on the secondary side of the transformer results in an increase in the length of the HV winding, thus increasing both inductance and resistance. The change in per unit values is reflected in the following equations:

$$U_{HV} = (1 + 1.5\% \cdot tap) \cdot U_2 \tag{6.05}$$

$$L_{HV} = (1 + 1.5\% \cdot tap) \cdot L_2 = (1 + 1.5\% \cdot tap) \cdot \frac{1}{2} z_k = L_2 + L_3 \tag{6.06}$$

$$L_3 = 1.5\% \cdot tap \cdot \frac{1}{2} z_k \tag{6.07}$$

Where L_2 is the basic inductance and L_3 is the inductance added by the taps. Only a portion of L_3 is connected based on the tap selection. Decreasing taps is accomplished by connecting the winding with taps in anti-phase, thereby reducing the total inductance.

Similarly, the resistance of the winding is computed.

$$R_3 = 1.5\% \cdot tap \cdot \frac{1}{2} P_k \tag{6.08}$$

Voltages are solved in a similar manner. Individual 1-Ph transformers on the LV side are connected in a delta configuration, while on the HV side, they are connected in a star

configuration. Let's not overlook the fact that the voltage across the winding on the HV side is $Un/\sqrt{3}$, due to the star connection.

7 Grid

As mentioned in previous chapters, the simulation is performed using phasor-based solution. This method is enabled for solving by utilizing the Simscape/Electrical/Specialized Power Systems library. The parameters of the grid at the connection point of the power generation unit, estimated by DNO, are summarized in the following table:

Table 8 Estimated parameters by DNO

Parameter	Value		Unit
V	132		(kV)
f_N	50		(Hz)
3-Ph Fault parameters			
	Minimum	Maximum	
S_K	2632	3690	(MVA)
Z/R ratio	4.191	5.673	(-)

The grid is modelled as a voltage 3-Ph source behind the impedance respecting grid strength. The impedance of the grid model has been calculated from 3-Ph fault parameters.

The grid source impedance is modelled using a 3-Ph series RLC branch (also from the Simcape library), with specified resistance R_K and inductance L_K.

$$Z_K = \frac{V^2}{S_K} \tag{7.01}$$

$$R_K = Z_K \cdot \frac{1}{Z/R\ ratio} \tag{7.02}$$

$$X_K = \sqrt{Z_K^2 - R_K^2} \tag{7.03}$$

$$L_K = \frac{X_K}{2 \cdot \pi \cdot f_N} \tag{7.04}$$

Table 9 Calculated parameters

Parameter	Value		Unit
V	132		(kV)
f_N	50		(Hz)
3-Ph Fault parameters			
	Minimum	Maximum	
S_K	2632	3690	(MVA)
Z/R ratio	4.191	5.673	(-)
Z_K	6.6201	4.7220	(Ω)
R_K	1.5798	0.8323	(Ω)
X_K	6.4288	4.6480	(Ω)

L_K (H)	0.0205	0.0148	(H)

If required, an ideal controlled source can replicate the FRT curve [1] using a look-up table. However, simulating faults on the HV terminals of the step-up transformer, such as a voltage dip of 140 ms, is rather our interest [1]. Therefore, the model needs to be equipped with a breaker that will perform the connection of phases (faults) at the PCC, not at the ideal source location. The faults are single-phase short circuit, phase-phase short circuit, two-phase short circuit with ground, and three-phase short circuit.

Finally, it's essential to resolve the voltage level at the point of connection, which differs from that at the ideal source connection point. We'll utilize the voltage source's adjustability and implement feedback control to regulate the voltage at the connection point. This will be achieved by employing an integral regulator with low gain. The regulation process will only occur within the initialization loop, after that, the regulator keeps a constant (nominal) value. The regulation is enhanced with reactive power control at the grid connection point for specific simulations that demand unity power factor or any other specific PF.

All voltage settings are hidden within the 3-Phase source block.

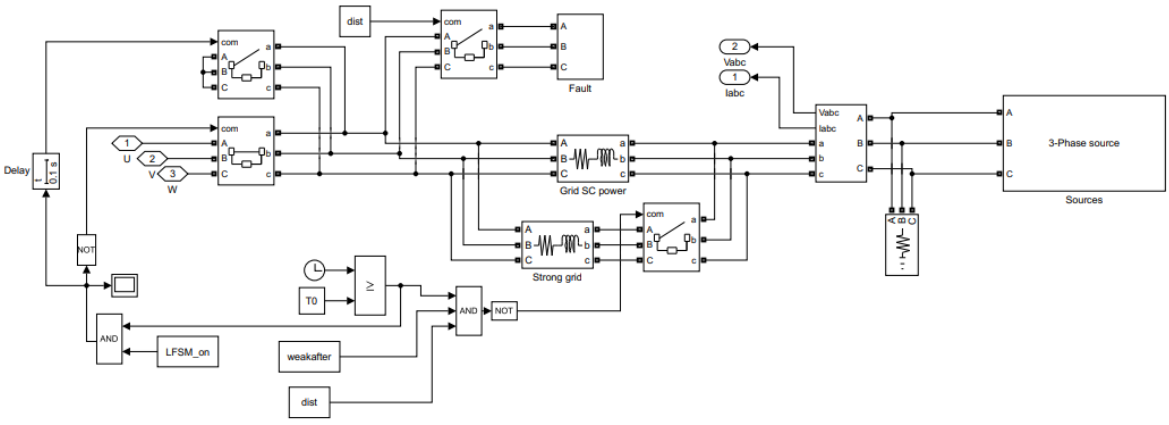

Figure 42 Complete grid implementation

As previously mentioned, the entire simulation utilizes a phasor-based solution. Complex values are entered into the controlled AC voltage sources, where the amplitude of each phase is the same and the phase difference between them is 120°.

Phasors (in p.u.) in various stages are depicted in Figure 43. The OLTC transformer causes vector shift of approximately 30°, while the equivalent reactance of OLTC transformer and equivalent reactance of network's strength results in only a slight vector shift.

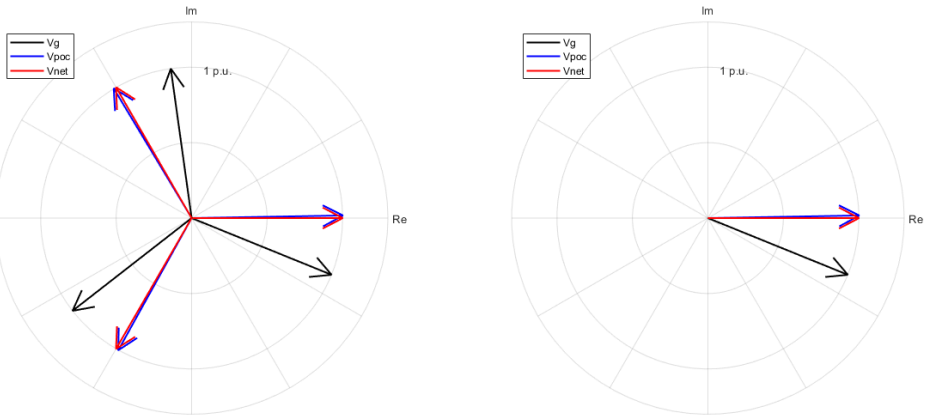

Figure 43 Voltage phasors, Positive sequence voltage phasors

Where Vg is generator terminal votlage, Vpoc is point of connection voltage and Vnet is voltage at controlled AC voltage sources.

The most effective way to depict the voltage levels and power flow associated with Figure 43 is via the load flow diagram. The tap of the step-up transformer was set to 0.

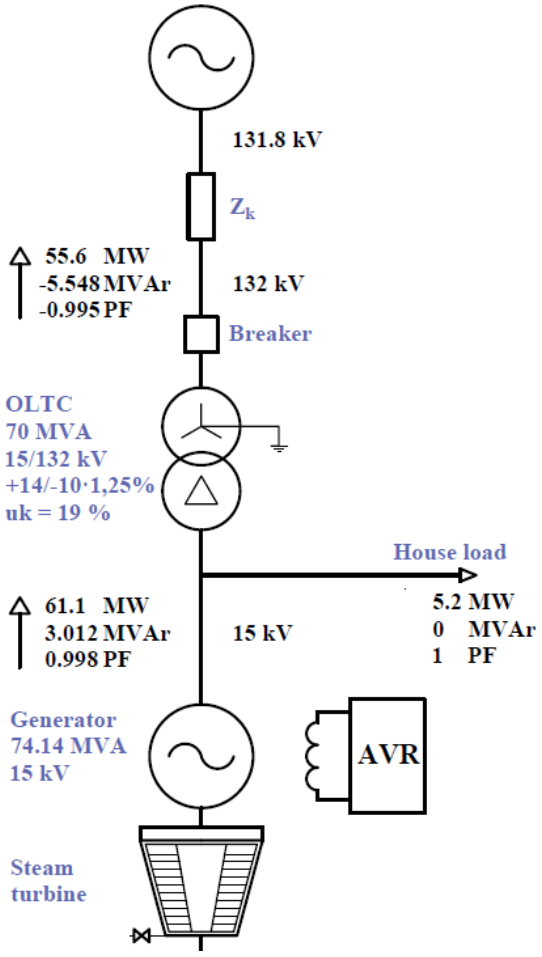

Figure 44 Load flow diagram of Power Generating Unit

8 PSS

8.1 Introduction

PSS (Power System Stabilizer) is a functionality in the voltage regulator that aids in damping frequency oscillations on generator terminals, primarily within the typical range of interest, which is typically 0.1 to 3 Hz. Damping is achieved by compensating for the phase lag of the voltage regulator, which significantly adds the synchronising torque to the shaft, particularly in the region of phase compensation.

Frequencies ranging from 0.1 to 1 Hz primarily represent inter-area modes that characterize the grid. However, these modes are not typically present in simplified grid models like ours. The oscillations within the range of 1-3 Hz, referred to as local mode frequencies, are caused by the interaction between the generator and the grid. This mode of oscillation is clearly visible from the simulations in Chapter 9. All these oscillations need to be damped to help keep the stability of the network.

Thanks to speed of digital voltage controllers and convenient frequency characteristics of the synchronous machines, the PSS quickly responds oscillations by adjusting the input signal to the excitation to damp frequency oscillations.

This section is dedicated to: describing the function of the specific PSS used in Chapter PSS2C, the Fourier analysis applied in the simulations in chapter 9.2, determination of the time constant of input washout filters and the calculation of the speed deviation signal entering the PSS, which is calculated from the load angle. Tuning of the PSS, i.e. the torsion filter and the main filter, is included in Chapter 9.2, while the parameters are summarized in Chapter 8.3.

8.2 PSS2C

The used PSS2C is formed in accordance with Std.421.5. The power system stabilizer of type PSS2C utilizes electrical active power and shaft speed as inputs. The output signal of the PSS is directed to the summing point of the voltage regulator (as indicated by the signal Vs in Figure 29).

Both input signals (1) and (2) are passed through a high pass filter to ensure that the PSS does not respond to slow changes in power. It is essential for both signals (1) and (2) to reach a comparable amplitudes of the local mode oscillations to ensure proper functioning. While it might appear simpler to adjust parameter KS3 to equalize the amplitudes of signals (1) and (2), it is necessary to achieve this by adjusting KS2 instead. The reason lies in the structure

of PSS2C and the way in which signal (2) is added and then subsequently subtracted to become signal (4).

Signals (1) and (2) are summed and filtered by a torsional filter. The signal state at point (4) shall be free of torsional higher harmonics. The main configuration of the PSS is defined by constants Ks1, T1-T4, T10-T13, which implement phase compensation.

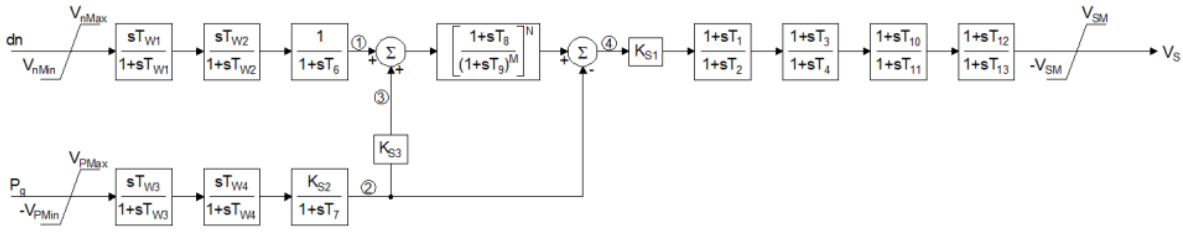

Figure 45 PSS2C structure

As previously mentioned, the PSS helps damping of grid frequency oscillations by voltage regulation loop phase compensation. Through Fourier analysis, the amplitude and phase of the terminal voltage loop can be identified within the specified frequency range from 0.2 to 3 Hz. Phase compensation is executed by setting constants T1-T4 and T10-T13, which determined by the simulation in Chapter 9.2.

The tuning of the PSS should be conducted in a closed loop, which involves injecting noise into the reference voltage and monitoring the output voltage at the generator terminals. As an alternative, the *linearize* function can be used, enabling the display of the linearized model in the frequency spectrum. Both results are illustrated in Chapter 9.2.

Following that, the power response to the reference voltage (Pg/Vref) is verified because power oscillation corresponds to frequency oscillations. The tuning of the PSS is also detailed in Chapter 9.2.

8.2.1 Washout configuration

The washout filters are composed of high-pass filters applied to both signals, filter time constant is set to 5 s. The low-pass filter with time constant T6 is not utilized (the constant is set to 0), high-pass filter is bypassed because the time constant Tw4 it's not used too. A washout constant of 5 seconds ensures reliable transmission of frequencies as low as 0.1 Hz, as depicted in the attached Figure 46.

The constants Ks2 and T7 should be set such that signal 2 similar to signal 1. This is accomplished by ensuring that T7 is the same as Tw3 and Ks2 = T7/2H = 0.7434 [8], [12]. All specified values are summarized in Table 11.

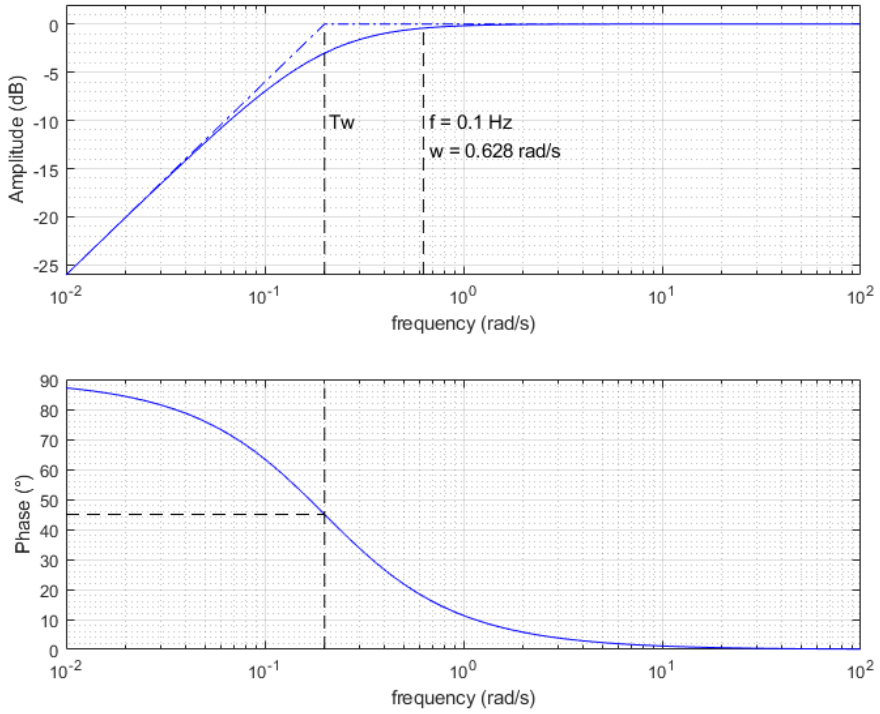

Figure 46 High-pass (washout) filter

8.2.2 Fourier analysis

As already mentioned, to convert a signal from the time domain to the frequency domain, Fourier transform is used. The equation for the Fourier transform of a continuous signal is:

$$F(f) = \int_{-\infty}^{\infty} f(t) \cdot e^{-j\omega t} dt \tag{8.01}$$

Where $F(f)$ is the function transformed into the frequency domain, and $f(t)$ is the function dependent on time. However, signal can only be sampled at specific time intervals for a limited duration. Therefore, the discrete Fourier transform (DFT) is utilized:

$$F(h) = \sum_{n=0}^{N-1} f_n \cdot e^{-j\frac{2\pi}{N}hn} \tag{8.02}$$

Where N is the last sample of the captured function and n denotes each single sample.

In Matlab, the function fft - Fast Fourier Transform can be used, which utilizes the similarities of many elements in the matrix W^{hn}.

$$W^{hn} = e^{-j\frac{2\pi}{N}} \tag{8.03}$$

FFT:

$$F(h) = \sum_{n=0}^{N-1} f_n \cdot W^{hn} \tag{8.04}$$

The sampling frequency must be at least twice as large as the maximum analysed frequency according to the Nyquist-Shannon theorem.

$$f_v \geq 2f_{max} \tag{8.05}$$

For our purposes, we are interested in the frequency range of 0.2-3 Hz. Therefore, a sampling period of 0.01 s is sufficiently distant from the Nyquist limit theorem, and the results within this frequency range can be considered valid. The fft function analyses samples with a sampling period of 0.01 s up to a frequency of ±50 Hz according to the theorem (see Figure 49).

The sampling interval of the signal determines the resolution of the analysed frequencies. If a sinusoidal signal of 1 Hz is sampled for Tw = 120 s, then the frequency of 1 Hz corresponds to the 120th harmonic frequency (121st - because Matlab indexes from 1, DC signal corresponds to index 1) and the 1st harmonic in the spectrum is 1/120 Hz, i.e. h = 0.00833 Hz.

Fourier analysis is conducted on the injected signal into the excitation reference voltage. The injected signal, used for verification, exhibits the following waveform:

$$0.01 \cdot (\sin(\omega t) + \sin(3\omega t)) \tag{8.06}$$

Figure 47 illustrates the amplitude spectrum obtained from the unadjusted Fourier transformation output.

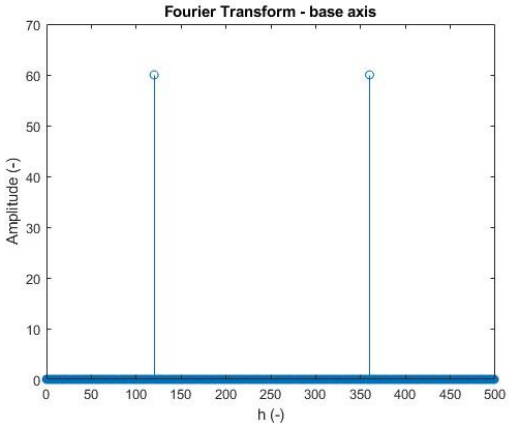

Figure 47 Harmonic spectrum

Calculation of amplitude and phase:

$$abs\left(V_{ref_{fft}}\right) = \sqrt{Re\left\{V_{ref_{fft}}\right\}^2 + Im\left\{V_{ref_{fft}}\right\}^2} \tag{8.07}$$

$$angle\left(V_{ref_{fft}}\right) = arctg\left(\frac{Im\left\{V_{ref_{fft}}\right\}}{Re\left\{V_{ref_{fft}}\right\}}\right) \tag{8.08}$$

The conversion of harmonic numbers to frequencies on the x-axis is applied in Figure 48.

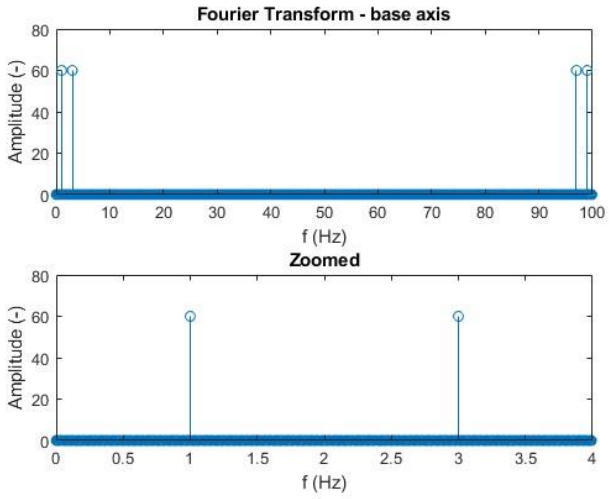

Figure 48 Entire frequency spectrum and zoomed frequency spectrum

The transformation produces a mirror copy representing the negative frequencies. Since MATLAB doesn't accommodate negative values in the spectrum, values above the 50 Hz frequency correspond to the range of -50 to 0 Hz. To enhance clarity, the fftshift() function is employed in Figure 49.

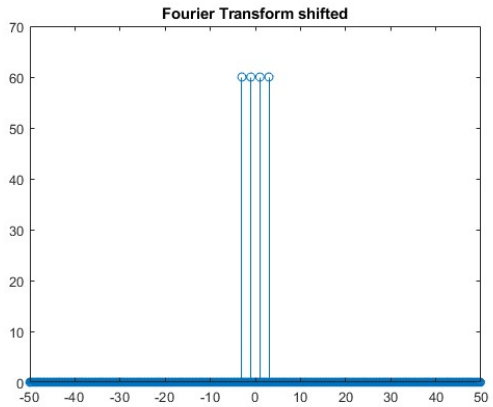

Figure 49 Visualization of the mirrored frequency spectrum

The number of frequency components of a harmonic signal in the spectrum is multiplied by $\frac{2}{N}$ because the analyzed signal is mirrored into positive and negative frequencies. As a result, the amplitude of the harmonic signal is obtained on the y-axis in the frequency spectrum.

$$k \cdot \frac{2}{N} = 60 \cdot \frac{2}{12000} = 0.01\ (amplitude) \tag{8.09}$$

Where k represents the number of frequency components, and N denotes the total number of samples. Similarly, the Fourier transform is applied to the measured terminal voltage of the generator.

To construct the Bode plot, we will utilize the following calculations for the signal's gain and phase.

$$|F_{db}| = 20 \log\left(\frac{abs(V_g)}{abs(V_{ref})}\right)\ (dB) \tag{8.10}$$

$$\sphericalangle F_{db} = angle(V_g) - angle(V_{ref})(°) \tag{8.11}$$

It might seem problematic that for an ideal representation of the transfer through Fourier transformation, the analysed function should be periodically repeating in an infinite time domain. Furthermore, it should be sampled throughout the entire period, not just a portion of the period as in the case of random noise.

If these conditions are not fulfilled, other frequency components may appear in the frequency spectrum, typically being relatively minor compared to the dominant correct components.

This is partially repressed by creating an analysis window that is half the size of the sampled data. The window is subsequently shifted from the first half of the data to the second half of the data. The results from the Fourier analysis are averaged. 50 cycles are used, resulting in 50 averaged values for each frequency, along with 50 shifts from the initial to the final position of the window.

The application of Fourier analysis processed in this manner is depicted in Figure 52, where noise containing the entire desired analysed spectrum (0.2 - 3 Hz) was injected.

In Figure 52, the Fourier analysis is also compared to the Bode diagram of linearized model using the function *linearize*.

8.2.3 Speed derivation from load angle

The speed signal entering the Power System Stabilizer is not directly measured in practice but derived from the measured electrical variables at the terminals of the generator. The similarity of load angle deviation to speed deviation is utilized. The load angle is computed from the measured variable levels thus the angle remains constant in steady state. The change in rotational state is then calculated by taking the derivative of this angle.

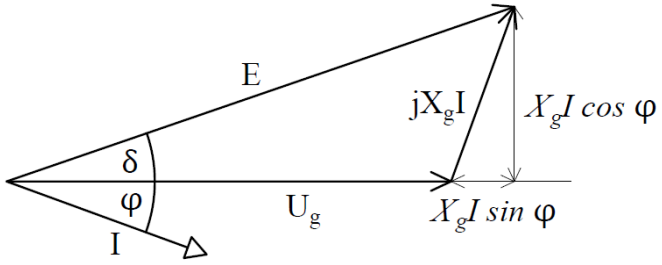

Figure 50 Load angle

The calculation of the angle is as follows:

$$tg\ \delta = \frac{X_g \cdot I \cdot cos\varphi}{V_g + X_g \cdot I \cdot sin\varphi} \tag{8.12}$$

Active and reactive power are measured at the generator terminals.

$$P = 3 \cdot V_{g_f} \cdot I \cdot cos\varphi \rightarrow I \cdot cos\varphi = \frac{P}{3 \cdot V_{g_f}} \tag{8.13}$$

$$Q = 3 \cdot V_{g_f} \cdot I \cdot sin\varphi \rightarrow I \cdot sin\varphi = \frac{Q}{3 \cdot V_{g_f}} \tag{8.14}$$

By substituting the expressions from (8.13) and (8.14) into equation (8.15), we obtain:

$$tg\ \delta = \frac{X_g \cdot \frac{P}{3 \cdot V_{g_f}}}{V_{g_f} + X_g \cdot \frac{Q}{3 \cdot V_{g_f}}} \cdot \frac{3 \cdot V_{g_f}}{3 \cdot V_{g_f}} = \frac{X_g \cdot P}{3 \cdot V_{g_f}^2 + X_g \cdot Q} = \frac{X_g \cdot P}{V_g^2 + X_g \cdot Q} \tag{8.15}$$

$$\delta = arctg\left(\frac{X_g \cdot P}{V_g^2 + X_g \cdot Q}\right)\ (rad) \tag{8.16}$$

The resulting angle is expressed in radians. By taking the derivative of the angle, we obtain the speed deviation in radians per second. Therefore, a conversion of speed to per unit is subsequently applied.

$$\frac{d\delta}{dt} = \Delta\omega\ \left(\frac{rad}{s}\right) \rightarrow \Delta\omega = \frac{d\delta}{dt} \cdot \frac{1}{\omega_s} = \frac{d\delta}{dt} \cdot \frac{1}{2\pi \cdot 50}\ (p.u.) \tag{8.17}$$

8.3 PSS Parameters

The PSS filter and RT filter are configured based on simulation (detailed in the Chapter 9.2).

Table 10 PSS Parameters

PSS Parameters			
Tw1	Frequency washout time constant 1	5	s
Tw2	Frequency washout time constant 2	5	s
Tw3	Power washout time constant 2	5	s
Tw4	Power washout time constant 4	0	s
T1	Lead-lag PSS filter time constant 1	0.09	s
T2	Lead-lag PSS filter time constant 2	0.01	s
T3	Lead-lag PSS filter time constant 3	0.09	s
T4	Lead-lag PSS filter time constant 4	0.01	s
T6	Frequency filter time constant	0	s
T7	Power filter time constant	5	s
T8	Lead-lag RT filter time constant 8	0.75	s
T9	Lead-lag RT filter time constant 9	0.13	s
T10	Lead-lag PSS filter time constant 10	0.11	s
T11	Lead-lag PSS filter time constant 11	0.1	s
T12	Lead-lag PSS filter time constant 12	0.9	s
T13	Lead-lag PSS filter time constant 13	1	s
Ks1	PSS gain 1	15	(p.u.)
Ks2	PSS gain 2	0.7434	(p.u.)
Ks3	PSS gain 3	1	(p.u.)
Vsm	PSS output limitation	0.05	(p.u.)
M	Torsion filter parameter grade M	5	(-)
N	Torsion filter parameter grade N	1	(-)

9 Simulation

9.1 Introduction

The Power Generating Unit comprises steam turbine and generator. In the pressure control, the guaranteed value of 55.6 MW exceeds the registered capacity of 55 MW in the connection offer. All simulations should be associated with the guaranteed registered capacity. The estimated house load of the power plant is about 5.5 MW (with includes step-up transformer loss of 306 kW). The turbine-connected generator can operate with a nominal apparent power of 74.12 MVA.

The Power Generating Unit operates at the voltage of 15 kV and is connected to the grid at 132 kV through step-up transformer with a nominal power of 70 MVA. Reactive power control can be achieved not only by adjusting the generator excitation but also by tapping the winding of transformer. A single tap adjustment results in a 1.25% change of the nominal voltage of HV side, the tap control range is from -10 to +14.

All the simulations are carried out in accordance with the instructions in the Engineering Recommendation G99 ([1]) and Grid Code ([2]).

Legend

Sn – nominal power of generator (74.12 MVAr = 1 p.u.)

Pm – turbine shaft power

Pg – generator power (61.1 MW = 0.823 p.u.)

HL – house load (5.5 MW = 0.074 p.u.)

Vg – generator voltage (15 kV = 1 p.u.)

Vgcp – voltage at grid connection point (132 kV = 1 p.u.)

Efd – generator rotor voltage (162V = 1 p.u.)

Ifd – generator rotor current (1162 A = 1 p.u.)

Vfe – exciter voltage (67.7 V = 1 p.u.)

Ife – exciter current (13 A = 1 p.u.)

PSS – injected voltage to AVR by PSS

dw – speed deviation (50 Hz = 1 p.u.)

delta – Angle between generator rotor and remote grid voltage

The blue text in the following subchapters represents excerpts taken from the Grid Code or G99, i.e. it is not part of this thesis.

9.2 PSS

C.7.2.1 In the case of a Synchronous Power Generating Module with a Power System Stabiliser the Power System Stabiliser tuning simulation study report required by the Grid Code C.1.2.5.6 shall be submitted in accordance with Grid Code EPC.A.3.2.1.

ECP.A.3.2.1 In the case of a Synchronous Power Generating Module with an Excitation System Power System Stabiliser the Power System Stabiliser tuning simulation study report required by ECC.A.6.2.5.6 or required by the Bilateral Agreement shall contain:

(i) the Excitation System model including the Power System Stabiliser with settings as required under the Planning Code (PC.A.5.3.2(c)).

The torsional frequency was calculated to 21.22 Hz and the local mode frequency is around 1.59 Hz in accordance with Table 12. Thus, the torsional filter must damp higher frequencies than 20 Hz and gives phase shift 180° at 1.59 Hz. The signal damping at 21.22 Hz is around -80 dB (as you can see in the Figure 51).

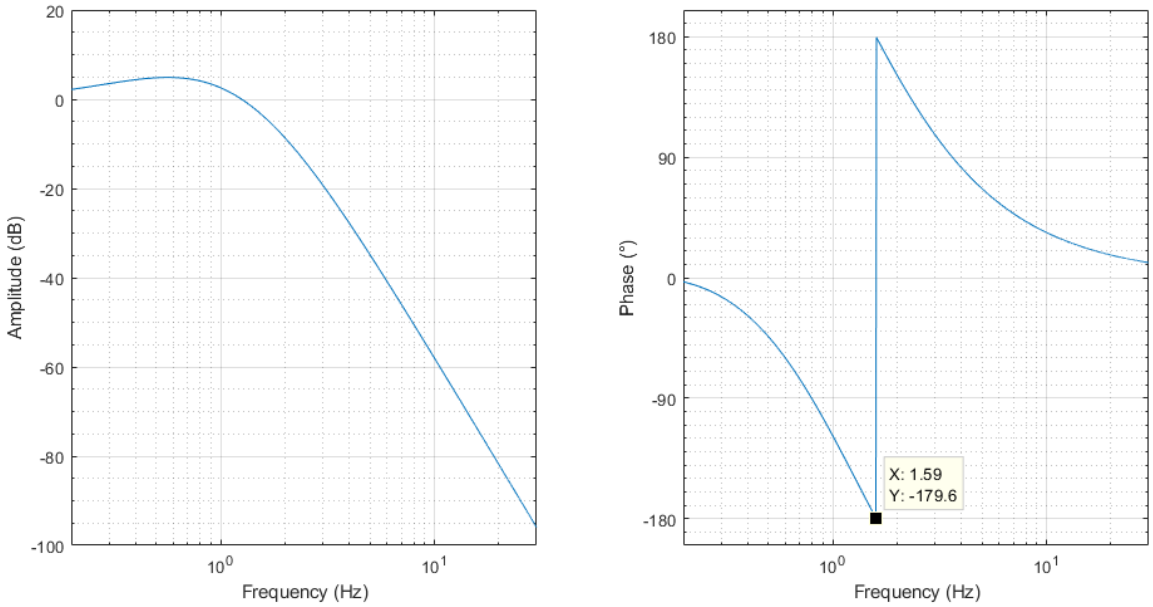

Figure 51 Torsional filter

To perform voltage phase compensation, the noise signal Vs is injected to the voltage reference summing point. By applying Fourier analysis (described in detail in Chapter 8.2.2) to the recorded reference and terminal voltage, a Bode diagram is constructed, as depicted in Figure 52.

Alternatively, the *linearize* function can be used to linearize the entire model, followed by using the *bode* function to extract frequency, magnitude, and phase data for constructing the Bode diagram.

The main PSS filter (already linearized) is tuned to compensate for voltage response in a closed loop (Vg/Vref). The compensated phase should ideally be 0°, However, it's essential for the PSS not to overcompensate the phase. Phase compensation is illustrated in Figure 52.

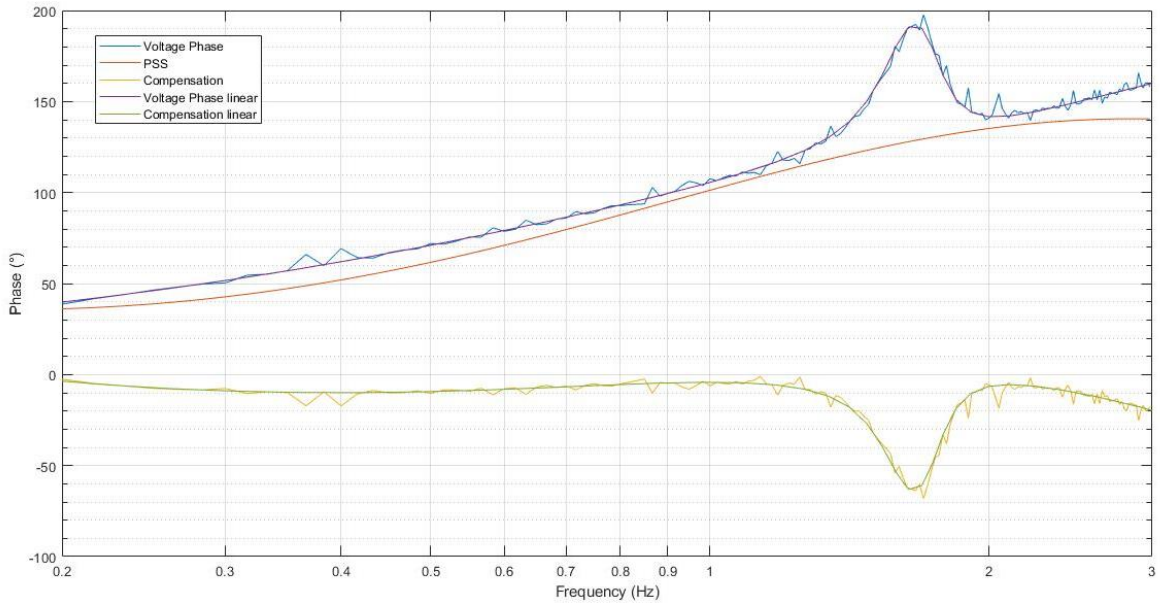

Figure 52 Voltage response and phase compensation by PSS

Note: The voltage response is reversed in Figure 52 for a better graphical tuning of the PSS phase. In reality, PSS phase is summed with the phase of the voltage response.

(ii) open circuit time series simulation study of the response of the Excitation System to a +10% step change from 90% to 100% terminal voltage.

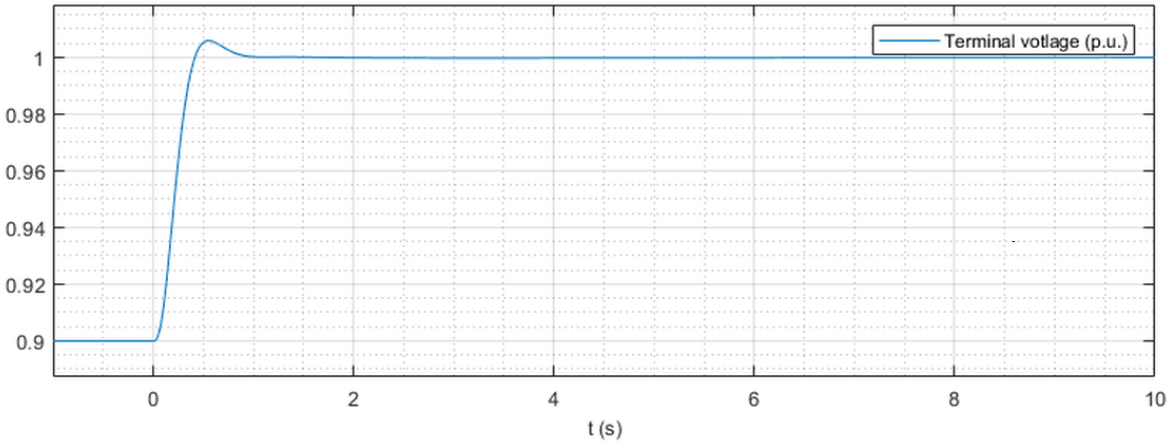

Figure 53 Step at terminal voltage

This simulated waveform demonstrates the correctness of the excitation controller tuning. Tuning the excitation controller directly influences the frequency spectrum of the voltage response.

(iii) on load time series dynamic simulation studies of the response of the Excitation System with and without the Power System Stabiliser to 2% and 10% steps in the reference voltage and a three phase short circuit fault applied to the higher voltage side of the Synchronous Power Generating Module transformer for 100ms. The simulation studies should be carried out with the Synchronous Power Generating Module operating at full Active Power and maximum leading Reactive Power import with the fault level at the Supergrid HV connection point at minimum or as otherwise agreed with The Company. The results should show the Synchronous Power Generating Module field voltage, terminal voltage, Power System Stabiliser output, Active Power and Reactive Power output

The simulations were performed with full active power and maximum leading reactive power at the point of connection, which is the HV side of the step-up transformer. The reactive power was adjusted to -24.95 MVAr using the tap on the step-up transformer, which exceeds the maximum leading reactive power of -23.69 MVAr with a significant margin.

$$P_{reg} \cdot \tan(arccos(PF)) = 55.6 \cdot \tan(\arccos(-0.92)) = -23.69\ MVAr \quad (9.01)$$

The simulation displays time series outputs that was simulated as demanded.

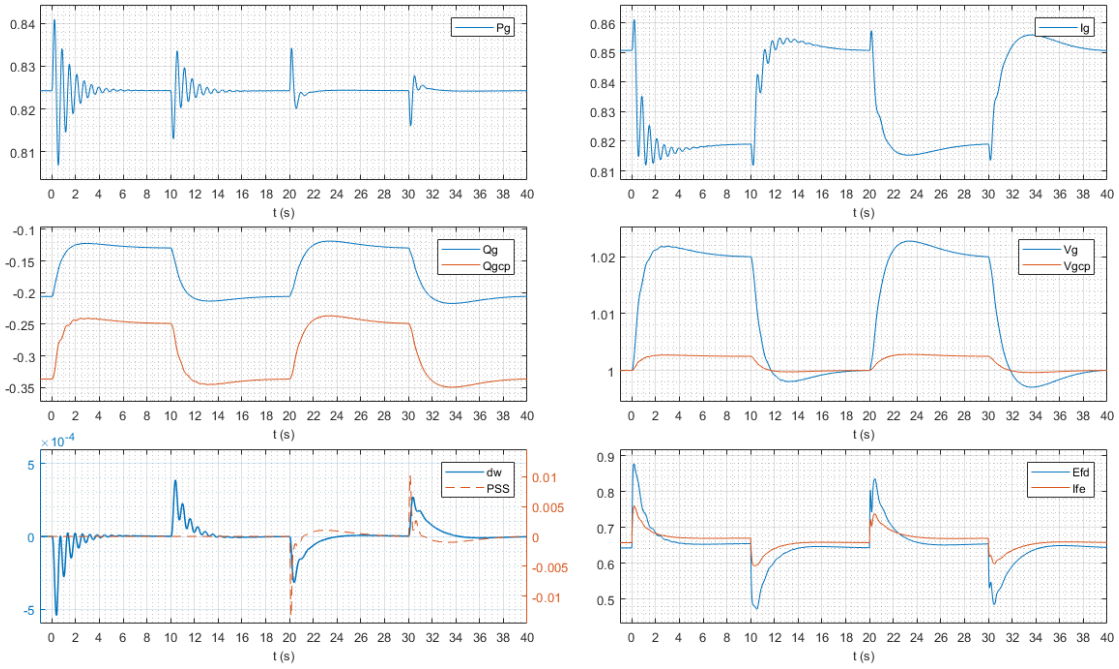

Figure 54 Step in the reference voltage 2% (time < 20 s – without PSS, time > 20 s – with PSS)

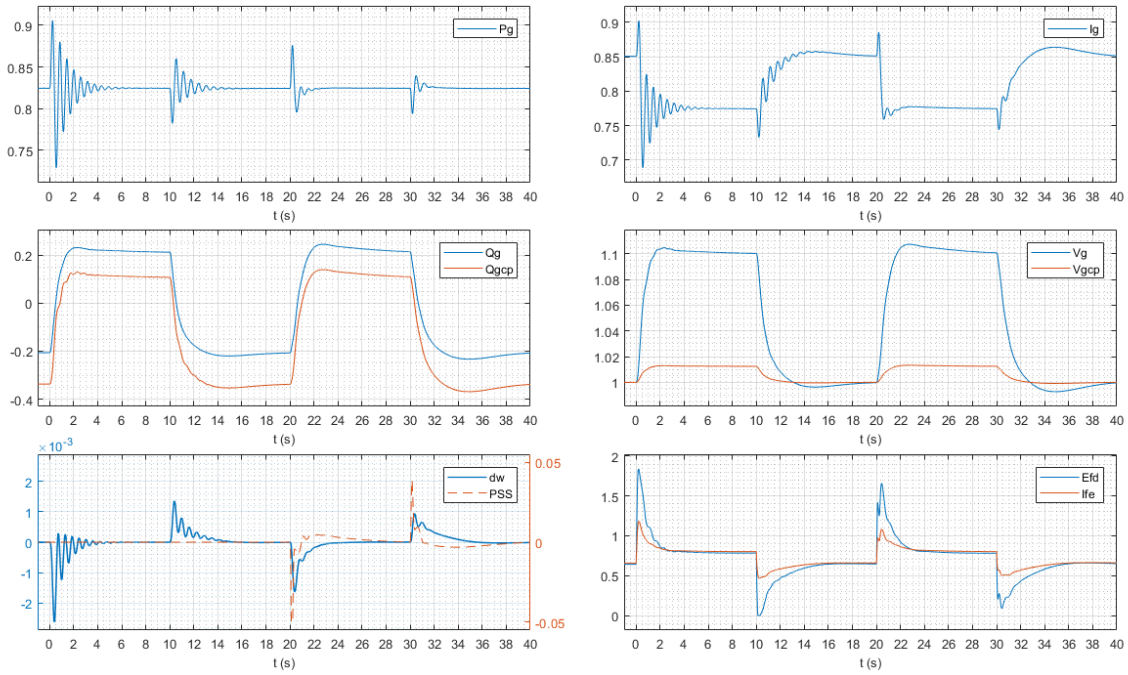

Figure 55 Step in the reference voltage 10% (time < 20 s – with PSS, time > 20 s – without PSS)

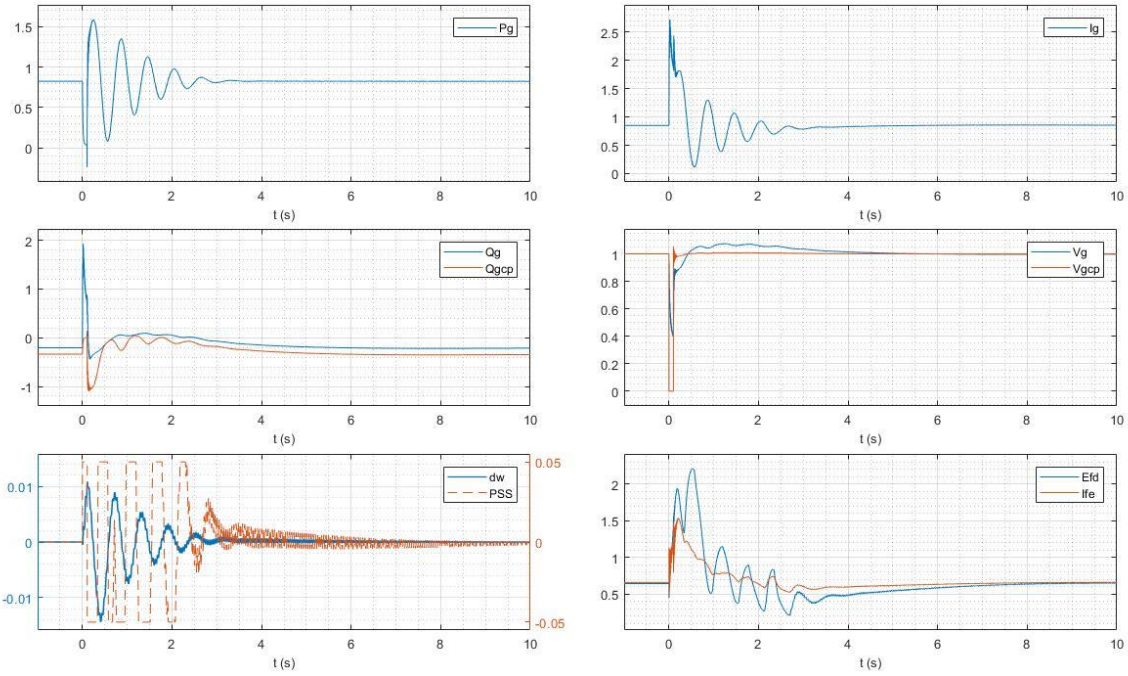

Figure 56 Voltage dip of 100 ms at HV terminal of the transformer - PSS ON

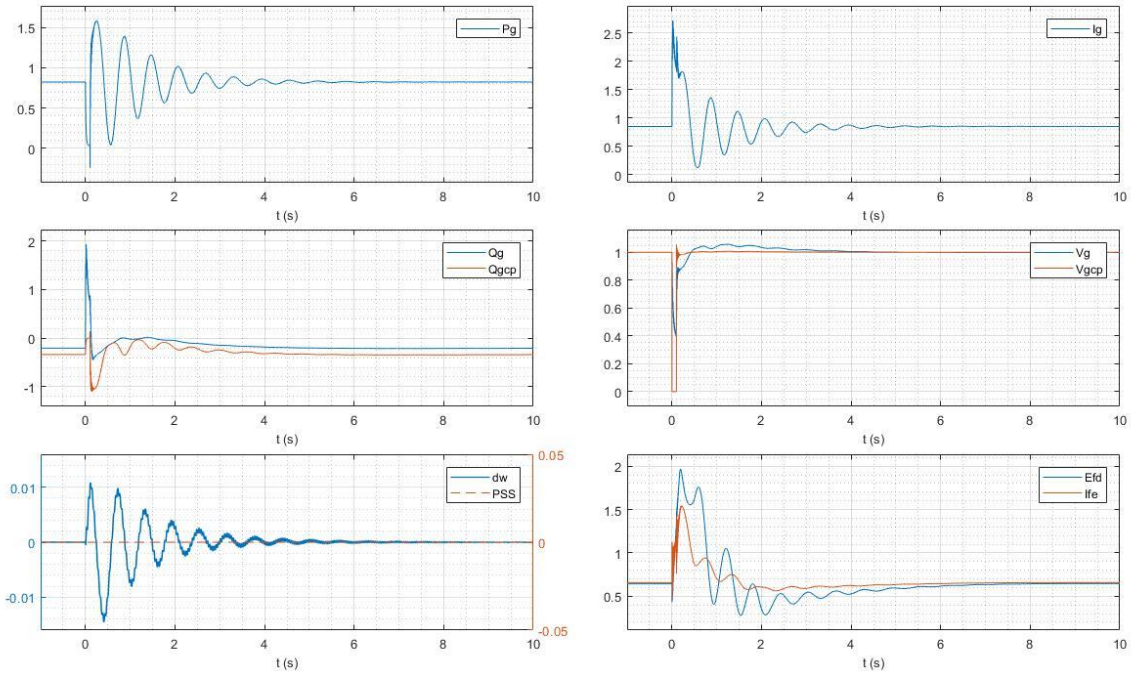

Figure 57 Voltage dip of 100 ms at HV terminal of the transformer - PSS OFF

(iv) gain and phase Bode diagrams for the open loop frequency domain response of the Synchronous Power Generating Module Excitation System with and without the Power System Stabiliser. These should be in a suitable format to allow assessment of the phase contribution of the Power System Stabiliser and the gain and phase margin of the Excitation System with and without the Power System Stabiliser in service.

The Bode diagram for open loop was performed terminal voltage (Vg/Vref). Figure 58 shows sufficient safety in phase and safety in amplitude for all three states (without PSS, Ks1 = rated and Ks1 = 3 x rated).

The phase margin is around 91.2° for Ks1 = 0, 87.25° for Ks1 = 15, 80.5° for Ks1 = 45. The amplitude margin (when the phase is at -180°) is around -15.65 dB for Ks1 = 0, -34.3 dB for Ks1 = 15, and -36.55 dB for Ks1 = 45.

The phase margin higher than 40° and the amplitude margin higher than 6 dB is generally accepted in accordance with [13].

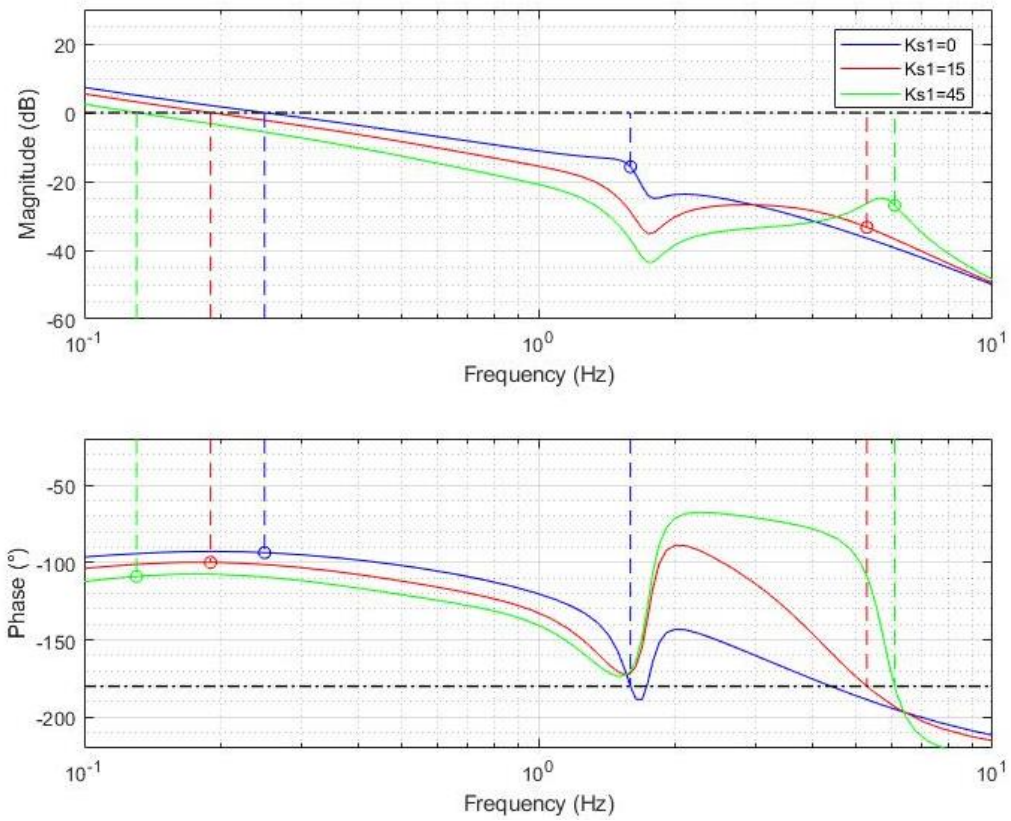

Figure 58 Bode plot Vg/Vref in open loop

(v) an eigenvalue plot to demonstrate that all modes remain stable when the Power System Stabiliser gain is increased by at least a factor of 3 from the designed operating value

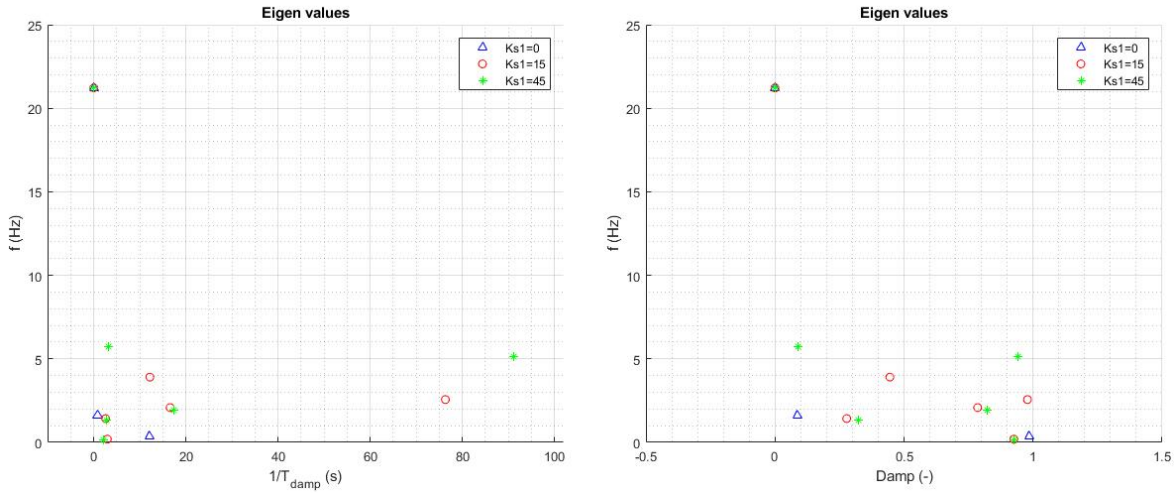

Figure 59 a) Eigenvalues plot, b) Damping factor plot

Eigenvalues represent the characteristic roots of the transfer function within the complex frequency domain, commonly referred to as the s-plane [13]. The eigenvalues were applied to a linearized approximation of the model. Poles indicate the damping of oscillations, which

are damped more rapidly with a larger damping factor (Damp). Eigenvalues closer to the imaginary axis are damped more slowly, while eigenvalues further from the real axis oscillate at higher frequencies. The accurate eigenvalues are given in the Table 12.

From the real and imaginary parts of the eigenvalues, damping factor is determined using the formula: Damp = - Re{eigenvalue} / abs{eigenvalue}. The eigenvalue oscillation frequency can be calculated as: frequency = Im{eigenvalue}/2π and damping time constant can be calculated as: .

The eigenvalues plot for PSS off, PSS with rated output gain - Ks1 = 15 and PSS with 3x rated output gain - Ks1 = 45, are simulated as the response of mechanical power to a signal injected into the reference voltage. Mechanical power is interesting because of its close correlation with frequency oscillations, which corresponds to the following point (vi).

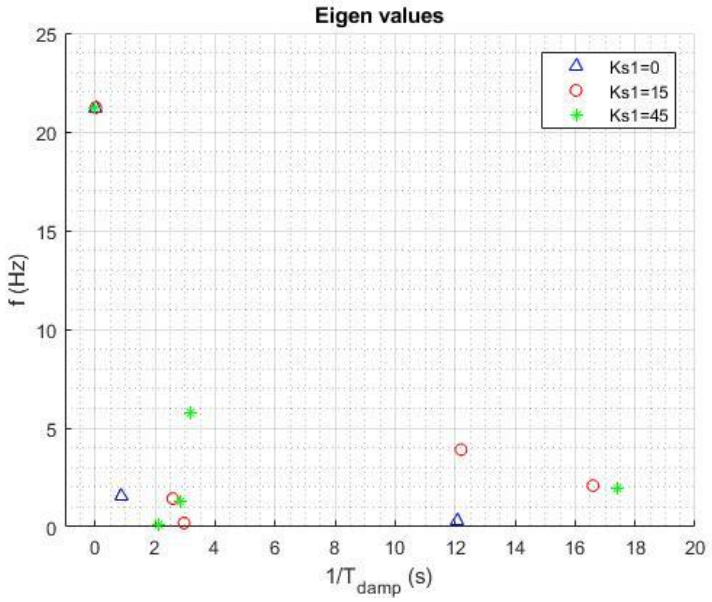

Figure 60 Significant damping time constants (zoomed)

The Table 12 shows local mode frequency around 1.59 Hz and shaft torsional frequency about 21.22 Hz. In Figure 60, it is evident that augmenting the output PSS gain does not lead to instability. As the output gain of the PSS increases, the time constant of damping (T_{damp}) decreases around the local mode frequency. The utilization of PSS deforms the dominant local mode frequency into few frequencies with significantly higher damping factor. It demonstrates stable operation when the PSS gain is increased.

Table 11 Parameters of eigenvalues

	frequency (Hz)	Re (-)	Im (-)	T_{damp} (s)	Damp (-)
Ks1 = 0	111.883	-27.284	702.981	0.037	0.039
	111.865	-27.433	702.867	0.036	0.039
	21.222	-0.031	133.342	32.557	0.0002
	1.586	-0.864	9.966	1.157	0.087
	0.347	-12.071	2.178	0.083	5.543
Ks1 = 15	111.833	-33.136	702.668	0.030	0.047
	111.822	-33.285	702.597	0.030	0.047
	21.222	-0.025	133.340	39.897	0.0002
	2.564	-76.308	16.109	0.013	0.978
	3.908	-12.201	24.557	0.082	0.445
	2.085	-16.597	13.099	0.060	0.785
	1.426	-2.593	8.961	0.386	0.278
	0.193	-2.969	1.215	0.337	0.925
Ks1 = 45	111.822	-33.285	702.597	0.030	0.047
	21.221	-0.013	133.336	77.929	0.0001
	5.156	-91.135	32.399	0.011	0.942
	5.745	-3.178	36.095	0.315	0.088
	1.923	-17.394	12.083	0.057	0.821
	1.318	-2.837	8.279	0.352	0.324
	0.139	-2.136	0.875	0.468	0.925

(vi) gain Bode diagram for the closed loop on load frequency domain response of the Synchronous Power Generating Module Excitation System with and without the Power System Stabiliser. The Synchronous Power Generating Module operating at full load and at unity power factor. These diagrams should be in a suitable format to allow comparison of the Active Power damping across the frequency range specified in ECC.A.6.2.6.3 with and without the Power System Stabiliser in service.

ECC.A.6.2.6.3 A facility to inject a band limited random noise signal into the Automatic Voltage Regulator voltage reference shall be provided for demonstrating the frequency domain response of the Power System Stabiliser. The tuning of the Power System Stabiliser shall be judged to be adequate if the corresponding Active Power response shows improved damping with the Power System Stabiliser in combination with the Automatic Voltage Regulator compared with the Automatic Voltage Regulator alone over the frequency range 0.3Hz – 2Hz.

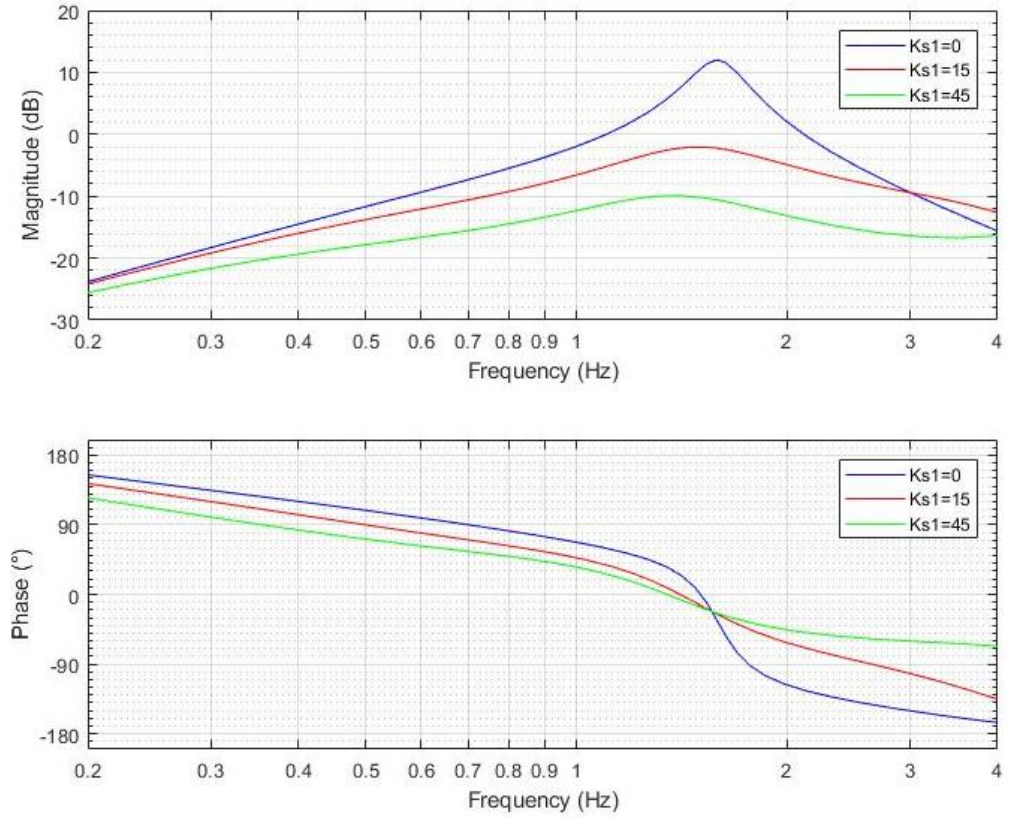

Figure 61 Bode plot Pm/Vref in closed loop

The closed-loop simulation was performed in accordance with ECC.A.6.2.6.3 in the range 0.3 – 2 Hz for active power response to an injected noise signal into the AVR, allowing for comparison of active power damping across the frequency range in accordance with ECP.A.3.2.1 (vi). As required, the simulation was performed with full load and unity power factor at generator terminals. Here, we are dealing with two different loops, therefore the amplitude margin and phase margin are not involved. Instead, Figure 61 shows the increase in damping eigen frequency.

9.3 Reactive Capability across the Voltage Range

C.7.3.1. For Synchronous Power Generating Modules the Generator shall demonstrate the capability to meet Section 13.5 by submission of a report containing load flow simulation study results showing:

- *(i) the maximum lagging Reactive Power capability when the Connection Point voltage is at 105% of nominal.*
- *(ii) the maximum leading Reactive Power capability when the Connection Point voltage is at 95% of nominal.*
- *(iii) the maximum lagging Reactive Power capability at the Minimum Stable Operating Level when the Connection Point voltage is at 105% of nominal.*
- *(iv) the maximum leading Reactive Power capability at the Minimum Stable Operating Level when the Connection Point voltage is at 95% of nominal.*

The terminal voltage in the simulation should be the nominal voltage for the machine.

The simulation was conducted within the voltage variation range at the connection point in the range from 0.95 pu to 1.05. Achieving the specified conditions ([1] capture 13.5, Figure 13.11) for the reactive power control range based on the voltage at the connection point is viewed at UQ diagram. The UQ diagram shows the maximum requested operating leading reactive power PF = -0.92 and maximum lagging reactive power PF = 0.92 for both voltage limits at the connection point. The simulation is conducted with a registered capacity of 55.6 MW, considering a house load of 5.5 MW.

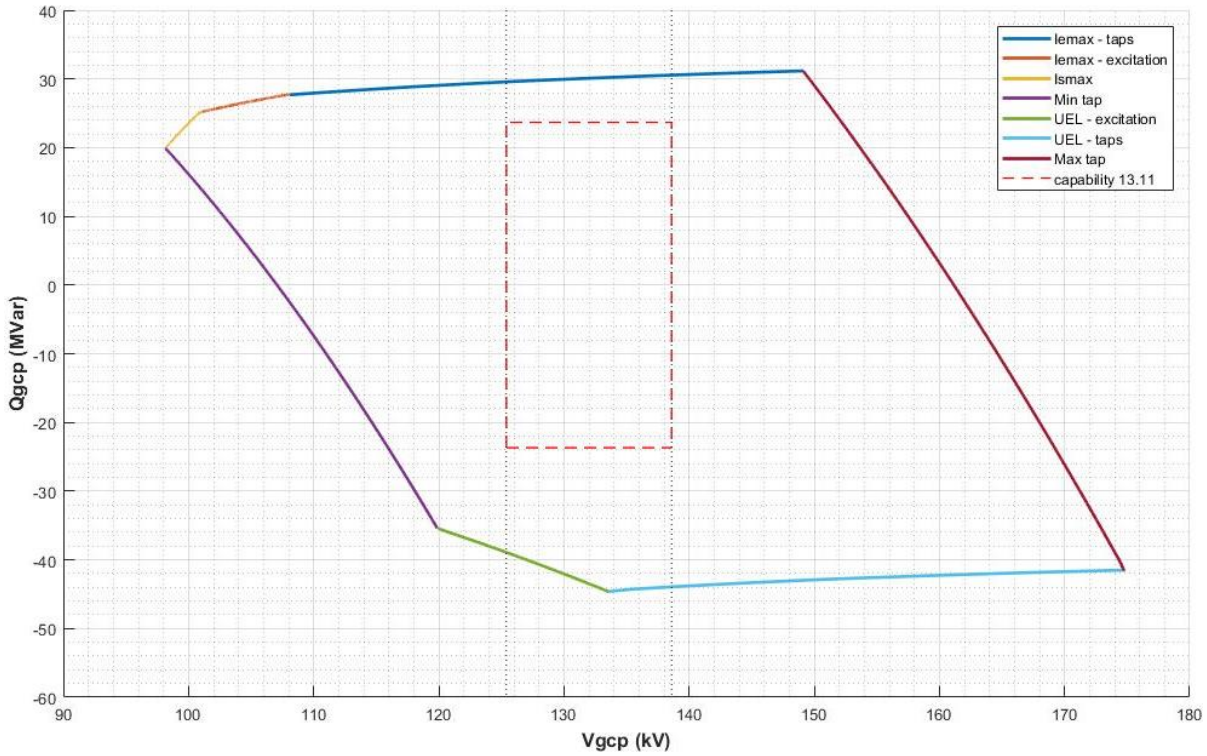

Figure 62 UQ capability diagram

The generator is designed to regulate voltage within the range of 0.95 to 1.05 at its terminals. In addition to excitation-based regulation, regulation is also performed by the tap changer

on the OLTC transformer, which is equipped with a single tap change of 1.25%, including +14 taps for an increase and 10 taps for a decrease voltage.

Legend of capability diagram:

Iemax – taps … Maximum limit of generator field current, regulated by taps.

Iemax – excitation … Maximum limit of generator field current, regulated by excitation.

Ismax … Maximum limit of generator stator current, regulated by excitation.

Max tap …The Power Generating Module operates with maximum tap, Vg = 1.05 pu.

Min tap …The Power Generating Module operates with minimum tap. Vg = 0.95 pu.

UEL – excitation … Under Excitation Limiter, regulation by excitation.

UEL – taps … Under Excitation Limiter, regulation by taps.

To satisfy the requirements of C.7.3.1., the voltage at the generator terminals must be kept constant. Reactive power regulation is performed only by the tap changer, while excitation keeps the nominal terminal voltage. The following Figure presents the simulation according to C.7.3.1. (i) and (ii).

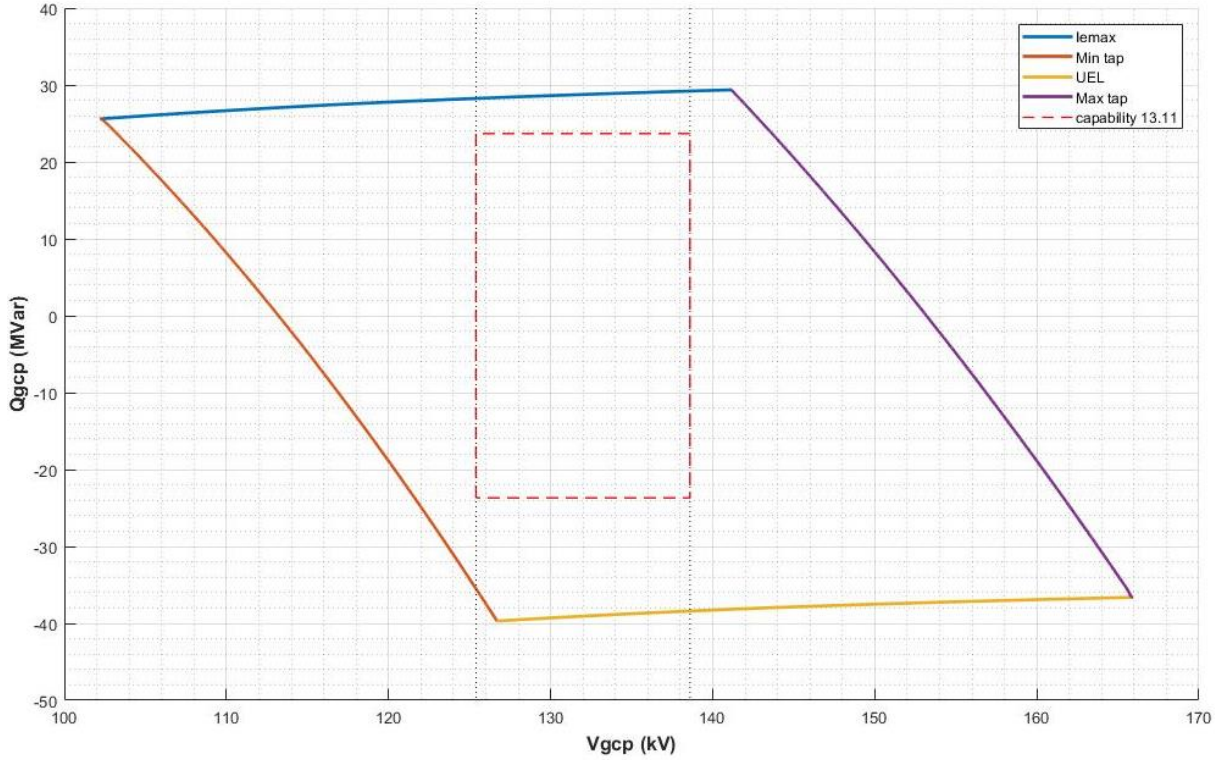

Figure 63 UQ capability diagram complying with specified conditions (i) and (ii)

Further simulation was performed for the minimum stable operating level in accordance with C.7.3.1. (iii) and (iv). The house load remained consistent, while the generated power is adjusted to 36.1 MW and power to the grid is adjusted to 30.6 MW. The Synchronous Power

Generating Module must still be able to continuously operate with reduced power at any point within the Reactive Power capability limit identified by the rectangle in Figure 13.11 of [1].

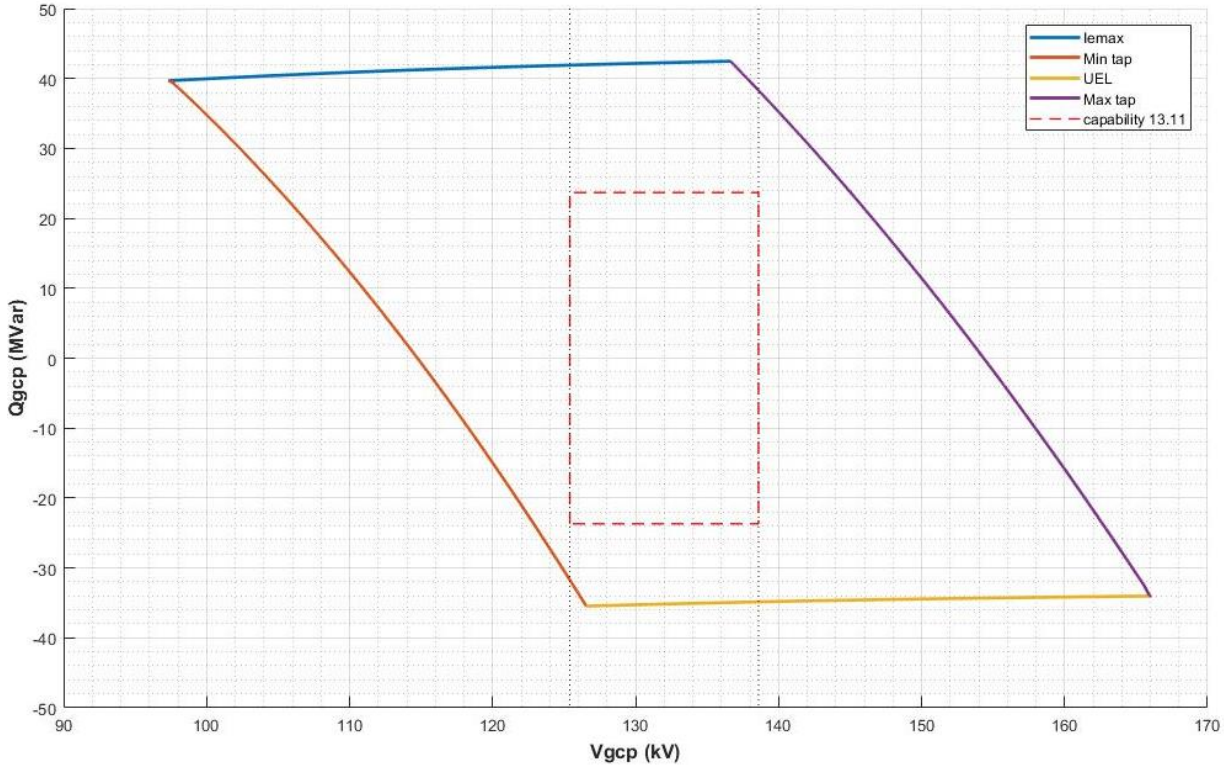

Figure 64 UQ capability diagram complying with specified conditions (iii) and (iv)

Reactive capability across voltage range is performed with very slow Vgcp change to keep steady state within the simulation. The maximum field and stator current is limited to 1.0 p.u., while UEL is simulated according to the limiter settings configured by the generator manufacturer.

Legend of capability diagram:

Iemax … Maximum limit of generator field current.

Max tap …The Power Generating Module operates with maximum tap.

Min tap …The Power Generating Module operates with minimum tap.

UEL … Under Excitation Limiter

capability 13.11 … Capability rectangle in accordance with Figure 13.11 in [1]

9.4 Fault Ride Through

C.7.5.2 The Generator shall supply time series simulation study results to demonstrate the capability of Synchronous Power Generating Modules and Power Park Modules to meet paragraph 13.3 and paragraph 13.6 by submission of a report containing:

(i) *a time series simulation study of a 140 ms three phase short circuit fault with a retained voltage as detailed in Table C.7.1 applied at the Connection Point of the Power Generating Module.*

(ii) *a time series simulation study of 140 ms unbalanced short circuit faults with a retained voltage as detailed in Table C.7.1 on the faulted phase(s) applied at the Connection Point of the Power Generating Module. The unbalanced faults to be simulated are:*

1. *a phase to phase fault*
2. *a two phase to earth fault*
3. *a single phase to earth fault.*

C.7.5.3 The simulation study should be completed with the Power Generating Module operating at full Active Power and maximum leading Reactive Power and the fault level at the Connection Point at minimum as notified by the DNO. A minimum short circuit power of 50 MVA is a generic minimum fault level that should be assumed. For the few cases where the fault level is lower than this the DNO will advise the Generator regarding the fault level assumptions to be used.

This section of simulations involves applying a short circuit to the terminals of the step-up transformer at the POC. The retained voltage for Type D from Table C.7.1 was found to be 0%. The time series simulations were performed with full active power and maximum leading reactive power as per C.7.5.3. Hence, the power factor was set less than -0.92 at the POC.

Maximum leading reactive power has been calculated according to equation (9.01) to be -23.69 MVAr. The reactive power set at -24.95 MVAr by adjusting the tap on the transformer to - 4. The simulation illustrates waveforms of 3-Ph short circuit (Fig. 65), 2-Ph to ground short circuit (Fig. 66), 1-Ph to ground short circuit (Fig. 67) and Ph-Ph short circuit (Fig. 68).

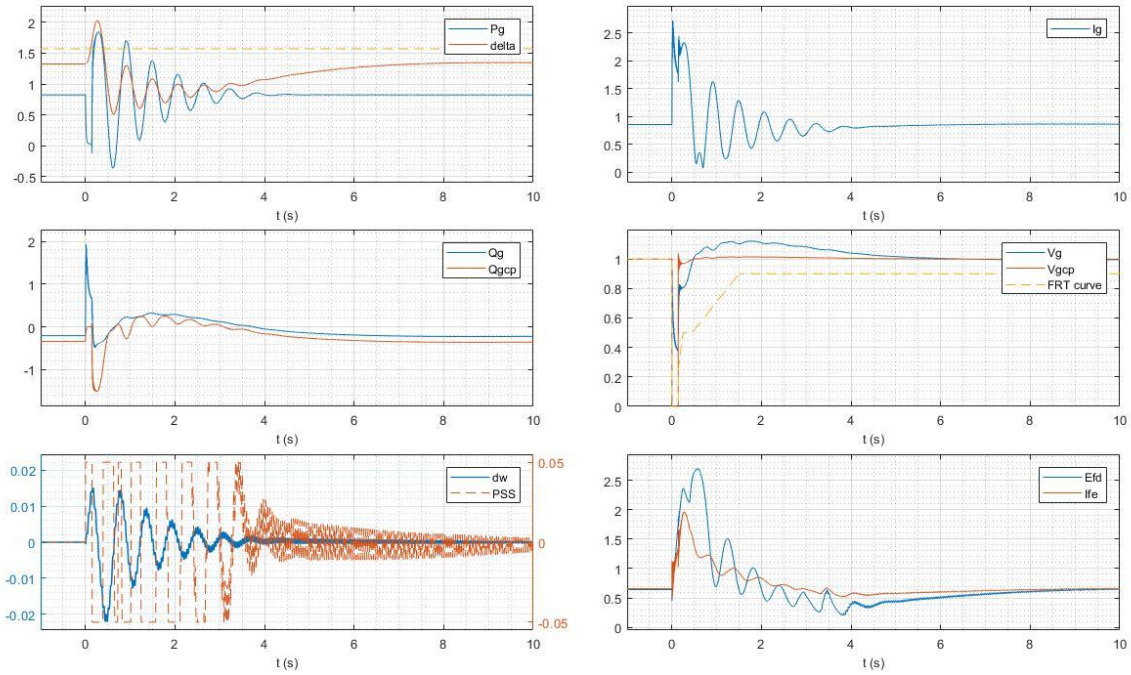

Figure 65 3-Ph short circuit at transformer terminals for 140 ms

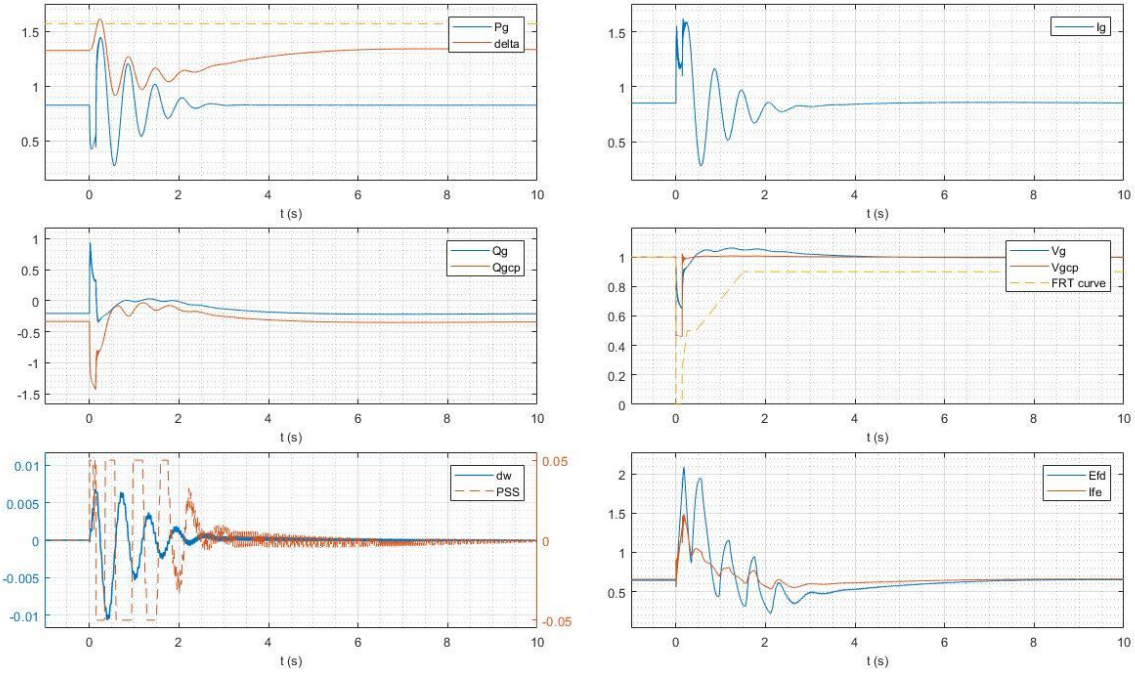

Figure 66 2-Ph to ground short circuit at transformer terminals for 140 ms

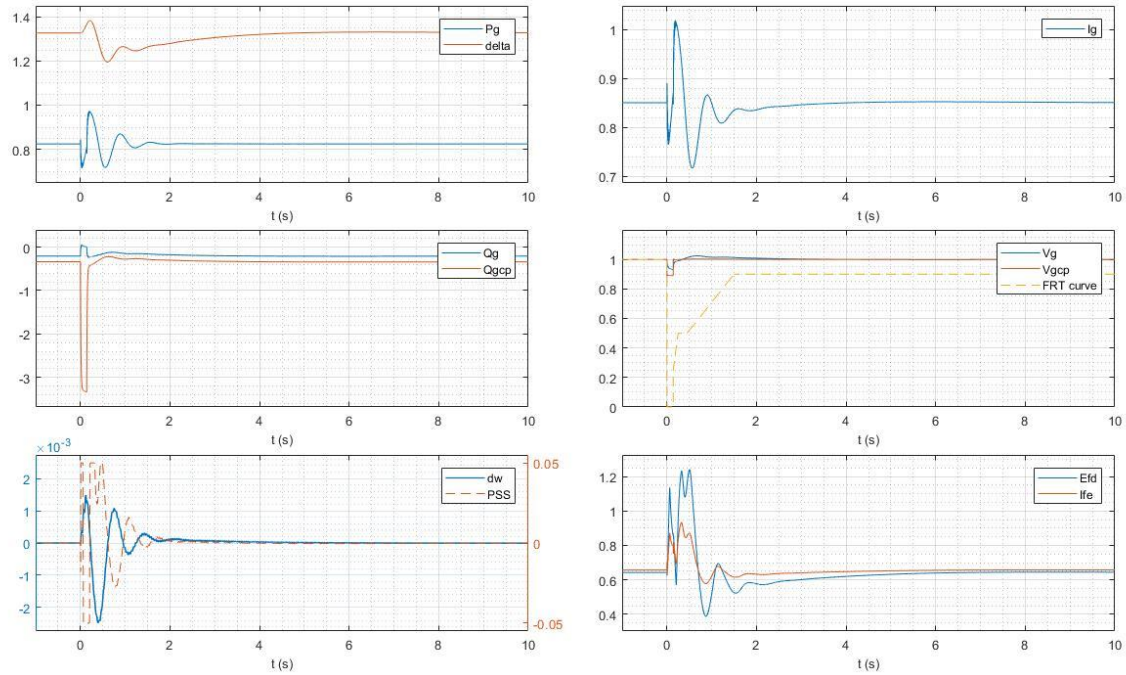

Figure 67 1-Ph to ground short circuit at transformer terminals for 140 ms

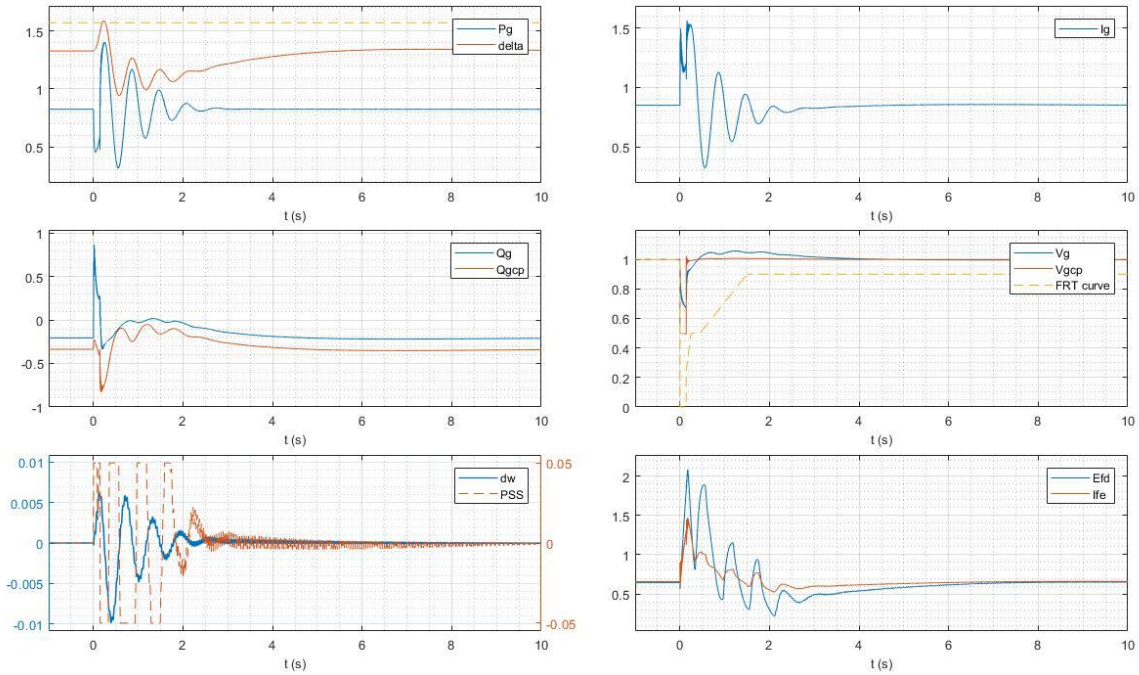

Figure 68 Ph-Ph short circuit at transformer terminals for 140 ms

The generator remains connected and stable for any fault, the voltage stays above black line of FRT curve from Figure 13.7 in [1].

C.7.5.4 The simulation study will show acceptable performance providing compliance with the requirements of paragraph 13.3.1.11 (e) are demonstrated.

e) Each Power Generating Module shall be designed such within 0.5 s of restoration of the voltage at the Connection Point to 90% of nominal voltage or greater, Active Power output shall be restored to at least 90% of the level immediately before the fault. Once Active Power output has been restored to the required level, Active Power oscillations shall be acceptable provided that:

- *The total active energy delivered during the period of the oscillations is at least that which would have been delivered if the Active Power was constant.*
- *The oscillations are adequately damped.*
- *In the event of power oscillations, Power Generating Modules shall retain steady state stability when operating at any point on the Generator Performance Chart.*

The voltage at the connection point is restored almost immediately to its nominal value. The active power oscillations are adequately damped and total active power delivered during the oscillations remains constant.

During a 3-phase fault, there is a significant overshoot of the angle stability point (90°) in the first period of oscillation. Subsequently, the rotor angle returns immediately back to the stable area and the generator keeps stability. Such a large deviation of the rotor angle is caused by significant under-excited generator, which is improbable during standard operation. The synchronism of generator is not lost.

9.5 Limited Frequency Sensitive Mode – Over Frequency (LFSM-O)

C.7.6.2 The simulation study should comprise of a Power Generating Module connected to the Total System with a local load shown as "X" in Figure C.7.1. The load "X" is in addition to any auxiliary load of the Power Generating Facility connected directly to the Power Generating Module and represents a small portion of the system to which the Power Generating Module is attached. The value of "X" should be the minimum for which the Power Generating Module can control the power island frequency to less than 52 Hz. Where transient excursions above 52 Hz occur the Generator should ensure that the duration above 52 Hz is less than any high frequency protection system applied to the Power Generating Module.

C.7.6.5 Simulation studies shall be performed in Limited Frequency Sensitive Mode (LFSM) and Frequency Sensitive Mode (FSM). The simulation study results should indicate Active Power and frequency.

The simulation was performed with maximum active power output 61.1 MW and house load 5.5 MW. The load "X" was connected at the point of connection, that means at the HV side of OLTC terminals.

Simulation studies were conducted with FSM mode and without FSM mode. LFSM has more impact than FSM because LFSM is not limited, therefore, it can rapidly adjust power production. When the turbine reaches a speed of 1.008 per unit (with a speed deviation of 400 mHz) as per section 13.2.4 of [1], it switches to LFSM mode. The simulation studies are performed for LFSM alone and for LFSM and FSM.

When the rotation frequency exceeds 50.4 Hz, a new reference value for the required power is reloaded. This reloaded value is determined by the electrical power at the generator terminals with a delay. This delay from the control loop is compensated for by setting the delay for loading the new reference power. The microcontroller loop delay, simulated as an aperiodic block, is 100 ms, and the reloading delay is set to 300 ms.

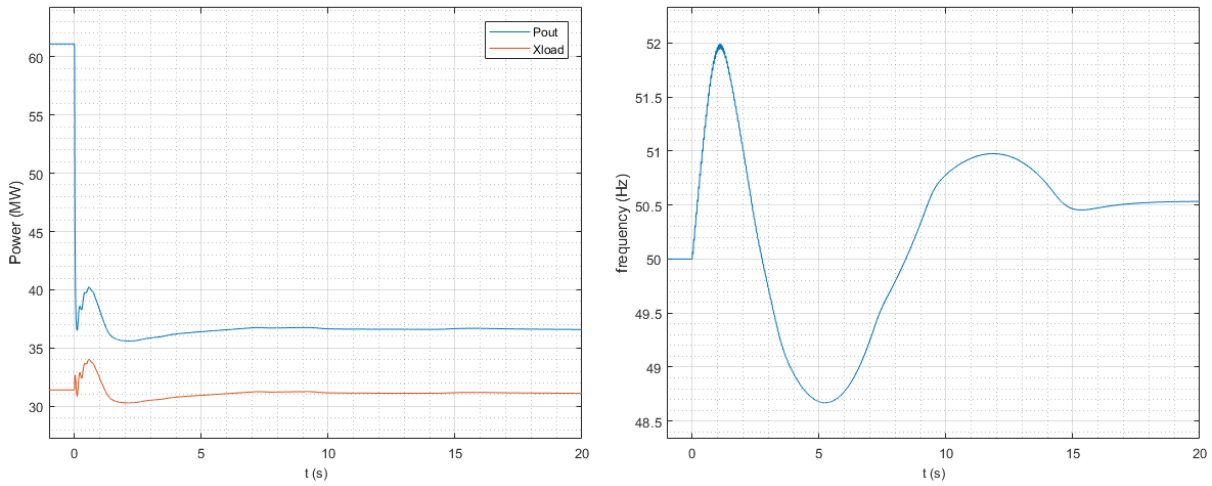

Figure 69 Grid cut-off with minimum possible connected load, LFSM

The maximum load that could be supplied from the Power Generating Unit after a grid cut-off occurs is 31.4 MW. The entire possible load, X load and house load, is 36.9 MW.

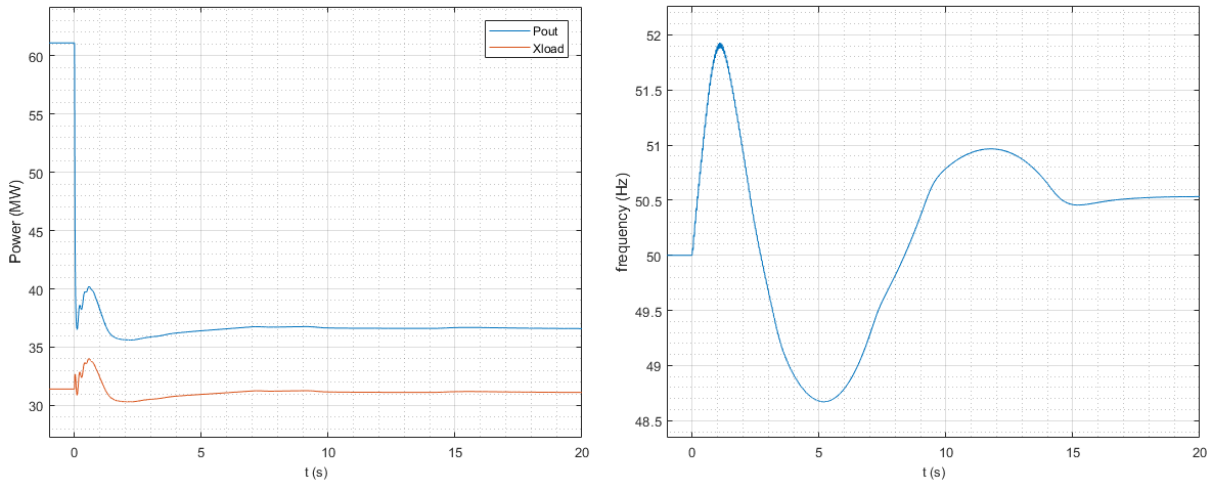

Figure 70 Grid cut-off with minimum possible connected load, LFSM and FSM

The difference between these 2 simulations is small, because FSM is limited to 10 % of registered power 5.56 MW. The combination of both modes may have a slightly better impact to keep turbine stability.

9.6 Limited Frequency Sensitive Mode – Under Frequency (LFSM-U)

C.7.7.2 To demonstrate the LFSM-U low frequency control when operating in Limited Frequency Sensitive Mode the Generator shall submit a simulation study representing the response of the Power Generating Module operating at 80% of Registered Capacity. The simulation study event shall be equivalent to:

(i) *a sufficiently large reduction in the measured system frequency ramped over 10 s to cause an increase in Active Power output to the Registered Capacity followed by*

(ii) *60 s of steady state with the measured system frequency depressed to the same level as in C.7.7.2 (i) as illustrated in Figure C.7.3 below.*

(iii) *then increase of the measured system frequency ramped over 10 s to cause a reduction in Active Power output back to the original Active Power level followed by at least 60 s of steady output.*

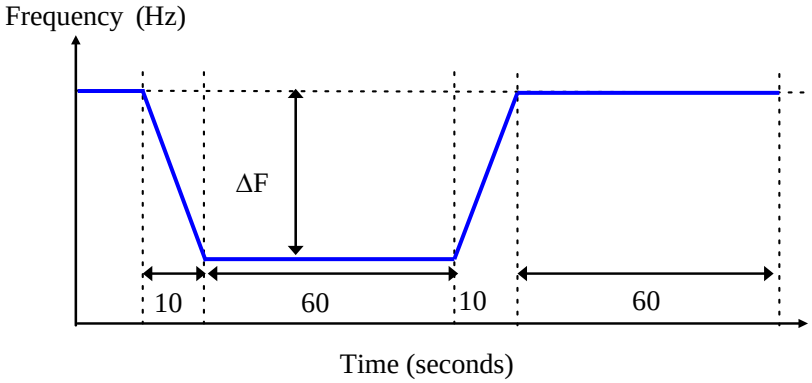

Figure 71 LFSM-U curve [1]

The LFSM-U simulation is not performed because it is not anticipated to operate in an inefficient mode to enable LFSM-U response (according to [1], section 13.2.5.1). LFSM-U operation is required for Power Generating Modules with headroom and the ability to increase Active Power output ([1], section 13.2.5.1 (a)). Power Generating Module in LFSM-U Mode shall be capable of providing a power increase up to its Registered Capacity ([1], section 13.2.5.1 (d)), which is exactly 61.1MW.

The most efficient operating mode of a Waste-to-energy Power plant is pressure control mode (pressure to the Turbine is controlled to defined value). In this mode, all available power is exported to the Grid at any time, and therefore, it has minimum capacity or reserve to provide LFSM-U.

9.7 Verification and validation controllers

C.7.8.2 To demonstrate the frequency control or governor/load controller/plant model the Generator shall submit a simulation study representing the response of the Synchronous Power Generating Module or Power Park Module operating at 80% of Registered Capacity. The simulation study event shall be equivalent to:

(i) a ramped reduction in the measured system frequency of 0.5Hz in 10 s followed by

(ii) 20 s of steady state with the measured system frequency depressed by 0.5Hz followed by

(iii) a ramped increase in measured system frequency of 0.3Hz over 30 s followed by

(iv) 60 s of steady state with the measured system frequency depressed by 0.2Hz as illustrated in Figure C.7.4 below.

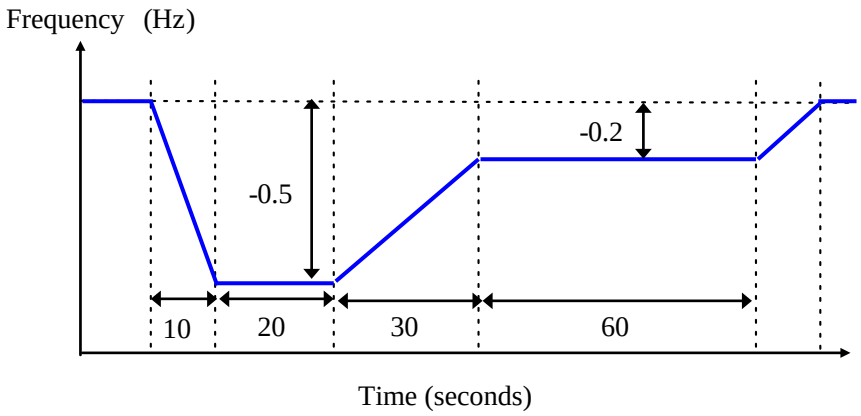

Figure 72 C.7.4 Controller simulation [1]

The simulation study shall show Active Power output (MW) and the equivalent of frequency injected.

At the start, the turbine operates at 80% of the registered output power, calculated as:

$$P_{ref} = P_{reg80\%} + P_{HL} = \frac{(55.6 \cdot 0.8 + 5.5)}{74.12} = \frac{49.98\ (MW)}{74{,}12\ (MVA)} = 0.6743\ (p.u.) \quad (9.02)$$

The FSM must be activated when the controller needs to respond to speed deviation. Speed deviation determines the increase in required power through droop.

Equation (4.03) is employed to compute the power level associated with frequency deviations of 0.2 Hz and 0.5 Hz. FSM droop is set to 5%. When the speed deviation Δf is 0.2 Hz (150 mHz insensitivity is included), The demanded power output is increased by:

$$\Delta P_{FSM} = \frac{(0.2 - 0.015)}{50} \cdot \frac{1}{0.05} \cdot \frac{55.6}{74.12} = \frac{4.114\ (MW)}{74.12\ (MVA)} = 0.0555\ (p.u.) \quad (9.03)$$

When the speed deviation Δf is 0.5 Hz, the demanded increased power is:

$$\Delta P_{FSM} = \frac{(0.5 - 0.015)}{50} \cdot \frac{1}{0.05} \cdot \frac{55.6}{74.12} = \frac{10.79\ (MW)}{74.12\ (MVA)} = 0.1456\ (p.u.) \quad (9.04)$$

Additionally, FSM power control is limited in accordance with equation (4.06) to 5.56 MW (0.075 p.u.). Therefore, a deviation of 0.5 Hz is too enormous for a linear FSM response. The maximum visualized power is calculated as 55.54 MW according to the following formula:

$$P_{max} = P_{reg80\%} + P_{HL} + \Delta P_{FSM_{MAX}} = \frac{(55.6 \cdot 0.8 + 5.5 + 55.6 \cdot 0.1)}{74.12} = \frac{55.54\ (MW)}{74{,}12\ (MVA)} = 0.749\ (p.u.) \quad (9.05)$$

The validation waveform clearly shows the speed of regulation with limits.

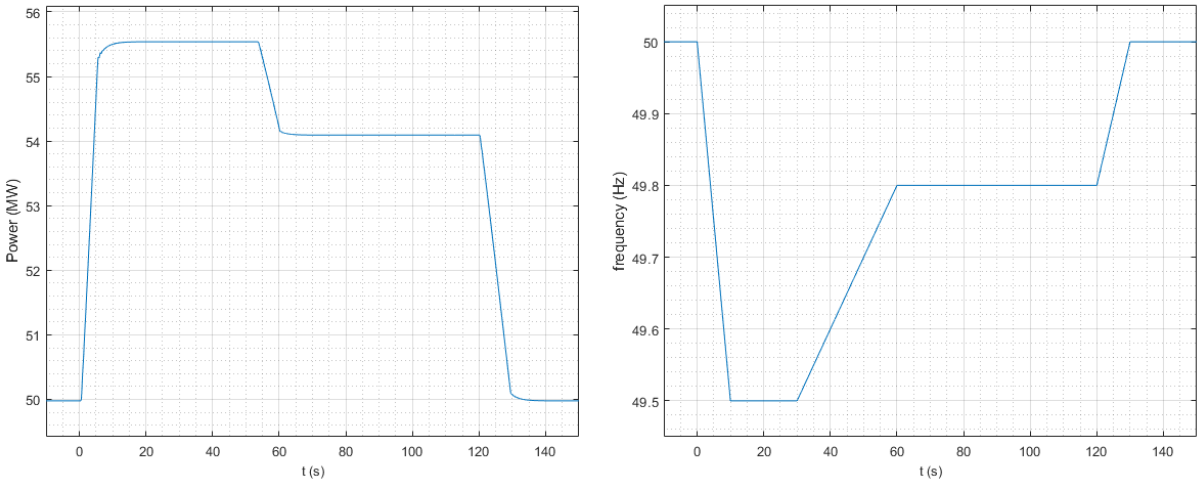

Figure 73 Frequency injection and power reaction

The PI controller is configured based on the turbine torque response to a speed change (0.2 Hz) when the FSM is activated.

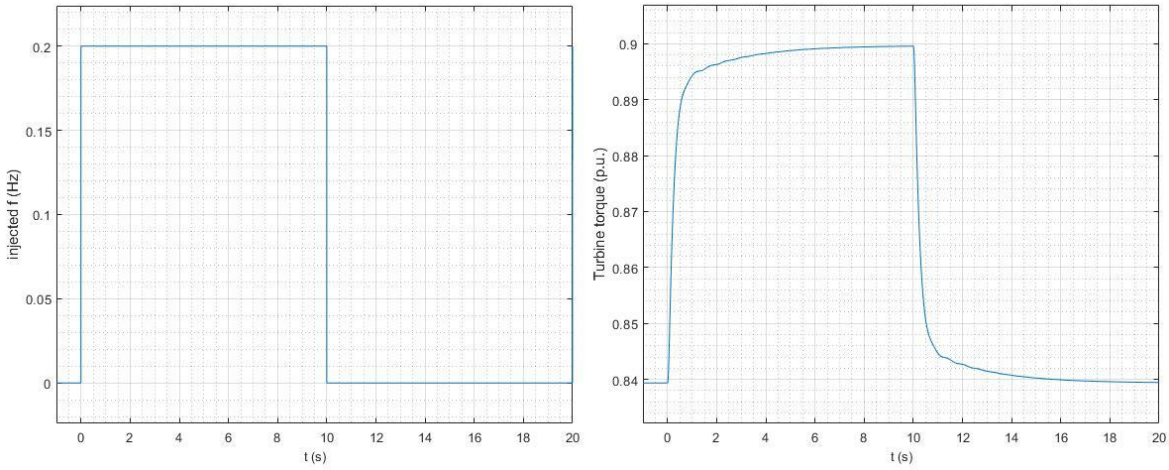

Figure 74 Turbine torque response to speed step

C.7.8.3 To demonstrate the Excitation System model the Generator shall submit simulation studies representing the response of the Synchronous Power Generating Module as follows:

(i) *operating open circuit at rated terminal voltage and subjected to a 10% step increase in terminal voltage reference from 90% to 100%.*

(ii) *operating at Registered Capacity, nominal terminal voltage and unity Power Factor subjected to a 2% step increase in the voltage reference. Where a Power System Stabiliser is included within the Excitation System this shall be in service.*

The simulation study shall show the Synchronous Power Generating Module terminal voltage, field voltage, Active Power, Reactive Power and Power System Stabiliser output signal as appropriate.

The terminal voltage and excitation response to a 10% step change in the required terminal voltage to the AVR is depicted in Figure 25. The step change was performed while the circuit was open. The measurable VA – specified value of field voltage of the exciter, I_{FE} – field current of the exciter are displayed in Figure 75 along with the voltage at the generator terminals. The generator field voltage E_{FD} is not shown, because it cannot be measured during real measurements.

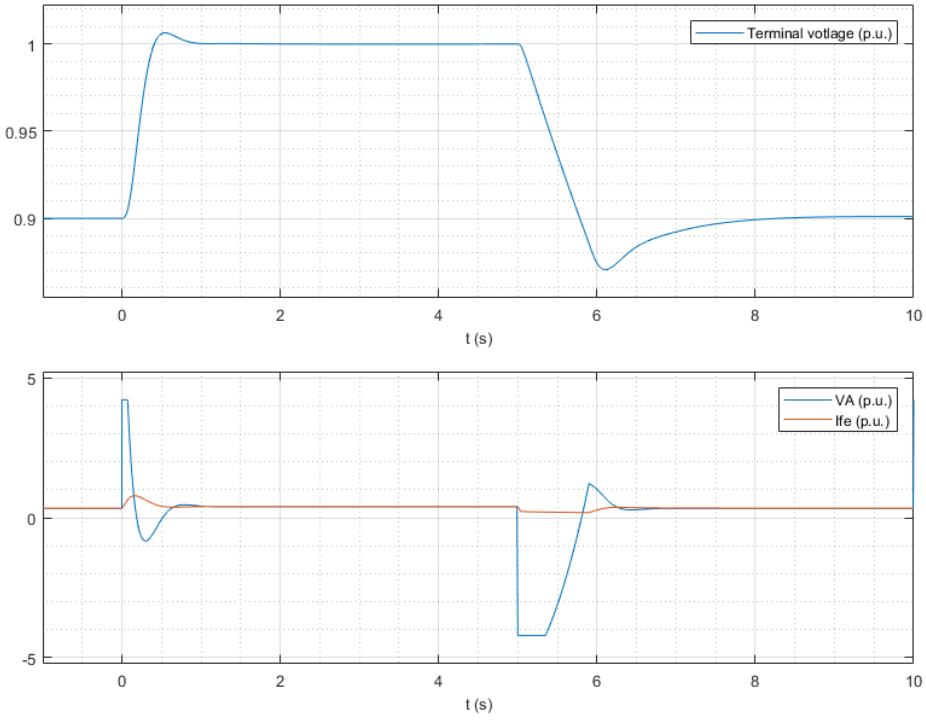

Figure 75 Reference voltage step from 90 % to 100%

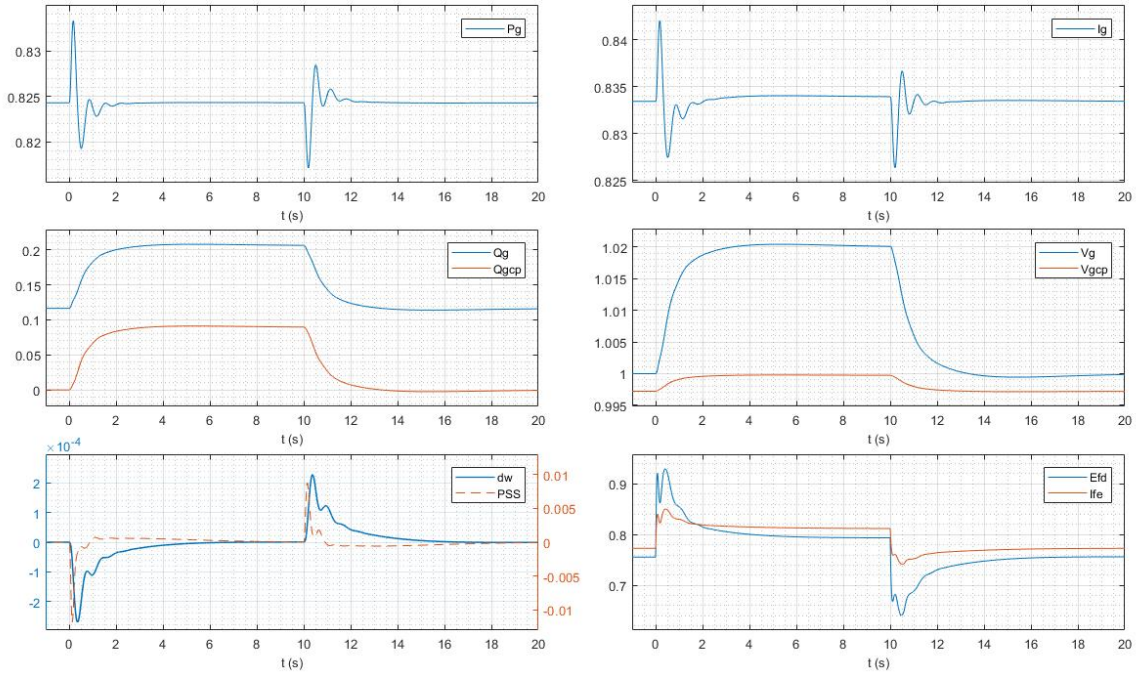

Figure 76 Voltage step change ± 2%

All requested outputs are displayed in Figure 76, showing the step change in the reference terminal voltage during operation. The simulation was conducted with a unit power factor.

Evaluation and Conclusion

The objective of the thesis was to assemble a power plant block in Simulink and subsequently simulate stationary issues (see Chapter 9.3, Reactive capability across the Voltage Range), conduct dynamic simulations of defined events, tune PI controllers and PSS, and especially to prove the compliance of the production unit according to the guidelines in G99 section C.7 based on the developed simulation model.

Due to the focus on RMS values instead of harmonic waveforms during simulations, the phasor-based solution has been selected. The mathematical models of Generator, Turbine, Excitation, Mass, OTLC, PSS operates with p.u. values.

The generator model has been realized by the Synchronous Machine pu Fundamental block from the Simscape/Power Systems library, which corresponds to the derived equations. The fundamental parameters have been derived from the standard parameters provided by the manufacturer.

The excitation model was designed in accordance with Standard Std. 421.5 utilized the exciter per-unit system. PI controller parameters have been determined from step injection to reference voltage simulation, as detailed in Capture 9.7. The turbine has been modelled according to IEEEG1 with a power controller, which is not a part of IEEEG1. While IEEEG1 with the Lead-lag block considers only a constant output from the load control, thus allows only frequency sensitive response, the PI controller is utilized for both load control and frequency sensitive response. Therefore, the Lead-lag block is inactive and replaced by a PI controller. In the Capture Mass, the transmitted power from the turbine to the generator is implemented via a flexible shaft connection. The inductance and reactance of the tap winding parts of OLTC transformer is calculated in p.u. from the provided parameters. The grid is modelled as an ideal controlled voltage source with impedance corresponding to the short-circuit power. The regulation of the RMS voltage level is carried out to adjust the voltage level at the point of connection (HV side of the transformer). This regulation can be done either for plotting the UQ diagram, or for the regulation of the voltage to the nominal level, or to achieve the desired power factor at point of connection.

According to G99 [1] and Grid Code [2], the simulations have been performed in Chapter 9 to demonstrate compliance with the connection conditions of the production unit, such as PSS, Reactive Capability across Voltage Range, Fault Ride Through etc. A detailed analysis is summarised in the following paragraph.

The torsional vibration filter of PSS has been configured to ensure that the PSS does not respond to torsional vibrations. In a closed loop, phase compensation of the voltage loop was performed to damp the turbine oscillations. Subsequently, simulations confirmed the correctness of this setting. Phase margin and amplitude margin were demonstrated by simulating the open voltage loop and plotting a Bode diagram. The Eigen values plot in the s-plane diagram demonstrates the improvement of the damping factor around the local mode frequencies. The damping of local mode frequencies was also illustrated by the Bode diagram of the power response to the reference voltage.

The reactive power capability requirements at the connection point as defined in Figure 13.11 in [1] has been satisfied by UQ diagram, which depicts the generator's operating limit curve.

The generator has been demonstrated to be capable of keeping stable operation under all specified fault types listed in Capture 9.4.

LFSM-O determined the minimum load that can be connected for an instantaneous islanding. According to G99 [1], it is not necessary to simulate LFSM-U if it is not anticipated that the generating unit will operate in an inefficient mode. For a Waste-to-energy Power plant, we assume that it will operate typically in constant pressure mode. In this mode, all steam produced by the boiler flows directly to the turbine, enabling the turbine to operate in the most economical manner and produce maximum power.

In the last Chapter 9.7 the controllers are verified and validated according to [1].

All defined objectives were successfully achieved at a specific power production unit in the UK, namely the Rivenhall Waste-to-energy Power Plant.

Literature

[1] ENERGY NETWORKS ASSOCIATION. Engineering Recommendation G99. Issue 1 – Amendment 9. 3 October 2022.

[2] National Grid ESO. THE GRID CODE. ISSUE 6. REVISION 16. 5 January 2023.

[3] KUNDUR, Prabha. Power System Stability and Control. New York, c 1994. ISBN 978-0-07-035958-1.

[4] Synchronous Machine pu Fundamental. Online. MathWorks. R2023b. Dostupné z: https://www.mathworks.com/help/sps/powersys/ref/synchronousmachinepufundamental.html?searchHighlight=synchronous%20machine&s_tid=srchtitle_support_results_6_synchronous%20machine. [cit. 2024-02-01].

[5] "IEEE Guide for Test Procedures for Synchronous Machines Part I—Acceptance and Performance Testing Part II—Test Procedures and Parameter Determination for Dynamic Analysis," in IEEE Std 115-2009 (Revision of IEEE Std 115-1995), vol., no., pp.1-219, 7 May 2010, doi: 10.1109/IEEESTD.2010.5464495.

[6] BAGHZOUZ, Y. Online. In: EE 742 – Chap 4 Electromagnetic Phenomenon. Dostupné z: http://www.egr.unlv.edu/~eebag/EE%20742%20Chap%204.pdf. [cit. 2024-02-08].

[7] "IEEE Standard Definitions for Excitation Systems for Synchronous Machines," in IEEE Std 421.1-2021 (Revision of IEEE Std 421.1-2007) , vol., no., pp.1-45, 17 March 2022, doi: 10.1109/IEEESTD.2022.9737077.

[8] "IEEE Recommended Practice for Excitation System Models for Power System Stability Studies," in IEEE Std 421.5-2016 (Revision of IEEE Std 421.5-2005) , vol., no., pp.1-207, 26 Aug. 2016, doi: 10.1109/IEEESTD.2016.7553421.

[9] Liu, Guangshi & Sun, Zhiyuan & Dou, Qian & Liu, Mosi & Zhang, Yihui & Wang, Xiaoming. (2018). Analysis about modeling MEC7000 excitation system of nuclear power unit. IOP Conference Series: Earth and Environmental Science. 121. 042030. 10.1088/1755-1315/121/4/042030.

[10] M. F. M. Yakub, W. Martono and R. Akmeliawati, "Vibration control of two-mass rotary system using improved NCTF controller for positioning systems," 2010 IEEE Control and System Graduate Research Colloquium (ICSGRC 2010), Shah Alam, Malaysia, 2010, pp. 61-67, doi: 10.1109/ICSGRC.2010.5562522.

[11] Multi-Winding Transformer. Online. MathWorks. R2023b. Dostupné z: https://www.mathworks.com/help/sps/powersys/ref/multiwindingtransformer.html?search

Highlight=multiwinding%20transformer&s_tid=srchtitle_support_results_1_multiwinding%20transformer. [cit. 2024-02-06].

[12] Izdebski, Michał & Malkowski, Robert & Miller, Piotr. (2022). New Performance Indices for Power System Stabilizers. Energies. 15. 10.3390/en15249582.

[13] "IEEE Guide for Identification, Testing, and Evaluation of the Dynamic Performance of Excitation Control Systems," in IEEE Std 421.2-2014 (Revision of IEEE Std 421.2-1990) , vol., no., pp.1-63, 27 June 2014, doi: 10.1109/IEEESTD.2014.6845300.